REAUSTENITISATION OF SOME ALLOY STEELS

by

URSULA RUTH LENEL

DARWIN COLLEGE

CAMBRIDGE

A dissertation submitted for the degree of Doctor of Philosophy in the University of Cambridge, October 1980

PREFACE

This dissertation, which is submitted for the degree of Doctor of Philosophy in the University of Cambridge, describes work carried out in the Department of Metallurgy and Materials Science under the supervision of Professor R.W.K. Honeycombe between October 1977 and September 1980. Except where acknowledgement and reference to previous work has been made, the work described is original and has been done without collaboration. The length of this dissertation does not exceed 60,000 words, and no part has been, or is being, submitted for a degree, diploma or any other qualification at any other University.

U. R. LENEL

October 1980

ACKNOWLEDGEMENTS

I would like to thank Professor R.W.K. Honeycombe for the provision of laboratory facilities, and for his continued advice and encouragement. I would also like to thank the members of the Alloy Steels Research Group for many useful and stimulating discussions; in particular I am grateful to Dr. P.R. Howell and Dr. H.K.D.H. Bhadeshia for the helpful interest they have shown during the course of this work. Thanks are also due to the technical staff of the Department, particularly D. Ackland and J. Leader, for maintenance of equipment and for technical advice.

This work was supported by the Science Research Council, to whom I am grateful for the provision of a Research Studentship.

Finally, I would like to thank my parents and my friends for all their encouragement and support; thanks particularly to Andrew Mackintosh for help with the proof-reading.

SUMMARY

This thesis reports a study of reaustenitisation of a variety of microstructures in some alloy steels, using several experimental techniques. Emphasis has been placed on the formation of austenite in the two-phase austenite plus ferrite temperature range, as the characteristics of such reactions, and their variation with alloying element content, starting structure and temperature, are not understood in detail. Moreover, such intercritical annealing of low alloy steels is carried out during the industrial production of dual phase steels, which display improved mechanical properties over conventional low alloy steels.

The starting materials for reaustenitisation in this study consisted of:

1. Low alloy steels, containing 0.1% to 0.25% C and 1% to 2% Mn or Ni, with microstructures of ferrite and spheroidised cementite, ferrite and pearlite, or martensite, and
2. A high alloy steel containing 0.2%C and 10%Cr, with a microstructure of ferrite and $M_{23}C_6$ type carbides.

The formation of austenite was studied using optical microscopy and transmission electron microscopy (TEM), while the kinetics of the reactions were investigated by isothermal dilatometry. Alloying element distributions were determined by microanalysis using an energy dispersive X-ray analysis system in conjunction with TEM and STEM (Scanning Transmission Electron Microscopy).

Several aspects of reaustenitisation have been studied: austenite nucleation behaviour and growth mode, austenite morphology, austenite-ferrite crystallography and interface type, and the effect of cementite or alloy carbide distributions on the ferrite to austenite transformation. The interdependence of these factors has also been examined. In addition, kinetic and microanalytical studies have elucidated the rate controlling factors of austenite formation in some alloy steels, and the conditions under which completion of the austenite reaction is achieved most rapidly have been determined, both in the two-phase region and at higher temperatures in the single phase austenite region.

CONTENTS

CHAPTER ONE

LITERATURE REVIEW

1.1 Introduction

In this chapter a review of the literature relevant to the subject of this thesis is given. In past work on steels, the transformation from ferrite, martensite and bainite to austenite has received a great deal less attention than the reverse transformation from austenite. The decomposition of austenite is relatively well understood, and as several reviews of the subject are available (eg Aaronson(1962), Honeycombe(1976)) no literature survey of the topic will be given here. However, some similarities between austenite decomposition and the reaustenitisation reactions are expected, and the austenite decomposition literature will be quoted where relevant.

Reaustenitisation is a complicated process, which has not been widely investigated in the past. The reaction is affected by many variables such as temperature and heating rate, and is particularly sensitive to the starting structure and alloy composition. A detailed review of the literature on reaustenitisation is given in section 1.2 of this chapter. The state of current knowledge on the reaction mechanisms, the austenite morphology, the effect of different starting structures and the effect of alloying elements on the austenite reaction is outlined.

In section 1.3, the development of dual phase steels is reviewed. The production of dual phase steels involves partial reaustenitisation and quenching, and it is the development of these steels which has led to renewed interest in austenite formation. Dual phase steels are generally low alloy, and hence low cost, steels, their importance lying in their good mechanical properties, which can be attributed to a composite microstructure of a hard phase (martensite) in a more ductile matrix (ferrite). The mechanical properties of such steels are therefore reviewed along with some theoretical models to describe their behaviour. Finally, the development of useful microstructures in dual phase steels is outlined.

1.2 Reaustenitisation

Reaustenitisation is an important industrial process, as it is a necessary part of the heat treatment of most steels. Although the austenite is replaced by other transformation products on cooling, the nature of the austenite which exists at high temperature affects the morphology, grain size and properties of the low temperature phases. In addition, steels which have been partially transformed to austenite, and then quenched to give a composite ferrite-martensite microstructure, are found to show improved properties over conventional steels. The early stages of austenitising are thus important in determining the size and distribution of the martensite in these so called dual phase steels (see section 1.3).

For these reasons, some studies of the formation of austenite have been made, but reaustenitisation has received a great deal less attention than the reverse transformation, the decomposition of austenite. In general, excluding transformations to or from martensite, carbides are present, and austenite formation cannot be a simple reversal of austenite decomposition. Whereas austenite decomposition involves the precipitation of carbides, during reaustenitisation the two low temperature phases, ferrite plus carbide, must react together to give a single phase, austenite (except in alloy steels in which carbides may remain in the austenite). Also, the kinetics of the reactions occuring on heating and cooling will be different. On heating, the driving force to form austenite and the rate of diffusion both increase with increasing temperature, whereas on cooling the driving force to form ferrite increases and the diffusion rate decreases as the temperature decreases.

In this section, the literature concerning reaustenitisation is reviewed. First the mechanism of austenite formation and the resultant austenite morphology are considered in general terms, followed by a survey of the reaustenitisation of particular microstructures, namely ferrite plus spheroidite, ferrite plus pearlite, and martensite or bainite. The effects of austenitising conditions on austenite grain growth and methods of austenite grain refinement (by heat treatment) are reported, and finally the effects of alloying elements are considered.

1.2.1 Transformation Mechanism

The mechanism of austenite formation may be either diffusionless shear (as in the decomposition of austenite to martensite) or nucleation and growth (as in the diffusional decomposition of austenite to ferrite).

Zerwekh and Wayman (1965) investigated the transformation to austenite in pure iron whiskers and observed a well defined shape change and ferrite-austenite habit plane at high superheating, indicating that the transformation was occurring by a cooperative shear (martensitic) mechanism. Krauss and Cohen (1962) and Krauss (1963) noted a high dislocation density in austenite formed during a reverse martensitic transformation in carbon-free Fe-34%Ni alloys. Kessler and Pitsch (1965) showed that this transformation was occurring by a shear mechanism, by observation of both surface relief and a ferrite-austenite orientation relationship (the Nishiyama-Wasserman orientation relationship). The dilatometric and metallographic experiments of Jana and Wayman (1967) on a similar alloy suggested that both diffusional and shear mechanisms occurred, the shear mechanism operating only at relatively high temperatures ie. high superheating, or under conditions of rapid heating. In pure iron and iron alloys with high Ni content, the ferrite to austenite transformation can therefore occur by either a shear or a nucleation and growth mechanism.

There is no convincing evidence for the operation of a shear mechanism during reaustenitisation of Fe-C alloys or steels. Sadovskiy (1962) and Albutt and Garber (1966) consider that a martensitic mechanism can occur during very rapid heating, although their evidence indicates only that the transformation is diffusionless, and not that it is occurring by cooperative shear, which is a necessary criterion of a martensitic transformation. During reaustenitisation of martensite, Matsuda and Okamura (1974a,b) observed the formation of acicular austenite grains, all of which had the same crystallographic relationship to the prior austenite grain in which they nucleated. This led them to believe that the reaustenitisation of martensite occurred by a diffusionless shear mechanism. However, the formation of acicular austenite grains has been shown to be due simply to the inheritance of the shape of the preceding ferrite (ie martensite lath) eg. by Nehrenberg (1950), while the constancy of the crystallogrphic relationship can be interpreted in terms of geometrical interfacial energy minimisation

(Watanabe et al 1976). On the other hand, many other reaustenitisation studies, eg Roberts and Mehl (1943), Speich and Szirmae (1969), Plitcha and Aaronson (1974), have provided evidence for the formation of austenite by a nucleation and growth mechanism.

It therefore seems that reaustenitisation of steels occurs only by a nucleation and growth mechanism and not by a martensitic shear mechanism.

1.2.2 Austenite Morphology

The morphology of austenite is strongly dependent on the starting structure, and this dependence will be discussed more fully in later sections. Here, an attempt will be made to outline the major factors affecting morphology.

In Fe-C alloys, the transformation from ferrite to austenite is always complicated by the presence of carbides or by a prior martensitic microstructure. The simpler case of a prior ferrite microstructure has been investigated by Grozier et al (1965), Pavlick et al (1966) and Fong and Glover (1975), who investigated the growth of austenite into carbon free ferrite during nitriding. The formation of austenite in this system depends on the penetration of nitrogen. The work of Grozier et al (1965) indicated that under conditions of nitrogen supersaturation of the ferrite, austenite grows with a platelet (Widmanstätten) morphology, whereas the austenite-ferrite interface is smooth when growth is controlled by nitrogen diffusion through austenite. The work of Pavlick et al (1966) can also be interpreted to support this. Fong and Glover (1975) independently investigated a similar system. At internal ferrite grain boundaries, austenite allotriomorphs, idiomorphs and primary sideplates were seen, (following the Dubé (1958) morphological classification), growth occurring usually only on one side of the boundary. Crystallographic data was obtained from electron diffraction patterns, and a Kurdjumov-Sachs (KS) orientation relationship,

$$\{111\}_\gamma \| \{110\}_\alpha \; ; \langle 1\bar{1}0\rangle_\gamma \| \langle 1\bar{1}1\rangle_\alpha$$

between austenite and ferrite was often found. In particular, the primary sideplates were found to be within 10° of KS with ferrite on both sides of the boundary, while allotriomorphs were KS with the grain into which they were not growing. Nemoto (1973) observed that a curved austenite-ferrite interface migrated much more rapidly than a planar interface, and also observed the passage of ledges across a planar

interface, in situ in a high voltage electron microscope.

Thus the morphology and growth mechanism of austenite seem to follow the same pattern as that shown by proeutectoid ferrite. Widmanstätten sideplates and other planar interfaces have been observed only when there is a definite orientation relationship between the phases, the interfaces being low energy boundaries which grow by the passage of ledges. Curved boundaries are thought to move by diffusional transfer of atoms across the interface.

The similarity between austenite growth and growth of proeutectoid ferrite breaks down if the starting structure for austenitisation is either martensitic or contains carbides, as is the case in most steels. For instance, the austenite grains may tend to take the shape of martensite laths (eg. Nehrenberg 1950), and carbides may act as both a carbon source for the reaction (eg. Hillert et al 1971) and as a barrier to growth (eg. Nemoto 1977). Thus the austenite morphology is largely dictated by the nature of the prior structure.

1.2.3 Reaustenitisation of Ferrite and Spheroidised Carbides

The homogeneous distribution of spheroidised carbides in ferrite, formed by tempering martensite or annealing pearlite, is one of the simpler steel microstructures, and as such has been the starting structure for several investigations of reaustenitisation.

That the transformation to austenite in this system occurs by nucleation and growth has long been known. Roberts and Mehl (1943) showed that both the nucleation and the growth of austenite were structure sensitive properties, and that in steels containing spheroidised cementite, nucleation occurred at a cementite-ferrite interface in a ferrite grain boundary. Growth was then accompanied by the dissolution of cementite, either in ferrite or austenite, depending on the carbon content of the steel.

A model for the reaustenitisation of spheroidite in low carbon steels was first developed by Judd and Paxton (1968). The model has a starting structure of identical cementite spheroids in a grain boundary free matrix of ferrite and assumes that the rate controlling process is the diffusion of carbon through austenite, that local equilibrium exists at all interfaces, that each carbide nucleates austenite and is immediately enveloped by austenite, and that carbon diffusion through

ferrite does not affect the reaction. The model is able to predict the rate of austenite growth and of cementite dissolution, and good correlation with experimental results for a pure iron-carbon system was obtained. However, the model is limited in that it cannot take account of grain boundary nucleated austenite (the most likely nucleation event), or carbon diffusion through ferrite as the rate controlling factor, which will be important for many carbide distributions. Hillert et al (1971) developed a more general model, in which different reaction types are proposed for different carbide distributions. The rate controlling factor is taken to be the diffusion of carbon through austenite or ferrite, and local equilibrium is assumed. The validity of these assumptions is supported by good agreement between calculated growth characteristics and experimental results for several systems. The treatment was extended to include the effect of substitutional alloying elements on the diffusion of carbon, and again some fairly good agreement with experimental data was obtained.

During reaustenitisation of a spheroidised steel, the carbides must dissolve, and the carbon must be redistributed between the ferrite and the austenite. Several investigations of carbide dissolution have been carried out. Speich and Szirmae (1969) observed the formation of an austenite shell around a carbide particle soon after nucleation, as suggested by Judd and Paxton (1968), showing that some carbide dissolution must occur in the austenite. Molinder (1956) studied the dissolution of cementite during reaustenitisation of a hypereutectoid steel. The ferrite transformed rapidly to austenite, followed by much slower dissolution of carbides in the austenite. The activation energy for dissolution was found to be higher than that expected for carbon diffusion control, which led Molinder to conclude that dissolution was controlled by a slow interface reaction. However, as Judd and Paxton (1968) point out, Molinder does not take into account the effect of alloying elements (Si, Mn and Cr) on boundary conditions for carbon diffusion, rendering the result inconclusive. Judd and Paxton (1968) and Hillert et al (1971) showed that dissolution of cementite in austenite was in fact controlled by carbon diffusion through austenite, and Hillert also showed that dissolution in ferrite was controlled by carbon diffusion through ferrite.

Nemoto (1973,1974,1977) was able to observe directly the dissolution of cementite using a high voltage transmission electron

microscope. Cementite dissolution in either austenite or ferrite was accompanied by the production of dislocations to relieve the strain arising from the volume difference between cementite and the matrix. During reaustenitisation, mobile austenite-ferrite interfaces are attracted to cementite particles in the ferrite, due to the higher carbon concentrations in the vicinity of the dissolving particles. The cementite dissolution rate increases markedly when an interface is in contact with the particle, and dissolution continues in the austenite after the interface has passed.

The morphology of austenite formed from spheroidite is generally equiaxed with curved interfaces, following the shape of carbon diffusion fields from dissolving cementite particles, or prior ferrite grain shapes. Non-equiaxed austenite growth was observed by Judd and Paxton (1968) in a coarse grained low carbon Fe-C alloy. They suggest that growth into ferrite supersaturated with carbon (due to a long nucleation incubation time) causes the observed platelet morphology.

Rose and Strassburg (1956) illustrated the sequence of events during reaustenitisation of a ferrite-spheroidite structure with time-temperature-transformation diagrams. In general, ferrite transforms rapidly to austenite, followed more slowly by the dissolution of cementite, a finer cementite distribution giving more rapid reactions.

1.2.4 Reaustenitisation of Ferrite-Pearlite

Early investigations of reaustenitisation in high carbon pearlitic steels established that nucleation occurs at a carbide ferrite interface, and that the most likely nucleation sites are in grain boundaries, at pearlite colony boundaries or at pearlite-ferrite interfaces. Bayertz (1942) and Roberts and Mehl (1943) observed that in high carbon steels the cementite lamellae do not disappear on passage of the austenite interface through pearlite, and that residual carbides and pearlite "ghosts" are present in the austenite for a long time. Roberts and Mehl (1943) also maintain that carbon concentration gradients remain in the austenite for some time, although this seems unlikely once the carbides have dissolved. (The variation in hardness they observed can be better attributed to an inhomogeneous distribution of substitutional alloying elements.) Digges and Rosenberg (1943) observed that austenite growth occurred predominantly along the lamellae rather than across them, as did Speich and Szirmae (1969), who noted that the austenite

interface was bowed between the cementite lamellae. Nemoto (1977) followed the growth of austenite through pearlite in situ in a high voltage electron microscope, and concluded that the cementite lamellae act as a barrier to growth as well as a source of carbon.

The rate of austenite growth has been reported to increase with decrease in pearlite interlamellar spacing (Roberts and Mehl 1943), while the austenite grain size decreases with a decrease in pearlite colony size (Bayertz 1942). A model for the growth of austenite in pearlite in steels of near eutectoid composition was developed by Speich and Szirmae (1969), along similar lines to models describing pearlite growth. For a hypereutectoid steel, assuming incomplete cementite dissolution, and that carbon diffusion is rate controlling, the experimental results were in fair agreement with the theory, although the observed growth rates were rather low.

Rose and Strassburg (1956) report that in a low carbon steel, the pearlitic regions transform rapidly, and the cementite dissolves quickly. The rate of transformation then decreases, as redistribution of carbon in the austenite to the interface allows more ferrite to transform. The same authors also present TTT curves for the reaction.

1.2.5 Reaustenitisation of Martensite and Bainite

The formation of austenite from martensite or bainite is complicated by the high number of effective grain boundaries (lath boundaries) which act as nucleation sites, as paths of easy diffusion, and also as barriers to growth (eg. Nehrenberg 1950). Further complications arise due to the crystallographic relationships between adjacent ferrite laths, and the possibility of the presence of carbide precipitates. Much of previous work has concentrated on the relation between the new austenite grain size and the prior austenite grain size. Whereas the austenitising conditions for attaining fine austenite grain size are fairly well documented, the underlying reasons for the behaviour are not. An attempt will be made here to rationalise the available data on reaustenitisation of martensite.

That austenite grows in martensite both in acicular (referring to two-dimensional sections) and equiaxed morphologies, has long been known. The proportions of the two morphologies and their effect on the final austenite grain size have been found to depend markedly on austenitising conditions such as time, temperature and heating rate.

Nehrenberg (1950) first suggested that the acicular nature of the austenite was simply due to the martensite lath boundaries acting as barriers to growth; thus the austenite took up the shape of the martensite laths. There have been some suggestions (Matsuda and Okamura 1974, Sadovskiy et al 1962) that acicular austenite forms by a shear mechanism, but no evidence in support of this has been reported. The acicular austenite has, however, been found to obey the Kurdjumov-Sachs orientation relationship with the surrounding ferrite (Matsuda and Okamura 1974, Watanabe and Kunitake 1976, D'Yachenko and Fedorov 1963) and in some cases it has been shown that austenite needles in any one prior austenite grain have an identical crystallographic relationship to that prior grain (eg. Watanabe and Kunitake 1976). Plitcha and Aaronson (1974) have shown that an austenite needle is in fact an allotriomorph which nucleated at a lath boundary; subsequent growth into both laths occurs. Because of the crystallographic relationship between adjacent laths and between the prior austenite and the laths, it is possible that one particular orientation of austenite (that of the prior austenite), and its twin related orientation, will be favourable, and that all nuclei of austenite will be in these orientations (Watanabe 1976b).

Austenite which forms at prior austenite grain boundaries is always equiaxed, and this morphology also sometimes forms at grain interiors. In order to explain the occurrence of intragranular equiaxed austenite, it is first necessary to examine the conditions under which the two austenite morphologies, acicular and equiaxed, form.

In the early stages of growth of austenite, the formation of acicular (rather than equiaxed) austenite is favoured by a low austenititising temperature (Matsuda and Okamura 1976, Watanabe and Kunitake 1976), by a slow heating rate (Matsuda and Okamura 1974, Kinoshita and Ueda 1974), by the presence of carbides in the lath boundaries (Watanabe and Kunitake 1976, Homma 1974) and by the presence of austenite stabilising alloying elements such as Ni or Mn (Plitcha and Aaronson 1974). This behaviour can be explained in terms of dominance of nucleation over growth, assuming that the lath boundaries act as barriers to growth. Fine carbides are likely to precipitate on lath boundaries during heating to the austenitisation temperature, and these may pin the austenite interface at lath boundaries. At low temperatures and low heating rates, the occurrence of acicular austenite can be explained on the grounds that the driving force available is not

sufficient to allow the austenite to grow past ferrite lath boundaries, although many nucleation events occur. Carbides in the boundaries provide many favourable nucleation sites, and the addition of austenite stabilising elements incraeses the driving force for austenitisation and so also enhances nucleation.

Thus equiaxed austenite may form in several ways. Firstly, if the driving force for growth is high, for instance at high temperatures, the austenite may be able to grow past the restraining ferrite lath boundaries. Secondly, the martensite lath boundaries themselves may migrate into lower energy configurations, eliminationg many boundaries and reducing the acicularity of the ferrite, thus allowing equiaxed austenite growth. Austenite nucleation on a lath boundary prevents easy migration of that boundary; conversely a low nucleation rate will leave many boundaries free to migrate and equiaxed austenite forms (Plitcha and Aaronson 1974). Thirdly, equiaxed austenite may form during the later stages of the reaction or at higher temperatures, by coalescence of the original needles (eg. Watanabe and Okamura 1974).

The development of the final austenite grain size will now be considered. Austenite which begins to grow under conditions favouring the formation of acicular austenite, ie nucleation dominated, will not allow recrystallisation of the martensite lattice. All austenite nuclei which form at lath boundaries (in one prior austenite grain) will therefore be in the same (or twin related) orientation (Watanabe and Kunitake 1976b). During further growth the needles coalesce, forming one large austenite grain (of similar size to the prior austenite grain), which contains many low angle sub-boundaries corresponding to the initial needle boundaries. The orientation of the new austenite which forms at the prior austenite grain boundaries is, however, not controlled by the orientation of adjacent laths, but by the orientations of the two prior austenite grains at the boundary. The grain boundary austenite may therefore be in a different orientation from, and will remain separate from, the matrix austenite. The resulting austenite structure is thus coarse grained with some fine grains at prior austenite boundaries.

In the other case, in which the nucleation rate is slow enough to allow martensite recrystallisation and lath boundary migration, the austenite nuclei may all have different orientations. Growth of these will then produce an austenite structure which has a considerably finer

grain size than the prior austenite.

The two structures, coarse and fine grained, will behave differently on continued heating. On passing a critical temperature (the recrystallisation or breakaway temperature, or Chernov b point) the coarse grained austenite undergoes recrystallisation, which is enhanced by the presence of sub-grain boundaries, and will become fine grained (D'Yachenko and Fedorov 1963). Grain growth may follow. The structure which is initially fine grained may exhibit abnormal grain growth below the recrystallisation temperature, particularly if the grain size distribution is inhomogeneous (following Sheard and Nutting 1979). Above the recrystallisation temperature, rapid grain growth can occur, although it may be inhibited by the presence of carbides on grain boundaries (Bayertz 1942).

To summarise, austenitising conditions favouring nucleation rather than growth result in many austenite nuclei, which are identically oriented in any one prior austenite grain. Growth and coalescence leads to a final grain size similar to the prior austenite grain size, apart from fine grains at the prior austenite grain boundaries. Grain refinement occurs by recrystallisation above a critical temperature. Austenitising conditions which inhibit nucleation allow substantial recrystallisation of the martensite before austenite nucleates, leading to fine grained austenite. Continued heating may cause grain growth.

Thus, if the heating rate or the austenitising temperature are low, if there are carbides in the lath boundaries, or if austenite stabilising alloying elements are present, the steel must be heated above the recrystallisation temperature to achieve a fine grain size. If austenite forms at high temperatures and heating rates, the steel must be kept below the recrystallisation temperature to retain the fine grain size which forms initially.

1.2.6 Grain Growth

The final austenite grain size obtained on reaustenitising depends both on the initial structure and on the austenitising conditions, as noted in the preceding section. In some steels, austenite grain growth is a particular problem.

Sheard and Nutting (1980) demonstrated that abnormal grain growth is likely to occur if the initial austenite grain size is highly

inhomogeneous, for instance during reaustenitisation of spheroidised pearlite, leading to very coarse austenite grains. Similar abnormal grain growth has been reported during reaustenitisation of other steels, for instance in a high speed steel (Kula and Cohen 1954), a vanadium steel (Webster and Allen 1962) and a Ni-Cr-Mo-V steel (Homma 1974). Abnormal grain growth was found to occur because of dissolving carbides at the austenite boundaries. Grain boundaries without carbides migrate rapidly at the expense of grain boundaries containing still undissolved carbides, leading initially to an inhomogeneous grain size, and after abnormal grain growth, to very coarse austenite grains.

1.2.7 Grain Refinement by Reaustenitisation

It is possible that grain refinement in steels may be accomplished by repeated transformations to austenite and then to ferrite. The importance of a fine ferrite grain size in ferritic steels is well known, and Grange (1966) has shown that an ultrafine prior austenite grain size leads to improved properties in many martensitic steels.

Cyclic reaustenitisation in martensitic steels can only produce grain refinement if the austenitising conditions are such that many austenite grains form in each prior austenite grain. The conditions were discussed in section 1.2.5. Cyclic rapid reaustenitisation and quenching has been investigated by Grange (1966,1971), Mahajan (1973) and Chraska and Dubsky (1979). Markedly improved mechanical properties were observed after the first cycle, and improvements continued until a critical number of cycles (usually four), after which the austenite grain size and mechanical properties of the martensite remained the same. Austenite grain sizes of a few microns were obtained, the size limiting factor being the instability of ultrafine grains.

Karlsson (1973) reports that cyclic reaustenitisation and normalising gives considerable refinement of ferrite grain size. He notes that the grain refinement which occurs during the austenite to ferrite transformation affects the mechanical properties more than that which occurs during reaustenitisation. Again, the most marked refinement occurs during the first cycle, and little change is seen after about three cycles.

Law (1977) investigated heat treatment cycles consisting of reaustenitisation and isothermal transformation to ferrite in a vanadium steel. Again, the ferrite grain size was refined, and the mechanical

properties improved, with each cycle up to about four cycles.

Thus it has been shown that rapid reaustenitisation is a means to refine grain size and improve mechanical properties in many ferritic or martensitic steels, particularly if several cycles of heat treatment are employed.

1.2.8 The Effect of Alloying Elements on Reaustenitisation

The effects of alloying elements on reaustenitisation are many and varied. Hillert et al (1971) treated the ternary Fe-C-X diffusion problem theoretically for reaustenitisation of ferrite-spheroidite steels. In general, the addition of small amounts of substitutional alloying elements shift the boundary conditions for carbon diffusion and hence affect the rate of diffusion and the reaction rate. The partitioning of the substitutional alloying element (involving diffusion in one or both phases) between austenite and ferrite has not been considered. Hillert et al (1971) studied reaustenitisation of a hypereutectoid Cr steel in the two phase austenite-cementite region, and concluded that the late stages of the reaction were controlled by Cr diffusion.

Many substitutional elements slow down the austenite reaction by solute drag at the interface, eg. Mn (Judd and Paxton 1968). Other effects of manganese, a common alloying element in steels, have been reported. Nemoto (1977) noted that manganese partitions preferentially to cementite during a spheroidisation treatment, and that during subsequent reaustenitisation, dissolution of cementite in ferrite is largely prevented by the manganese, while dissolution in austenite is unaffected. Fong and Glover (1975) noticed that the austenite interface is pinned by manganese nitrides during nitriding, and Pavlick et al (1966) reported similar effects with other nitride forming elements. Similarly, alloying elements which form carbides have a marked effect on reaustenitisation of carbon steels (eg. Webster and Allen 1962).

Plitcha and Aaronson reported that austenite stabilising elements, such as Ni, significantly increase the austenite nucleation rate, presumably due to the increased driving force.

Some alloying elements are known to inhibit austenite grain growth under certain conditions, for instance aluminium and silicon (Bayertz 1942) and vanadium (Webster and Allen 1962).

The reaustenitisation of a ferritic steel containing fine vanadium carbides was investigated by Law and Edmonds (1980). The carbides were found to dissolve during reaustenitisation and to reprecipitate in the austenite with a more favourable austenite-carbide orientation relationship. The dissolution of alloy carbides has been shown to be responsible for abnormal grain growth in some steels (Kula and Cohen 1954, Webster and Allen 1962).

In summary, during reaustenitisation, alloying elements affect the diffusion of carbon, the equilibrium compositions and proportions of the phases, the driving force of the reaction, and the migration of the austenite-ferrite interface, both by solute drag and by pinning with alloy carbides.

1.3 Dual Phase Steels

Reaustenitisation is an important step in the formation of many dual phase steels. These steels are generally low carbon, low alloy steels, which have been heat treated to give a microstructure of ferrite and martensite, the heat treatment usually consisting of partial reaustenitisation (during an intercritical anneal) followed by quenching. In recent years, the improved properties of dual phase steels have stimulated interest in this field and in that of reaustenitisation.

1.3.1 Development of Dual Phase Steels

The development of high strength, low cost, formable steels has been encouraged by automobile fuel consumption requirements stipulated by recent USA laws, as fuel consumption can be reduced by weight reduction of automobile parts. Weight reductions in parts traditionally made from mild steel sheet can be achieved by using thinner sections of higher strength materials.

Conventional higher strength steels are either expensive, eg. higher alloy steels, or have poor formability, eg. HSLA controlled rolled steels. Low alloy dual phase ferrite-martensite steels, while being as strong as conventional HSLA steels, have a lower yield stress and a higher work hardening rate, leading to improved formability.

The first attempts at making steels with composite microstructures were those of Cairns and Charles (1967a,b), who investigated the

formation and properties of fibrous martensite-ferrite structures. The microstructures were not easily reproducible, and the properties no better than those of conventional steels.

Early development of commercially useful dual phase steels was carried out by Hayami and Furukawa (1977) in Japan, who produced dual phase steels containing 10-30% hard phase, by intercritically annealing rolled sheet (ie. annealing in the two phase ferrite plus austenite temperature range) followed by air cooling. A typical alloy composition, giving good strength and ductility, was found to be Fe-0.1%C-1.4%Si-1.6%Mn.

Bailey (1976) and Bailey et al (1979) produced similar properties by intercritical annealing and water quenching cold rolled sheet of typical composition Fe-0.11%C-0.5%Mn. Water quenched steels were also developed in Japan eg. by Araki et al (1977a), while air hardenable steels, which are commercially more useful, were developed in the USA by Rashid (1976) (containing 1.5%Mn, 0.5%Si and some V) and Morrow (1978) (containing Mo and possibly V). Other developments included V steels, eg. Butler and Bucher (1979), Davies (1978a) and Si steels eg. Koo and Thomas (1977).

1.3.2 Mechanical Properties

Dual phase steels generally have a lower yield stress, a higher initial work hardening rate, and a greater total elongation than conventional HSLA steels of the same tensile strength (eg. Rashid 1976). Dual phase steels also yield continuously (eg. Davies 1978,1979), eliminating stretcher strains, which arise during the forming of many steels. In addition, the formability of dual phase steels is superior to that of conventional HSLA steels (Rashid 1976).

Tensile failure of dual phase steels is initiated by the separation of the ferrite-martensite interface, or by fracture of the martensite islands (Stevenson 1977), followed by extension of these microcracks into voids, and subsequent void coalescence. The best tensile properties are obtained when the martensite islands are unconnected (Kunio et al 1975) (minimising the propagation of microcracks), when the martensite-ferrite interface is free from crack initiators such as precipitates (Koo and Thomas 1979), and when the hard phase itself is relatively tough, eg. when the hard phase is low carbon martensite (Koo and Thomas 1979), tempered martensite, or bainite (Owen 1980).

The fatigue properties of dual phase steels have been found to be little different from those of conventional steels (Davies 1978a), and can be understood in terms of high work hardening rate (Sherman and Davies 1979).

1.3.3 Theoretical Aspects of the Deformation of Dual Phase Steels

The simplest theory describing the deformation of two ductile phases is that due to Mileiko (1969) and is essentially a law of mixtures, assuming equal strain in both phases. Davies (1978, 1979a) has reported good experimental agreement with this theory. The law of mixtures has been modified by Lagneborg (1979) and Araki et al (1977) who introduced an effective strain difference between the phases, and found good experimental agreement for hard phase volume fractions of less than 20%. Tomota et al (1976) developed a more general theory, taking into account internal stresses produced by inhomogenous strain distributions. Bhadeshia and Edmonds (1980) showed that Tomota's theory is generally able to describe the experimental behaviour of many dual phase steels.

Another approach is taken by Karlsson and Sundström (1974), who employ continuum mechanics to analyse the mechanical behaviour of dual phase steels, while Owen (1980) suggests that the deformation of dual phase steels can best be described by the application of Ashby's (1966) model of work hardening in dispersion strengthened systems.

1.3.4 Microstructure-Property Relationships

a) Formation of microstructure

Dual phase steels may be formed either by controlled cooling from austenite, allowing the formation of some ferrite (Davies 1978a), or by intercritical annealing of ferrite followed by quenching. The formation of dual phase steels by controlled cooling results in unconnected islands of martensite (or other hard phase) in ferrite. Kunio et al (1975) have shown that unconnected martensite leads to good ductility, but unfortunately the formation of reproducible microstructures by controlled cooling is difficult.

Most dual phase steels have therefore been made by intercritical annealing. Southwick (1980) has shown that the volume fraction of hard phase formed by intercritical annealing and air cooling of a commercial steel, is almost independent of the annealing temperature. This is due

to the increased austenite volume fraction being balanced by decreased hardenability as the annealing temperature is raised.

Varying volume fractions of hard phase are obtained by water quenching rather than air cooling. The yield stress, the ultimate tensile strength and the elongation have all been found to vary linearly with the volume fraction of hard phase (eg. Butler and Bucher 1979), the optimum volume fraction of hard phase being about 20%.

Unconnected islands of hard phase are obtainable by intercritical annealing when the starting structure is martensite, and Koo and Thomas (1977) have suggested that this may produce the optimum dual phase microstructure.

b) Strength and Composition of the Ferrite

The strength and superior properties of dual phase steels have been attributed to their fine ferrite grain size, obtained by intercritical annealing of rolled sheet (eg. Davies 1978c, Tamura et al 1973). The ferrite grain size is now not thought to be the overriding strength factor (Owen 1980). Koo and Thomas (1979) have suggested that the overall properties can be improved by substitutional solid solution strengtheners, such as silicon, in the ferrite.

c) Strength and Composition of the Hard Phase

Davies (1978c) holds that the strength and composition of the hard phase are not important in determining the mechanical behaviour, but Speich and Miller (1979) and Araki et al (1977b) have shown that this is not the case, and that the overall strength increases with increasing strength of the hard phase. The martensite can be strengthened by increasing the carbon content of the alloy, and thus of the martensite, but Koo and Thomas (1979) have shown that this reduces the overall toughness, due to increased brittleness of the martensite. They indicate that the carbon content of the martensite should be less than 0.3%, and thus that the alloy carbon content should be less than 0.1%.

d) Summary - Design of Dual Phase Steels

An optimum dual phase steel should contain about 20% martensite containing less than 0.3% C, and should have a fine ferrite grain size and solid solution strengthened ferrite, a good ferrite-martensite interface unbroken by precipitates, a fine distribution of unconnected martensite islands, and air hardenability. These characteristics can be obtained for example, by intercritical annealing of martensite in an

alloy containing less than 0.1%C, up to 2%Si, and possibly up to 1.5%Mn (Koò et al 1979).

The advantage of such a steel over conventional steels is its unique combination of high strength, good formability, ease of production and low cost.

CHAPTER TWO

REAUSTENITISATION OF FERRITE AND SPHEROIDISED CARBIDES

2.1 Introduction

A number of workers have investigated the reaustenitisation of ferrite containing spheroidised carbides (see chapter 1, section 1.2.3) and have established that the process is one of nucleation and growth, that nucleation occurs at carbides in ferrite grain boundaries, that carbides dissolve both in ferrite and austenite, that the rate controlling factor of the formation of austenite is the diffusion of carbon to the interface through ferrite or austenite, and that local equilibrium exists at all interfaces.

The present work was carried out with several purposes in mind, namely:

a) To study the reaustenitisation reaction specifically in the two phase ferrite plus austenite region, as this reaction may be relevant to the production of dual phase steels by intercritical annealing.

b) To study the austenite morphology and the austenite-ferrite interfaces and crystallography, using transmission electron microscopy.

c) To compare the effects on reaustenitisation characteristics of different initial ferrite grain sizes and carbide distributions within the same steel.

Section 2.2 outlines the experimental procedures. Three carbide distributions were prepared for reaustenitisation, the first having most of its carbides away from ferrite grain boundaries, the second having most of its carbides situated in grain boundaries, and the third having roughly equal proportions of free carbides and grain boundary carbides. Reaustenitisation of the three distributions is described in sections 2.3, 2.4 and 2.5 respectively. The concept of interfacial stability is then considered, and applied to the present system (section 2.6). The work is summarised in section 2.7.

2.2 Alloys and Heat Treatment

The basic alloy used in this work had a nominal composition of Fe-0.2%C (compositions are given in weight percent, and the exact analysis of this alloy, A, is given in Appendix A1). In a plain Fe-C alloy, carbides are unstable at all temperatures above the eutectoid temperature; reaustenitisation of this basic alloy was therefore always accompanied by carbide dissolution. A similar alloy, to which 2%Ni had been added to improve hardenability (alloy B, Appendix A1) was also used, and reaustenitisation was again carried out at temperatures at which carbides are unstable.

The ferrite-spheroidite starting structures were prepared from martensite by deforming and tempering. Three microstructures were obtained, in which the grain size and the carbide size, and hence the proportion of carbides in the grain boundaries, varied. The specimens for reaustenitisation were in the form of 0.5mm strip and heat treatments were carried out in a bath of molten tin. Reaustenitisation treatments consisted of a hold time of 3s to one hour, at a temperature in the two phase ferrite plus austenite region, such that partial reaustenitisation occurred. The specimens were then iced-brine quenched, to transform the austenite to martensite. In the Fe-C alloy the formation of a fine ferrite-carbide mixture at the austenite-ferrite interface during the quench could not be prevented, and it was thus not possible to relate the interface at low temperature to the austenite-ferrite interface which had existed at high temperature. The alloy containing nickel was therefore prepared; in this alloy the austenite transformed completely to martensite. Reaustenitisation treatments were carried out on both alloys, and qualitatively the reactions were similar. For detailed studies and quantitative work, the alloy containing nickel was used.

The microstructures after heat treatment were observed by optical and transmission electron microscopy, and a Quantimet image analyser was used to measure the degree of transformation.

2.3 Reaustenitisation of Coarse Grained Ferrite containing Fine Carbides

In order to obtain a microstructure in which only a small porportion of the carbides was located in grain boundaries (most of the carbides being in ferrite grain interiors) a quenched sample of the Fe-0.2%C alloy was tempered at 650°C for twenty-three hours. A microstructure of coarse grained ferrite (grain size of the order of 100 μm) and relatively fine spheroidal cementite particles (about 2μm in diameter) resulted, and the scale of the structure can be seen in Fig. 2.1.

The microstructure was not readily reproducible because of uneven ferrite grain growth, and for this reason, only limited reaustenitisation studies were carried out on this structure.

Specimens were reaustenitised for one minute at a temperature of 740°C (17°C above the Ac_1 temperature) and iced-brine quenched. Nucleation of austenite occurred mostly at carbides in ferrite grain boundaries, as previously reported (eg. Roberts and Mehl 1943). Fig. 2.1 shows several austenite nodules (now transformed to martensite), some of which appear to be intragranular. The austenite shows both curved and planar (facetted) interfaces with the ferrite; facetted interfaces are illustrated more clearly in the grain boundary sawteeth depicted in Fig. 2.2. Widmanstätten sideplates were also occasionally observed; an intragranular Widmanstätten plate is shown in Fig. 2.3.

Carbides were rarely seen in the austenite, although they were sometimes seen in contact with the the advancing austenite interface. Virtually all cementite dissolution must therefore occur either in the ferrite or in the interface, and hence diffusion of carbon to the interface through ferrite, or through the interface itself, must occur.

The rate of nucleation of austenite in this starting structure is low, no doubt due to the low density of grain boundary nucleation sites. The nucleation of austenite at an internal carbide-ferrite interface is rare, despite the abundance of such sites, indicating that the ferrite grain size is the more important factor in determining the nucleation rate.

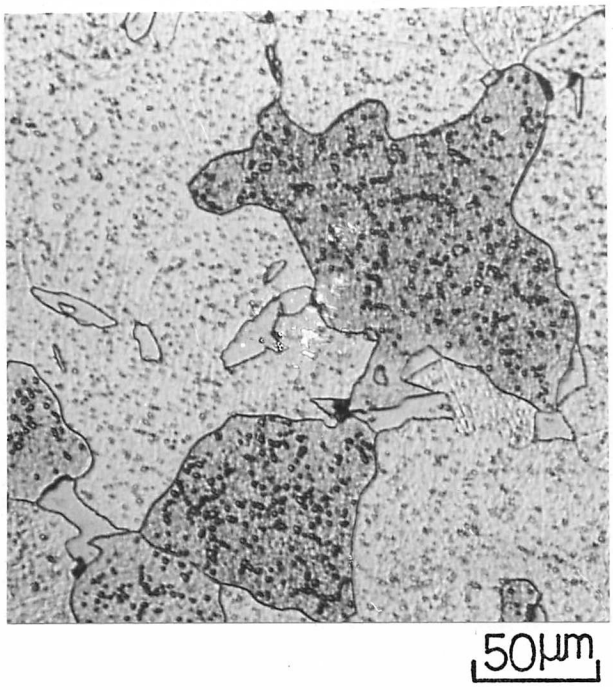

Fig. 2.1: Coarse grained ferrite containing fine spheroidal carbides. Partially reaustenitised 1 minute 740°C and quenched. Austenite (now martensite) appears light etched and bold outlined.

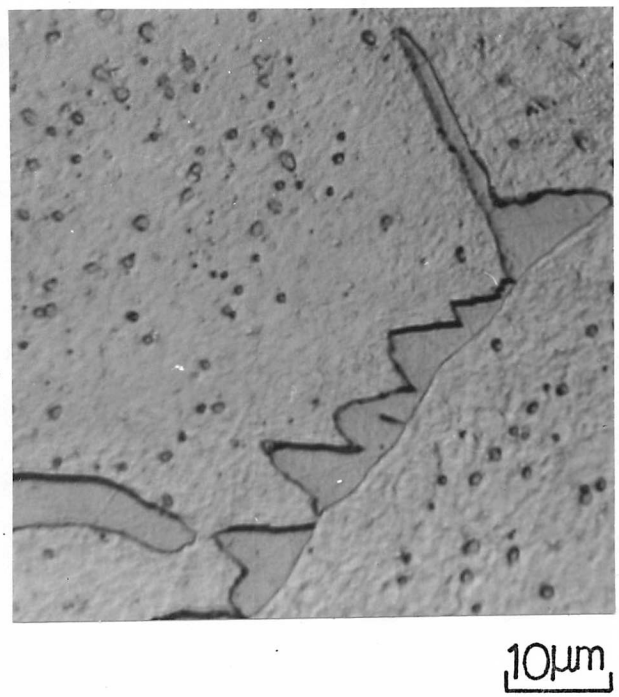

Fig. 2.2: Austenite sawteeth at a ferrite grain boundary. 1 minute 740°C.

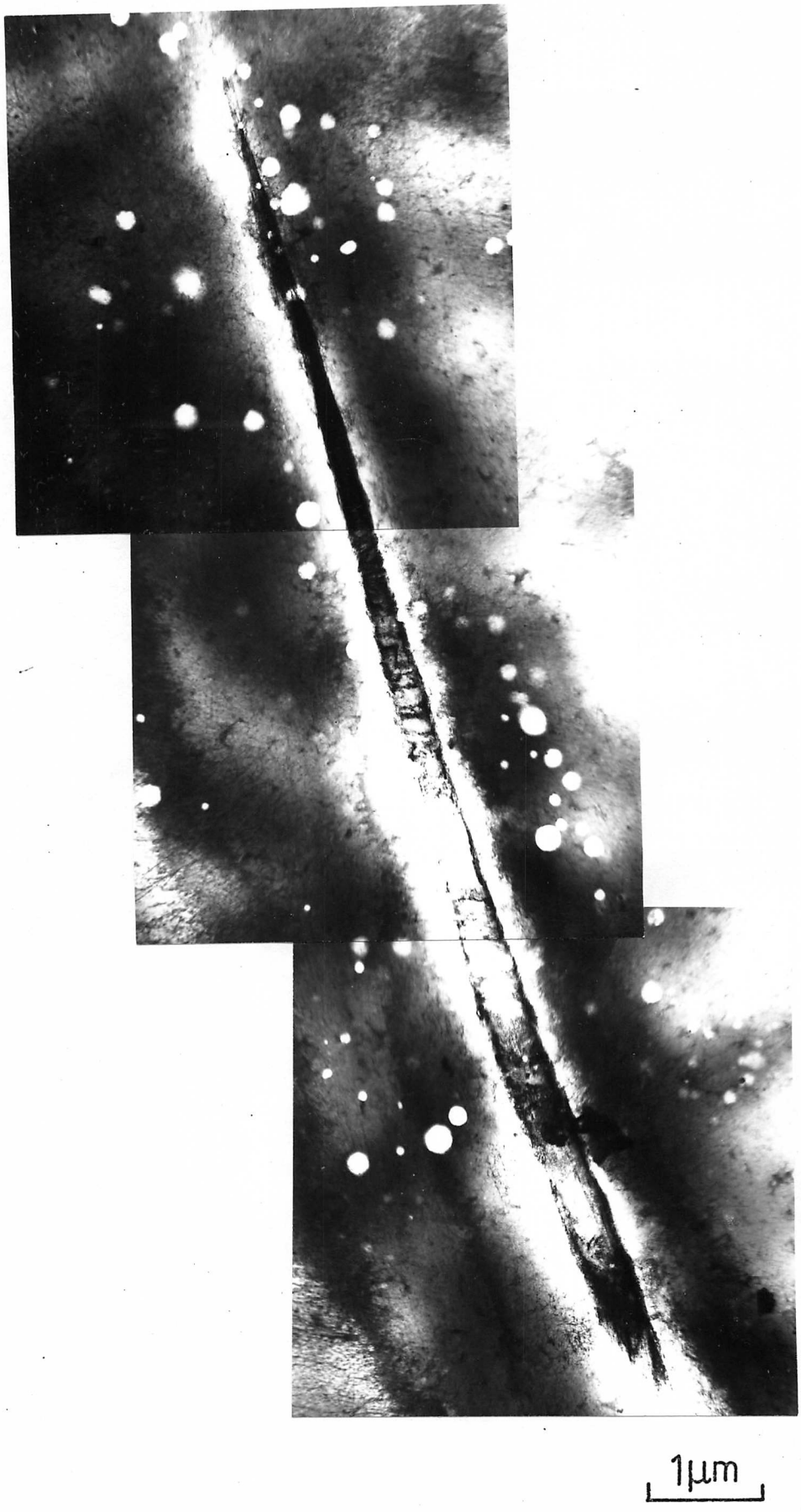

Fig. 2.3: Intragranular Widmanstätten austenite (now martensite) plate. Austenitised 1 minute 740°C.

2.4 Reaustenitisation of Fine Grained Ferrite containing Coarse Carbides

In this starting structure, virtually all the carbides are in grain boundaries. The microstructure was obtained in the Fe-2%Ni-0.2%C alloy by a heat and mechanical treatment consisting of austenitisation at 900°C for 15 minutes, water quenching, tempering at 600°C for one and a half hours, rolling to one quarter of the original thickness, and finally tempering at 600°C for 99 hours. The grain size was of the order of 5μm. The relatively coarse spheroidal carbides were about 1μm in diameter, and were located mostly at ferrite grain corners, as can be seen in Fig. 2.4a.

Reaustenitisation was carried out at 720°C (about 20°C above the eutectoid temperature) and the sequence of the reaction is shown in Fig. 2.4. In the early stages, austenite has nucleated at many carbides, and carbides are observed both in the austenite and in the ferrite. Optical and electron microscopy reveal that, at a later stage, virtually all the carbides have nucleated austenite; there are then carbides in the austenite, but none in the ferrite. Finally, all carbides dissolve.

The austenite morphology is blocky, as shown in Fig. 2.4, and Widmanstätten teeth or plates were never observed. The transformed fraction is plotted as a function of time at 720°C in Fig. 2.6. The transformation rate varies smoothly with time.

Since all carbides nucleate austenite relatively early in the reaction, there are no carbon sources available in the ferrite to feed growing austenite particles. The carbon necessary for the transformation must therefore always come from carbides dissolving within the austenite, leading to a carbon concentration gradient behind the advancing austenite interface. This tends to keep the interface smooth, as growth of any protruberance is unfavourable compared to growth of the bulk interface. Thus, the interfaces are smooth, and follow the carbon diffusion field from the carbide in the austenite; the absence of Widmanstätten sideplates is not surprising.

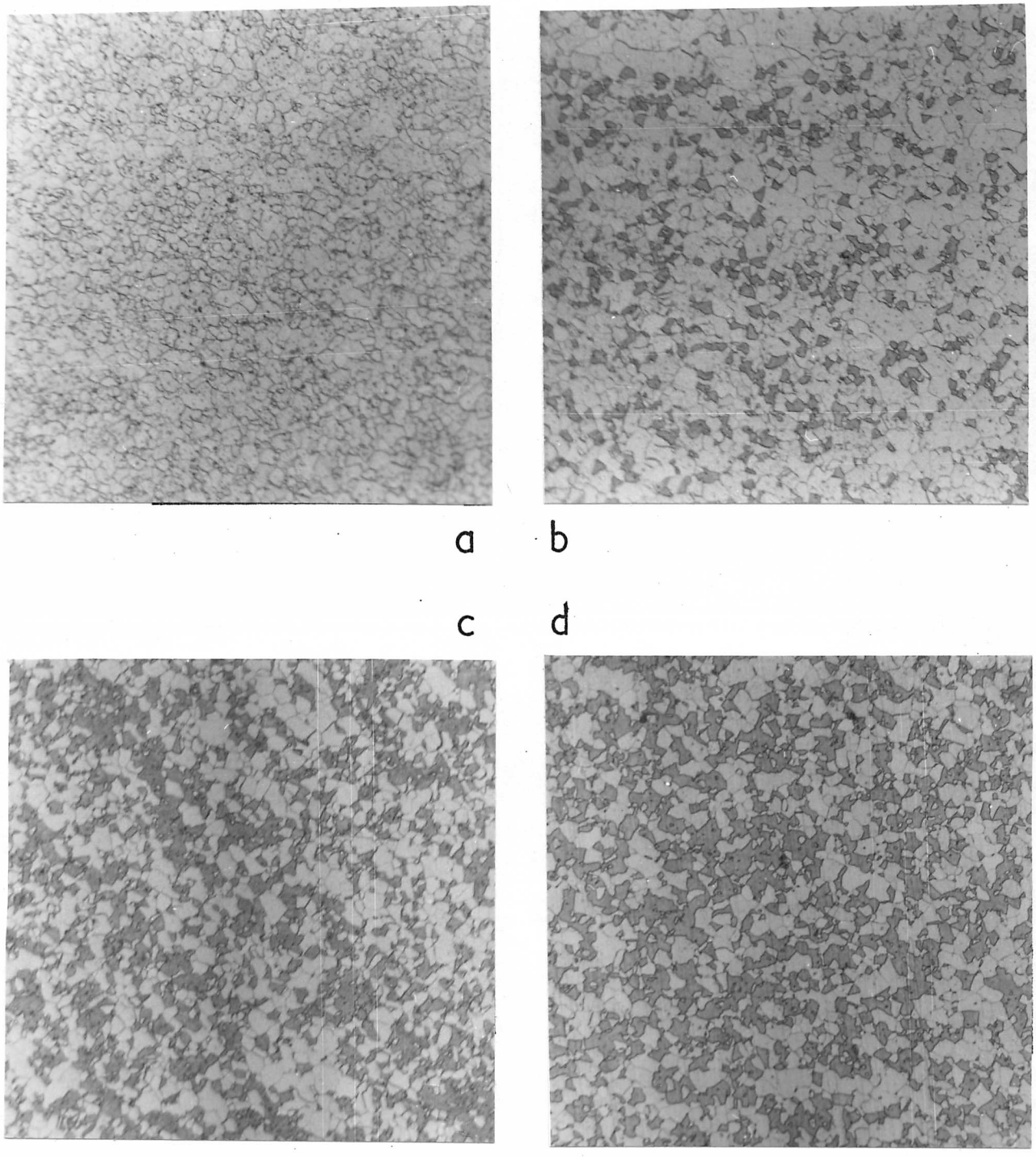

Fig. 2.4: Fine grained ferrite containing coarse spheroidal carbides. Austenite (now martensite) appears dark.

a) Starting structure.
b) Reaustenitised 10s 720°C.
c) Reaustenitised 32s 720°C.
d) Reaustenitised 100s 720°C.

2.5 Reaustenitisation of Fine Grained Ferrite containing Fine Carbides

In this microstructure, the grain size and carbide distribution are such that about half the carbides are in grain boundaries and the others are free in the ferrite, as shown in Fig. 2.5. The ferrite grain size of about 3μm and carbide diameter of a few tenths of a micron were obtained by a method similar to that used to produce the previous starting structure, except that the final temper was for only 2 hours rather than 99 hours.

2.5.1 Metallography

In the optical microscope, the austenite morphology after reaustenitisation at 720°C appears blocky at all times, as shown in the micrographs of Fig. 2.5. However, electron microscopy reveals that, at longer times, smooth interfaces may break down into groups of evenly spaced protrusions or sideplates.

The fraction of austenite as a function of time at 720°C is plotted in Fig. 2.7. The incubation period for nucleation of austenite is seen to be less for this starting structure than for the previous starting structure (see Fig. 2.6), which had a higher proportion of its carbides in grain boundaries, but a coarser grain size. The number of austenite nuclei is therefore seen to depend on the actual number of carbides in grain boundaries, which depends more strongly on the grain size than on the proportion of carbides in boundaries. The coarse grained starting structure (section 2.3) has a much lower nucleation rate than either of the finer grained structures.

Fig. 2.8 shows an austenite nodule, at an early stage of the reaction, associated with several carbides and displaying smooth interfaces. Fig. 2.9 shows perturbations at an austenite-ferrite interface at an intermediate stage. Figs. 2.10a,b and c are examples of fully developed austenite protrusions or sideplates which are exhibited by many interfaces during the later reaction stages.

It should be noted here that the ferrite-martensite interfaces in the micrographs are taken to correspond to the ferrite-austenite interfaces which existed at high temperatures (ie. no significant disruption of the interface has occurred during the quench). This assumption is supported by the observation of different interface types

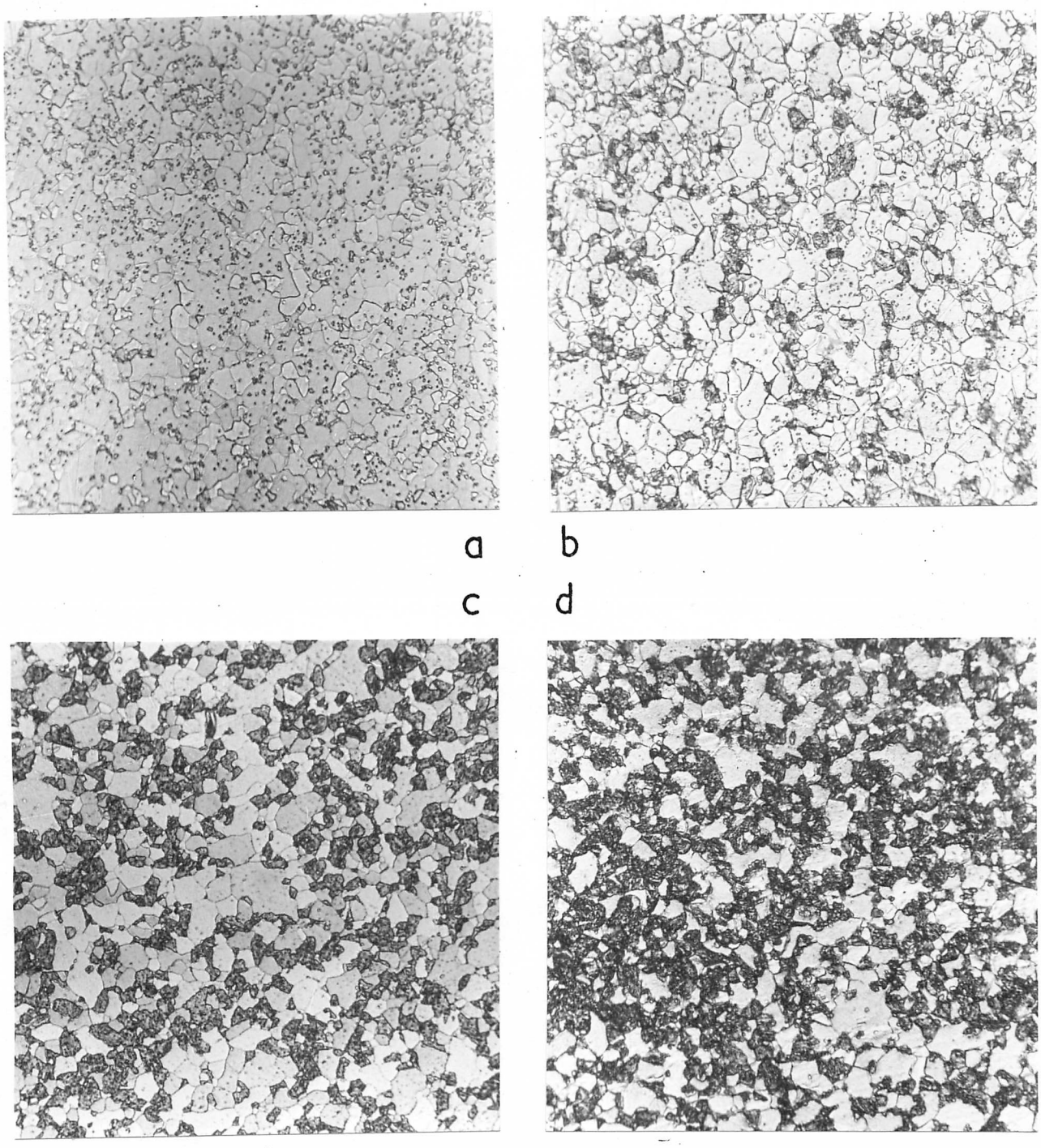

Fig. 2.5: Fine grained ferrite containing fine spheroidal carbides. Austenite (now martensite) appears dark.

a) Starting structure.
b) Reaustenitised 5s 720°C.
c) Reaustenitised 10s 720°C.
d) Reaustenitised 100s 720°C.

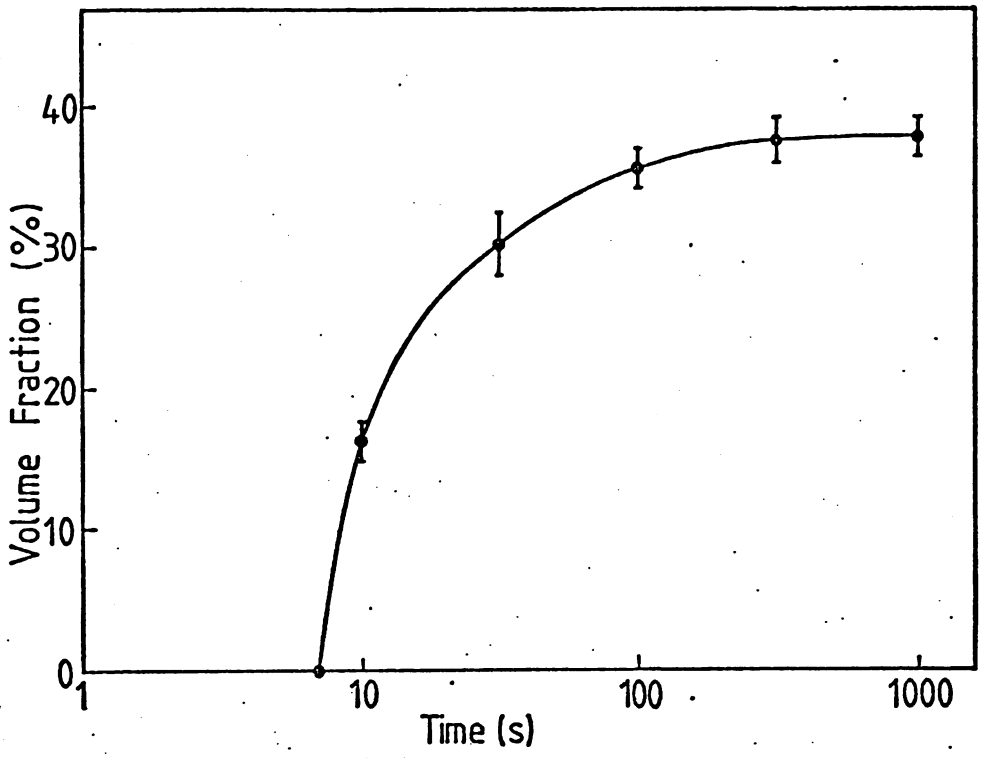

Fig. 2.6: Fine grained ferrite containing coarse carbides, fraction of austenite as a function of time at 720°C.

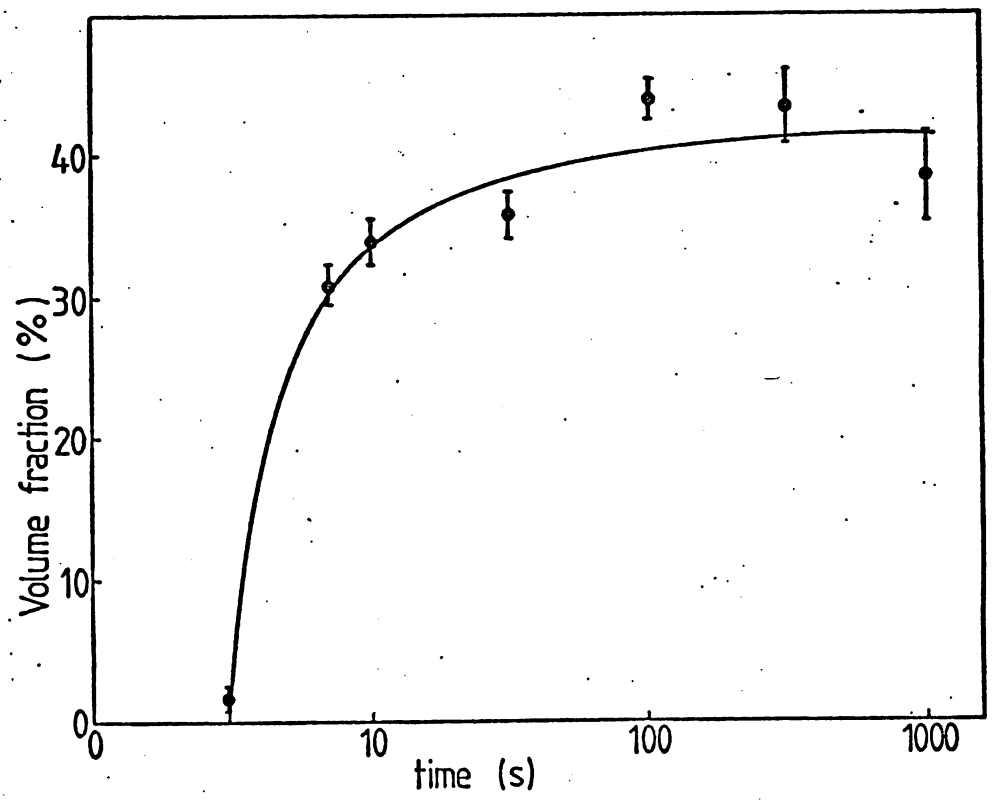

Fig. 2.7: Fine grained ferrite containing fine carbides, fraction of austenite as a function of time at 720°C.

Fig. 2.8: Austenite (now martensite, centre) associated with several rounded cementite particles (top and bottom). Reaustenitised 3s 720°C.

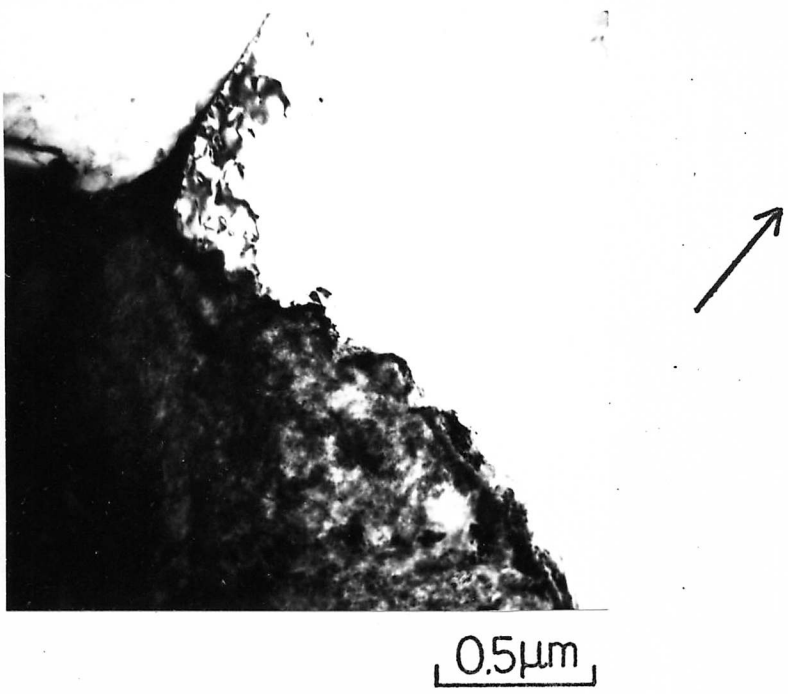

Fig. 2.9: Perturbations at an austenite-ferrite interface. Growth direction marked. Reaustenitised 10s 720°C.

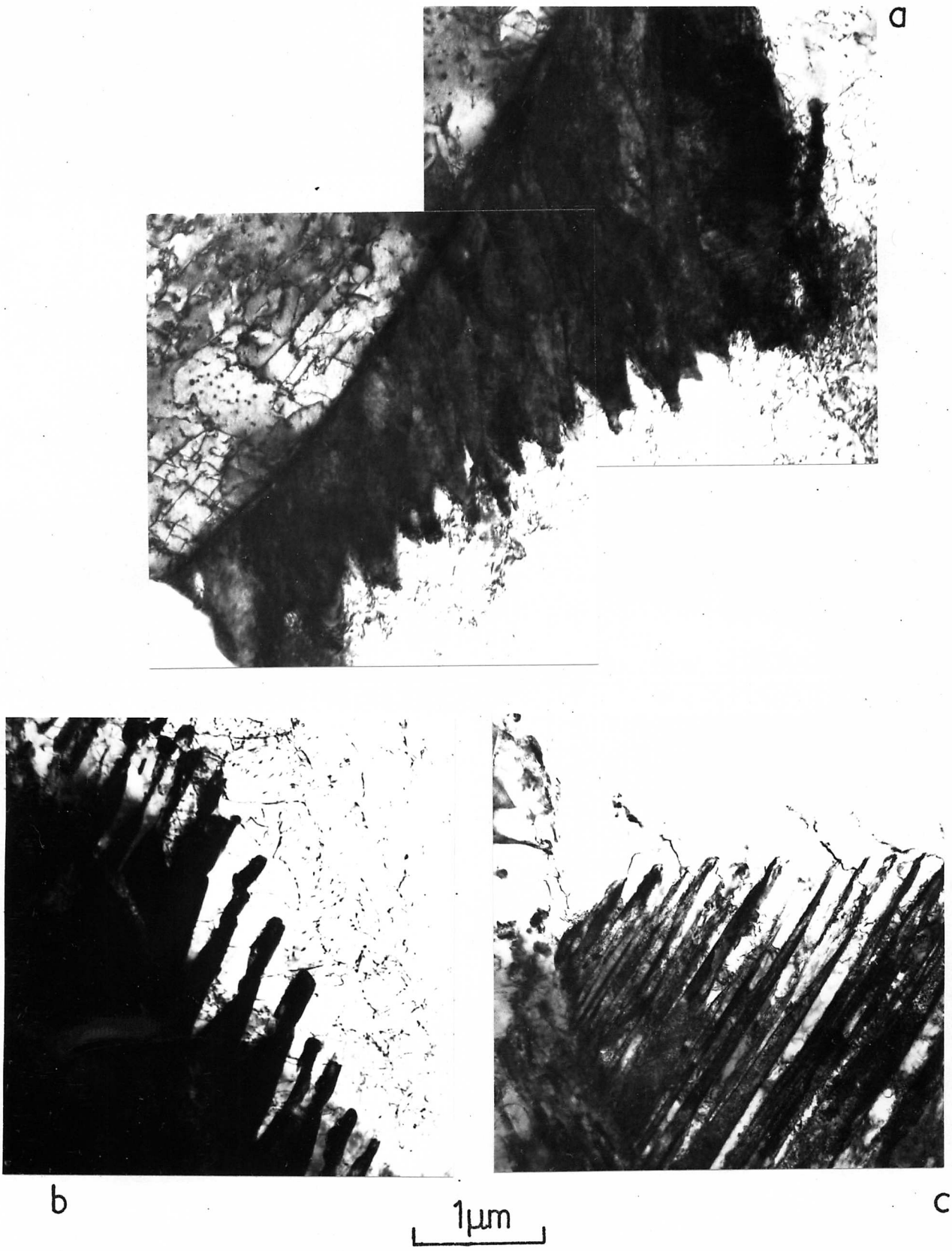

Fig. 2.10: Austenite (now martensite, dark) showing protrusions at an interface with ferrite.
a) Alloy containing Ni, 100s 720°C.
b) Ni-free alloy, 100s 740°C.
c) Ni-free alloy, 100s 740°C.

after different heat treatments. Marked change in contrast and dislocation density in the ferrite was observed in a few cases when interface motion during the quench had obviously occurred. It is therefore concluded that any interface which does not show this contrast change in the ferrite near the interface has not moved during the quench.

The sideplates which occur during the later part of the reaction are always evenly spaced, and the spacing, as measured from electron micrographs, always lies in the range 0.1 to 0.4μm, the average spacing being 0.2μm. As the measurements were made on two-dimensional sections, this figure is likely to be an overestimate of the true spacing.

Initially, carbides both free in the ferrite and associated with austenite are observed. During the reaction, the carbides in contact with austenite disappear first, such that after about 7s the only carbides remaining are those in the ferrite. Perturbations at the interface are first observed at about the same time as carbides in austenite disappear. On the metallographic evidence, it therefore seems reasonable to suggest that the early stages of growth involve carbon diffusion through austenite, and the later stages involve carbon diffusion through ferrite, which leads to interfacial breakdown and the growth of Widmanstätten sideplates. Some kinetic and crystallographic evidence to support this will now be presented. Then, in section 2.6, the breakdown of interfaces in concentration gradients will be theoretically considered, followed by the application of the theory to the present system.

2.5.2 Kinetics

Fig. 2.7 shows the fraction of austenite as a function of time at 720°C. Comparison with Fig. 2.6 shows that the reaction is complete within about 100s for both carbide distributions, and that the starting structure now under consideration leads to a less smooth curve of volume fraction against time. In this structure, the initial reaction rate is high, but falls off rapidly after a few seconds (see Fig. 2.7). The change in reaction rate can be understood in terms of a change in carbon diffusion rate, diffusion occurring through austenite in the early stages, and through ferrite in the later stages. The change in diffusion path is consistent with the observed disappearance of carbides associated with austenite at an intermediate time (about 7 seconds).

The smooth decrease in reaction rate in the starting structure with all its carbides in grain boundaries, Fig. 2.6, is consistent with a reaction occurring always by carbon diffusion through austenite.

2.5.3 Crystallography

If the sideplates are to be termed Widmanstätten, a crystallographic relationship between austenite and ferrite must be shown to exist, such that the plates may adopt broad low energy interfaces.

The austenite-ferrite orientation relationship in low carbon steels has been found to be the Kurdjumov-Sachs (KS) relationship by, for instance, Mehl et al (1933), who studied the relationship between austenite and proeutectoid ferrite. It is expected that the orientation relationship between austenite and ferrite during the formation of austenite should be similar.

The practical determination of the crystallographic relationship between austenite and ferrite is not straightforward, as the austenite has been transformed to martensite during the quench. Retained austenite was never observed in the martensite. If, however, the ferrite to austenite and austenite to martensite transformations both occur in accordance with the KS orientation relationship, ferrite and martensite will show some particular relationship to each other, although many different variants will be possible. In the first instance, the possibility that both reactions occur with a KS relationship involving the same $\{111\}$ austenite plane was investigated. The $\{110\}_\alpha$ plane parallel to the $\{111\}_\gamma$ plane contains two $\langle 1\bar{1}1\rangle_\alpha$ directions, which may be parallel to one of three $\langle 1\bar{1}0\rangle_\gamma$ directions. There are thus six possible KS variants involving the same $\{111\}_\gamma$ plane, and pairs of these variants lead to ferrite-ferrite crystallographic relationships involving simple rotation about a $\{110\}_\alpha$ plane normal. The angles of rotation have been shown to be 0°, 70°32', 10°, 60° and 49° (Speich and Swann 1965).

Pairs of electron diffraction patterns from either side of perturbed interfaces were taken, and were analysed for the above relationships. In all cases, the relationship between the ferrite and one martensite variant could be described by one of the above rotations about $(110)_\alpha$. The evidence is therefore consistent with austenite displaying a perturbed interface having a KS relationship with the

ferrite into which it is growing.

If the broad faces of the sideplates are indeed low energy interfaces, the sideplates should be stable during further annealing. That this is the case is demonstrated by the observation of sideplates after one hour at 720°C.

The plates can therefore be described as Widmanstätten plates with low energy partially coherent interfaces. These are normally assumed to grow by the passage of incoherent ledges (see eg. Aaronson 1962). Ledges can sometimes be seen at the interfaces of the sideplates (see Fig. 2.10b), but it is impossible to say whether such small scale features arose during reaustenitisation, or during the transformation to martensite.

2.6 Interfacial Stability

The breakdown of growing solid-solid interfaces in a concentration gradient can be considered in a similar manner to dendritic or cellular growth during solidification. A protruberance at the interface finds itself in conditions more favourable for growth than does the bulk interface; protruberances therefore grow at the expense of the bulk interface. During solidification, both temperature gradients and concentration gradients can lead to increased supercooling ahead of the interface, and thus to interfacial breakdown. Solid-solid interfaces, however, are subject to higher constraining forces than solid-liquid interfaces, and interfacial breakdown is less likely. In particular, the surface tension between two solid phases is high and tends to keep the interface smooth. A protruberance at the interface will only grow if the concentration gradient into which it is growing provides enough driving force to overcome the surface energy. Protruberances in solid-solid systems are therefore most likely to occur in orientations that minimise the surface energy between the two phases; hence the growth of Widmanstätten plates with broad, low energy, partially coherent interfaces.

The conditions under which breakdown can occur will now be considered, in a review of the literature on the subject.

2.6.1 Theory

Mullins and Sekerka (1963) consider the morphological stability of a spheroidal particle during diffusion controlled growth, and a brief outline of their treatment is given here. They assume that the effects of strain energy, anisotropy and diffusion in the interface are negligible, and that local equilibrium exists at all interfaces. They consider expansion of the particle in spherical harmonics; any harmonic whose amplitude increases with time will cause instability, and the harmonic with the highest rate of increasing amplitude will dominate.

Consider an alloy whose composition is c_∞ far from the interface, in which a product phase of composition c is growing. The composition of the parent phase at a planar interface is c_o, and at a curved interface is c_s. The velocity, v, of diffusion controlled growth is given by

$$v = \frac{D}{c-c_s}\frac{\partial c}{\partial n} \qquad (2:1)$$

where D is the diffusion coefficient of the solute in the parent phase, and $\frac{\partial c}{\partial n}$ is the concentration gradient normal to the interface. In the simplest case, the concentration gradient, G, on the surface of a sphere of radius R can be given by

$$G = \frac{\partial c}{\partial n} = \frac{c_\infty - c_o}{R} \qquad (2:2)$$

but in general, $\frac{\partial c}{\partial n}$ varies as the interface moves.

Assuming that $c-c_s \gg c_\infty - c_s$, and superimposing sinusoidal perturbations on the interface, Mullins and Sekerka were able to calculate the diffusion field during growth, and the amplitude of any harmonic (ie. perturbation with a particular wavelength). The growth rate of the amplitude of a perturbation was then found to be proportional to the concentration gradient, and negatively proportional to the surface tension. Thus the growth of each harmonic consists of two opposing factors, one leading to growth and one to decay. There must exist a harmonic of wavelength λ_o for which the opposing factors are equal, and for which neither growth nor decay occurs. Mullins and Sekerka find that

$$\lambda_o = 2\pi\left(\frac{\Gamma c_o}{G}\right)^{\frac{1}{2}} \qquad (2:3)$$

where $\Gamma = \frac{\gamma\Omega}{RT}$, and γ = interfacial free energy (surface tension), Ω = increment of precipitate volume per mole of added solute, R = gas

constant and T = absolute temperature. Harmonics for which $\lambda > \lambda_o$ grow, while $\lambda < \lambda_o$ leads to decay. Thus, λ_o is the minimum wavelength which can cause instability. For a perturbation to arise, initial concentration fluctuations are necessary over a distance of the order of the wavelength. For a diffusional fluctuation therefore, the wavelength must be less than $\sqrt{Dt}$, approximately (where t is time). Thus, if the supersaturation is small and the surface tension is large, λ_o is large and the interface is stable to very long times.

For any set of conditions G, Γ, c_o, the amplitude growth rate varies with wavelength in such a way that there is a maximum growth rate at a particular wavelength, λ_m. It is found that:

$$\lambda_m = \sqrt{3}\lambda_o = 2\pi \left(\frac{3\Gamma c_o}{G}\right)^{1/2} \qquad (2:4)$$

This harmonic dominates, and perburbations of spacing λ_m result.

Mullins and Sekerka obtain a similar solution for perturbations at a planar interface, and Shewmon (1965) finds that $\lambda_m = 4^{1/3}\lambda_o$ when the effects of interfacial diffusion are taken into account. Shewmon also points out that diffusion in the precipitating phase may be important, and considers the effects of strain energy, which he concludes are small.

Townsend and Kirkaldy (1968) compare the experimentally determined growth rates and spacings of secondary Widmanstätten ferrite plates with the predicted values. Good agreement leads them to conclude that growth of Widmanstätten ferrite is controlled by carbon diffusion through austenite, that it is affected by anisotropic surface tension, that local equilibrium pertains, and that neither an interfacial reaction nor interfacial diffusion is rate-controlling. They point out that an interface which is initially planar will not be easily perturbed, as it lies in a low energy configuration. Perturbations which lead to plates having low energy partially coherent interfaces will be favoured, as the surface tension factor inhibiting growth will be minimised.

2.6.2 Discussion - Interfacial Instability during Reaustenitisation of Spheroidite

During the early stages of reaustenitisation of spheroidite, the carbide at which austenite nucleated dissolves, and provides carbon for austenite growth. The concentration gradient behind the interface and the surface tension act together to stabilise a smooth interface.

If there are carbides in the ferrite after the carbides in the austenite have dissolved, there will be a diffusive flux of carbon through ferrite to the austenite interface, enabling further growth. This can occur, for instance, during the later stages of reaustenitisation of the fine grained structure containing fine carbides, in which interfacial instabilities were indeed observed. Growth continues until all carbides have dissolved and austenite and ferrite have achieved their equilibrium proportions and compositions.

The model of Mullins and Sekerka (1963) considers the growth of a precipitate into a concentration gradient. In the present case, the concentration gradient in the ferrite ahead of the interface is minimal, as the solubility of carbon in ferrite is very low, and the concentrations of ferrite in local equilibrium with austenite and cementite are fairly similar. However, the growth of austenite allows the dissolution of carbide far from the interface, and in this way a steady flux of carbon from carbide to austenite is set up. There is thus an effective concentration gradient ahead of the interface.

If only a small amount of austenite has already been formed, the average composition of the remaining ferrite and carbides together is of the order of the composition of the alloy (c_∞), which in this case is 1%C (composition in atomic percent). The composition of ferrite at the interface (c_o) is about 0.1% (ignoring the effct of Ni). The effective concentration gradient at the interface under these conditions is estimated as being the difference in bulk and interface compositions (c_∞ and c_o respectively), divided by half the distance between austenite nodules. In the fine grained starting structure containing fine carbides used in the present work, the distance between austenite nodules is of the order of the initial ferrite grain size, d, ie about 3μm. The estimated initial concentration gradient, G, is thus given by

$$G = \frac{c_\infty - c_o}{d/2} = 6\times10^3\ m^{-1} \qquad (2:5)$$

Following Mullins and Sekerka, the wavelength of the dominant perturbaion is given by Eqn.(2:4):-

$$\lambda_m = 2\pi\left(\frac{3\Gamma c_o}{G}\right)^{1/2}$$

Γ is of the order of 10^{-7}cm, and hence

$$\lambda_m = 0.14\mu m$$

Following Townsend and Kirkaldy (1968) the final spacing of Widmanstätten plates is given by the wavelength of the initial perturbation, which is determined by the initial concentration gradient. Thus the spacing of the plates in the present case is expected to be 0.14μm, which is in good agreement with the measured spacing of about 0.2μm.

The good agreement between observed and calculated spacings is, of course, fortuitous, as large approximations have been made. In particular, the effect of the interface velocity on the concentration gradient has been ignored, although in the case when there is a steady flux of carbon from a distant carbide, this effect will be small. In addition the compositions of the bulk ferrite plus carbide constituent and of the ferrite at the interface are not known exactly.

Since perturbations arise due to diffusional fluctuations, over a distance of the order of a wavelength, the incubation time, t_o, before perturbations are likely to be observed can be estimated from

$$\lambda_m \simeq \sqrt{Dt_o} \qquad (2:6)$$

Thus, in the present case, $t_o \simeq 10^{-7}$s. Perturbations should therefore arise virtually as soon as the flux of carbon from carbide to austenite through ferrite is established. Since no sideplates are observed at times of up to about 7s at 720°C, no carbon flux through ferrite can exist during this time, and growth must occur solely by diffusion of carbon through austenite behind the interface. Austenite nodules containing dissolving carbides were never observed to display perturbed interfaces or sideplates.

Sideplates are most likely to grow when the initial interface is not a low energy interface, but when nevertheless an orientation relationship exists such that the sideplates can adopt low energy interfaces. Austenite is expected to nucleate at a ferrite-ferrite grain boundary such that it has a low energy interface with one grain, and a less coherent, more intrinsically mobile interface with the other grain (Smith 1953). A crystallographic orientation relationship (probably KS) exists across the planar interface, but no orientation relationship is necessary across the less coherent interface. However, by analogy with the formation of proeutectoid ferrite (King and Bell 1975), the austenite may in many cases nucleate such that it is approximately KS related to both grains, the interfaces displaying both

low energy facets and less coherent sections. The less coherent sections of these interfaces are then the most likely interfaces to show instability.

Austenite nodules exhibiting a KS relationship with both ferrite grains were indeed observed. Several cases were also seen in which an austenite nodule displayed a stable, planar interface with one grain, and a more mobile interface with the other grain, at which instability, leading to formation of protrusions, occurred at the later reaction stages. An example is given in Fig. 2.10a.

The last small amount of austenite to transform does so after all carbides have disappeared. In this starting structure, most of the transformation has occurred, and most of the carbides have dissolved, by 10s at 720°C, while the reaction is not actually complete until over 100s. This last stage of the reaction must involve the removal of carbon concentration gradients in ferrite, allowing further austenite growth. The concentration gradients are very small, as the maximum solubility of carbon in ferrite (in contact with cementite) is very close to the equilibrium solubility. The existence of excess carbon in the ferrite is evidenced by the presence of fine carbide precipitates on dislocations in the quenched samples, as shown for instance in Figs. 2.10a and b. Accurate data for carbon concentrations in iron alloys containing nickel are not available. The solubilities of carbon in ferrite in pure iron-carbon alloys at a temperature 20°C above the eutectoid temperature (taken from Hansen 1958), are 0.120 %o (maximum) and about 0.088 %o (equilibrium). Considering a structure consisting of 70% ferrite and allowing the ferrite composition to fall from 0.120%o to 0.088%o, it can be calculated that enough carbon is released to allow the formation of a maximum of about 1% more austenite of composition 3.1%C. Thus more austenite can indeed form after all the carbides have dissolved, although rather more than the estimated increase of 1% is actually observed. However, the presence of nickel may well increase the maximum solubility of carbon in ferrite, thus increasing the amount of carbon available for the reaction.

An analysis of interfacial stability similar to that given above, indicates that austenite growing in the coarse grained starting structure (as described in section 2.3) should show sideplates with a spacing of up to about 1μm. Some sideplates were indeed occasionally observed, but unfortunately systematic measurement of their spacing was

not carried out.

Austenite growing in the fine grained starting structure (section 2.4) never experiences a carbon flux in the ferrite ahead of the interface. The interface shoud therefore always remain stable, as is observed.

Finally, it is noted that the addition of 2%Ni does not qualitatively alter the types of reaction which occur in a pure Fe-C alloy. A substitutional alloying element is expected to slow down the reaction by solute drag, and also to alter the boundary conditions for carbon diffusion. Since similar morphologies were observed for alloys with and without nickel, it is concluded that these factors have little effect on austenite morphology, although the rate and extent of transformation may be altered. The effect of alloying elements on the kinetics of reaustenitisation will be considered in chapter 6.

2.7 Summary

Reaustenitisation of three distributions of spheroidised carbides in ferrite at temperatures low in the two-phase austenite plus ferrite region has been carried out. Both the rate of austenite nucleation and the mode of austenite growth have been found to be determined by the initial ferrite grain size and the carbide size, and more specifically on the relationship between these parameters, and hence on the location of the carbides.

Nucleation occurs mostly at carbide-grain boundary junctions. The strongest factor affecting nucleation incubation time, for a given carbon content, is the grain size. The number of carbides in the grain boundaries determines the number of austenite nuclei which form. Thus the carbide to grain size ratio is more important than the carbide size itself, and the finest austenite grain size is achieved from a structure of fine grained ferrite in which all the carbides are in grain boundaries.

The growth of austenite is accompanied in all cases by dissolution of carbides, and involves the diffusion of carbon from cementite to the austenite interface. Initially the diffusion path is through austenite to the interface, from dissolving carbides within the austenite, and subsequently, diffusion of carbon from carbides dissolving in the

ferrite may occur. It has been shown that, locally, diffusion through both austenite and ferrite simultaneously does not occur. The diffusion path is determined by the number of austenite nuclei and hence by the initial carbide distribution.

The morphology of the austenite and the rate of transformation also depend on which carbon diffusion path is operative. Austenite growth involving carbon diffusion through itself, follows the carbon diffusion field and displays smooth interfaces. Interfacial instability occurs when austenite is growing into ferrite under conditions of carbon flux through ferrite, leading to Widmanstatten sideplates of well defined spacing. The observed interfacial instability is in good agreement with that predicted by the model of Mullins and Sekerka (1963). Widmanstatten growth is observed only when diffusion occurs ahead of the interface, and never when diffusion is occurring behind the interface, within the growing phase.

In certain circumstances, examples indicating that austenite nucleates at a grain boundary or grain corner such that it has a KS relationship with both grains, have been found. Interfaces across which KS relationships exist, but which are not low energy, low mobility interfaces, are likely to become unstable.

Intercritical annealing of a homogenous distribution of spheroidised carbides in ferrite has been shown to lead to a homogenous distribution of martensite islands in ferrite, when the initial ferrite grain size is fine. The formation of austenite and the dissolution of carbides is rapid even at temperatures low in the two phase austenite plus ferrite region, and even when a substitutional alloying element is present. The finest distribution of martensite islands is produced from a fine grained starting structure in which all the carbides are in grain boundaries.

CHAPTER THREE

REAUSTENITISATION OF FERRITE - PEARLITE AGGREGATES

3.1 Introduction

Ferrite-pearlite microstructures are readily obtainable in low carbon steels by transforming austenite at a wide range of cooling rates. Ferrite-pearlite aggregates thus provide the starting structure for reaustenitisation of many steels during industrial heat treatment, and in particular are relevant to the intercritical annealing of dual phase steels.

Previous work on reaustenitisation of pearlite has centred on high carbon steels often near eutectoid composition, as outlined in chapter 1, section 1.2.4. A few studies of lower carbon steels have also been carried out eg. by Rose and Strassburg (1956), Sheard and Nutting (1980). It has been established that austenite nucleation occurs at boundaries between pearlite colonies or at interfaces between ferrite and pearlite. Also, growth of austenite into pearlite has been found to occur rapidly by local diffusion of carbon. In high carbon steels, carbides may remain in the austenite after all the ferrite has transformed to austenite, and these residual carbides are slow to dissolve (eg. Speich and Szirmae 1969). In low carbon steels, the pearlite regions transform first, accompanied by dissolution of cementite, followed by the transformation of the bulk ferrite which takes place more slowly (Rose and Strassburg 1956).

The aims of this work were:

a) To investigate in more detail the reaustenitisation of a low carbon alloy, the composition of the alloy being characteristic of dual phase steels.

b) To study the partial transformation in the two phase austenite plus ferrite region, again bearing in mind the relevance to intercritical annealing of dual phase steels.

c) To compare the formation of austenite in different ferrite-pearlite microstructures as a function of temperature.

Characterisations of the initial microstructures are given in the next section (3.2) followed by the results of metallographic examination

of partially reaustenitised specimens in section 3.3. Section 3.4 deals with the methods and results of a crystallographic analysis of the relationship between the growing austenite and ferrite, and in section 3.5 some kinetic data are presented. The work is summarised in section 3.6.

3.2 The Ferrite - Pearlite Structures

The alloy used in this work had a nominal composition of Fe-1.2%Mn-0.1%C. Two casts of this alloy were made (alloys C and D, appendix A1) and two distributions of ferrite and pearlite were obtained, one from each cast. In both cases, homogenised, rolled strip was fully reaustenitised at 1000°C for 10 minutes, after which furnace cooling led to the first, coarser, starting structure (alloy C), and air cooling gave a second, finer, structure (alloy D).

3.2.1 Coarse Ferrite - Pearlite

The coarser structure consisted of ferrite grains (grain size a few tens of microns) with pearlite colonies at grain corners, as shown in Fig. 3.1. Inspection of the pearlite colonies by electron microscopy showed that although they consisted of fine mixtures of ferrite and cementite, the structures were not always lamellar, the cementite sometimes existing in fibrous or particulate form.

Lamellar cementite in a single colony was observed to have a single orientation, but other forms of cementite often displayed more than one orientation in one area. The non-lamellar structures cannot therefore be described as classical pearlite, the formation of which requires lamellar growth of ferrite and cementite by a cooperative mechanism. However, for convenience, the ferrite-cementite mixtures will be termed pearlite colonies throughout this work.

Fig. 3.2 shows such a colony containing lath-like carbides. Boundaries between the ferrite in the colony and the adjacent ferrite grains can be seen on all sides. This may be taken to imply that the formation of pearlite requires a separate nucleation event. However, in several cases, pearlitic ferrite continuous with the ferrite in an adjacent grain was observed. It seems therefore that the last austenite to transform, which is enriched with carbon, does so by the further growth of one of the ferrite grains surrounding the austenite island.

The ferrite growth is accompanied by carbide precipitation which often, but not always, occurs in a classical pearlitic manner. There are then boundaries between the colony ferrite and the other adjacent ferrite grains.

The carbides are often coarser in the colony-ferrite interface, as shown in parts of Fig. 3.2, indicating that coarsening occurred during the furnace cool. Coarse carbides were also sometimes found in ferrite grain boundaries.

3.2.2 Fine Ferrite - Pearlite

An optical micrograph of the finer structure, formed by air cooling, is shown in Fig. 3.3. The grain size and colony size here are considerably less than in the coarser structure (compare Figs 3.1 and 3.3), as is the lamellar spacing (Figs 3.2 and 3.4). The ferrite and cementite morphologies in the colonies are seen to be fairly similar in the two structures. The ferrite grain boundaries in the finer structure are heavily decorated by carbides, which are often in the form of grain boundary films.

3.3 Morphological Studies of Reaustenitisation

Preliminary experiments showed that austenite first begins to form at temperatures a little below 700°C, and that, for this alloy composition, the transformation to austenite is complete at about 850°C. Reaustenitisation treatments were therefore carried out at temperatures between 700°C and 850°C, for times of a few seconds to several minutes. During quenching, the austenite transforms to martensite, which is distinguishable from the original ferrite and pearlite.

The general characteristics of the reaction are that:

a) austenite forms preferentially at boundaries between ferrite and pearlite colonies, and

b) austenite also precipitates on ferrite grain boundaries. The nature of these precipitates varies with time, temperature and starting structure.

3.3.1 Optical Metallography

Figs 3.5 to 3.7 are optical micrographs illustrating the general features of the reaction. During reaustenitisation of the coarser

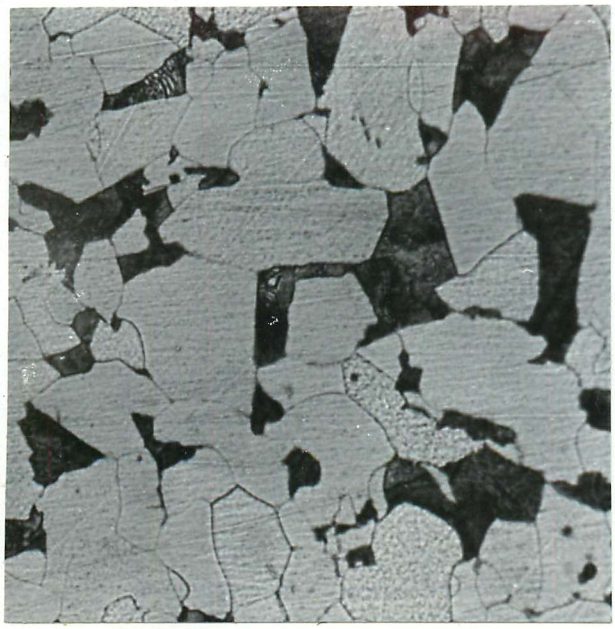

Fig. 3.1: Optical micrograph. Pearlite etched dark.

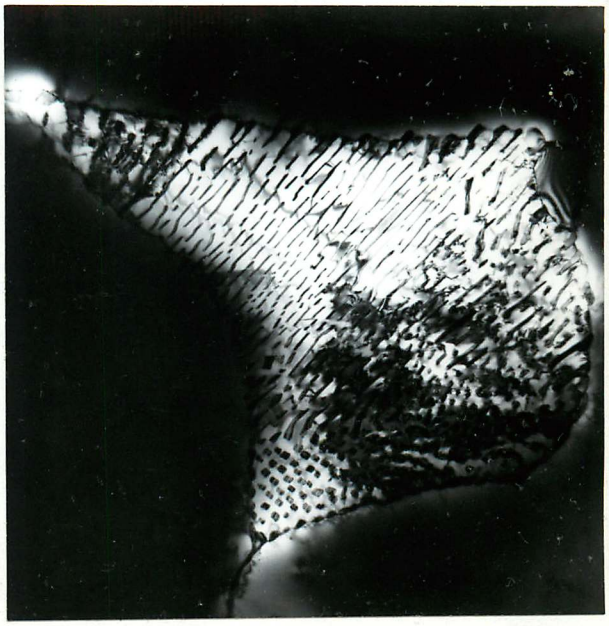

Fig. 3.2: Electron micrograph.

Figs. 3.1,3.2: Coarse ferrite-pearlite microstructure, obtained by furnace cooling from austenite.

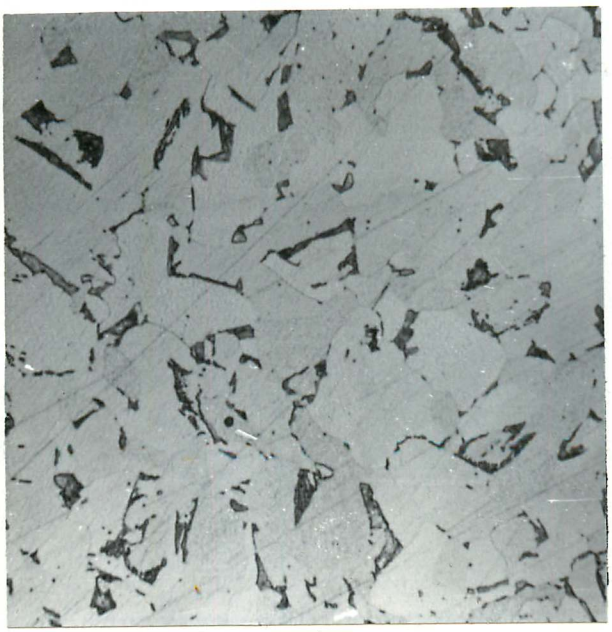

Fig. 3.3: Optical micrograph.

Fig. 3.4: Electron micrograph.

Figs. 3.3,3.4: Fine ferrite-pearlite microstructure, obtained by air cooling from austenite.

starting structure at 700°C, the reaction is fairly slow, and austenite is first seen to form at pearlite colony boundaries (Fig. 3.5a). At longer times, much of the pearlite disappears, the austenite islands become large and blocky, and many austenite precipitates on ferrite grain boundaries are also seen (Fig. 3.5b). The reaction in the finer starting structure is similar, but results in a finer distribution of austenite, see Fig. 3.5c. A little pearlite remains at 700°C even after very long reaction times (30 minutes), indicating that all three phases (ferrite, austenite and cementite) are stable at this temperature. At 725°C, no pearlite remains after 3 minutes, showing that this temperature is in the two phase austenite plus ferrite range.

The reaction rate increases rapidly with increasing temperature. Fig. 3.6a shows the extent of the transformation after only 2s at 751°C (in the coarser starting structure). All the pearlite disappears by 5s, and by 100s a stable volume fraction of austenite is reached. Again there are both large, blocky austenite areas, and fine grain boundary austenite precipitates (Fig 3.6b). Fig. 3.7 illustrates the transformation in the finer structure at the higher temperature of 800°C, showing rapid disappearance of carbides (less than 2s, Fig. 3.7a), and the formation of large connected areas of austenite (Fig. 3.7b). At 845°C, almost all the ferrite disappears in less than 20s, although small amounts of ferrite remain to long reaction times, showing that this temperature is just within the two phase austenite plus ferrite region.

3.3.2 Electron Metallography

a) Austenite formed at Pearlite-Ferrite Boundaries

Electron microscopy shows that the first austenite always forms at pearlite-ferrite boundaries, and initially growth occurs predominantly along the boundary, as in Fig. 3.8. Many nucleation events occur at each colony, and subsequent growth occurs both into the ferrite and the pearlite. The pearlite colony is consumed fairly rapidly, resulting in several small austenite grains which soon impinge, and subsequently transform to one large martensite region on quenching.

In these alloys, the cementite dissolves rapidly, such that pearlitic carbides are rarely seen in the austenite. Examination of the austenite-pearlite interface in Fig. 3.9 indicates that a little cementite may dissolve in the ferrite ahead of the austenite interface,

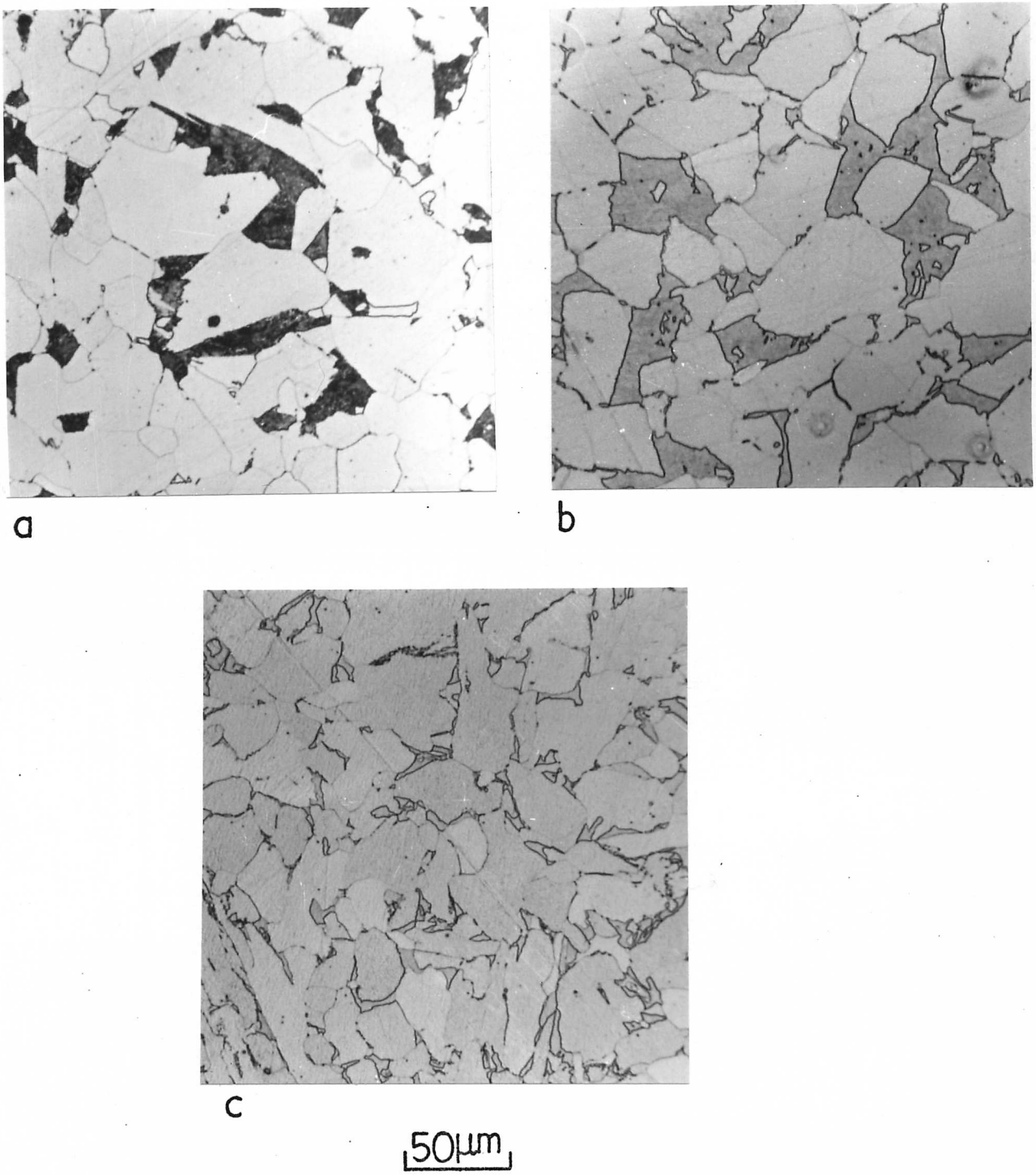

Fig. 3.5: Ferrite-pearlite, partially reaustenitised at 700°C.
a) Coarser structure, 2s transformation. Pearlite dark, austenite (now martensite) bold outlined.
b) Coarser structure, 180s transformation. Martensite dark.
c) Finer structure, 300s transformation. Martensite dark.

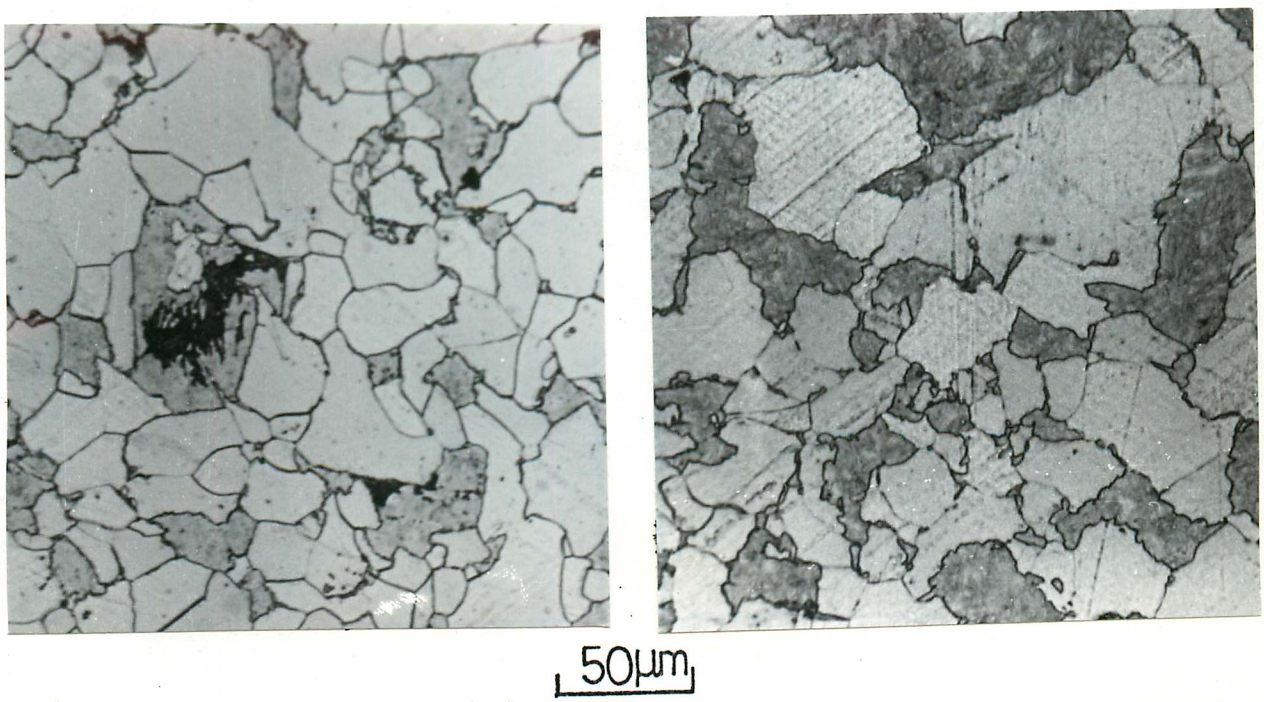

Fig. 3.6: Ferrite-pearlite, partially reaustenitised at 751°C. Coarser starting structure.
a) 2s transformation. Pearlite dark, martensite tinted.
b) 100s transformation.

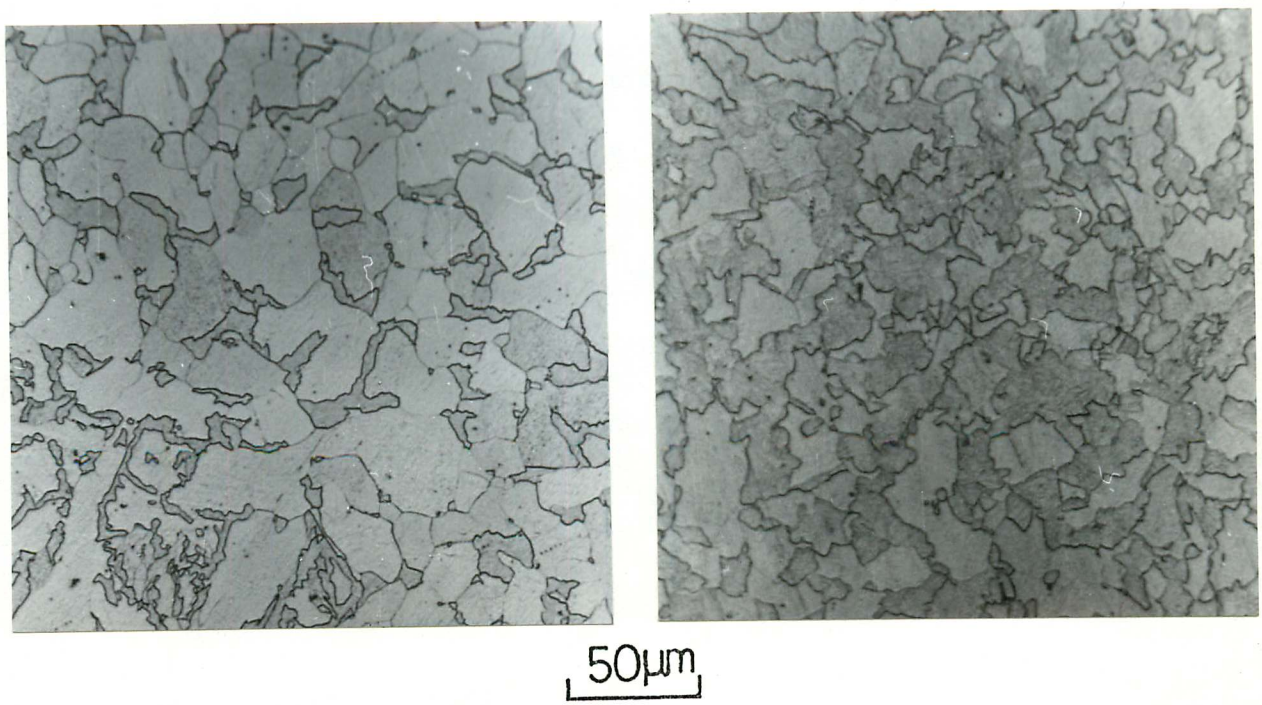

Fig. 3.7: Ferrite-pearlite, partially reaustenitised at 800°C. Finer starting structure.
a) 2s transformation.
b) 180s transformation.

Fig. 3.8: Austenite (now martensite) growing at a boundary between ferrite (left) and pearlite (right). Austenitised 100s 700°C.

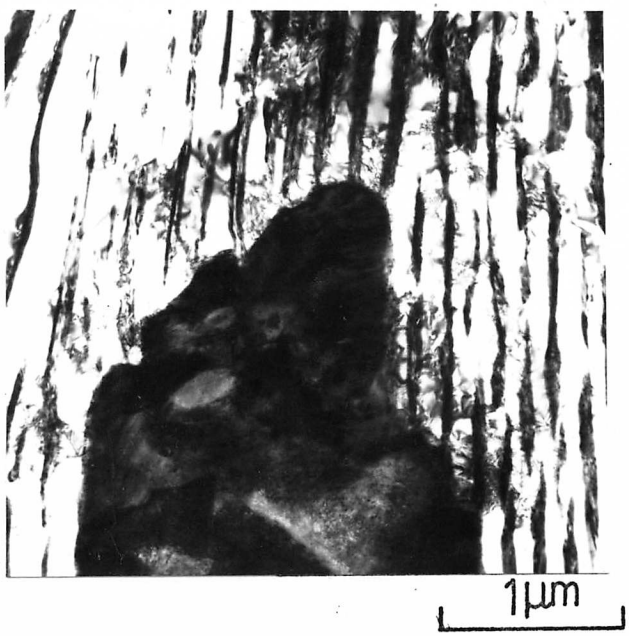

Fig. 3.9: Austenite growing into a pearlite colony. Austenitised 100s 700°C.

but that most of the dissolution occurs in the interface itself. At an intermediate temperature (750°C), a few small rounded carbides were observed in the austenite after a reaction time of 2s, indicating that the reaction rate was too rapid to allow complete cementite dissolution in the interface. These small carbides are unstable, and rapidly dissolve.

b) Austenite formed at Ferrite Grain Boundaries

Austenite also forms at ferrite grain boundaries, and examples of the precipitate morphologies, which are similar to those displayed by proeutectoid ferrite (as classified by Dubé et al 1958), are given in Figs 3.10 to 3.13. Although nucleation probably occurs at a carbide in the grain boundary (particularly in the finer structure, where many such sites exist), grain boundary carbides are very rarely seen in association with austenite, and thus must disslove rapidly. An opportunity therefore exists to study the growth of austenite into carbide free ferrite, a reaction analogous to the growth of proeutectoid ferrite into austenite. Since the morphology of the grain boundary austenite precipitates, and the conditions under which they occur, differ in the two starting structures, the coarse and fine starting ferrite-pearlite aggregates will now be considered in turn.

In the coarser starting structure, grain boundary austenite precipitates are not seen at short times at low temperatures (eg. less than about 100s at 700°C). The number of grain boundary precipitates increases with time and with temperature, and some typical morphologies (grain boundary film, allotriomorph and saw-tooth) are shown in Fig. 3.10. At low temperatures, the grain boundary austenite tends to be in the form of lenticular precipitates, or films, while at higher temperatures the austenite grows out into one or both ferrite grains, and often becomes facetted, as in Fig. 3.11. Widmanstätten sawteeth and sideplates were sometimes observed, as in Fig. 3.12, particularly at higher temperatures. The crystallographic relationship between austenite and ferrite, and its effect on morphology, are considered in section 3.4.

Grain boundary austenite is seen at all temperatures during reaustenitisation of the finer starting structure. At low temperatures, the many grain boundary carbides disappear rapidly, and are replaced by austenite films. At higher temperatures, the rapid growth of the pearlite-nucleated austenite removes many of the ferrite grain

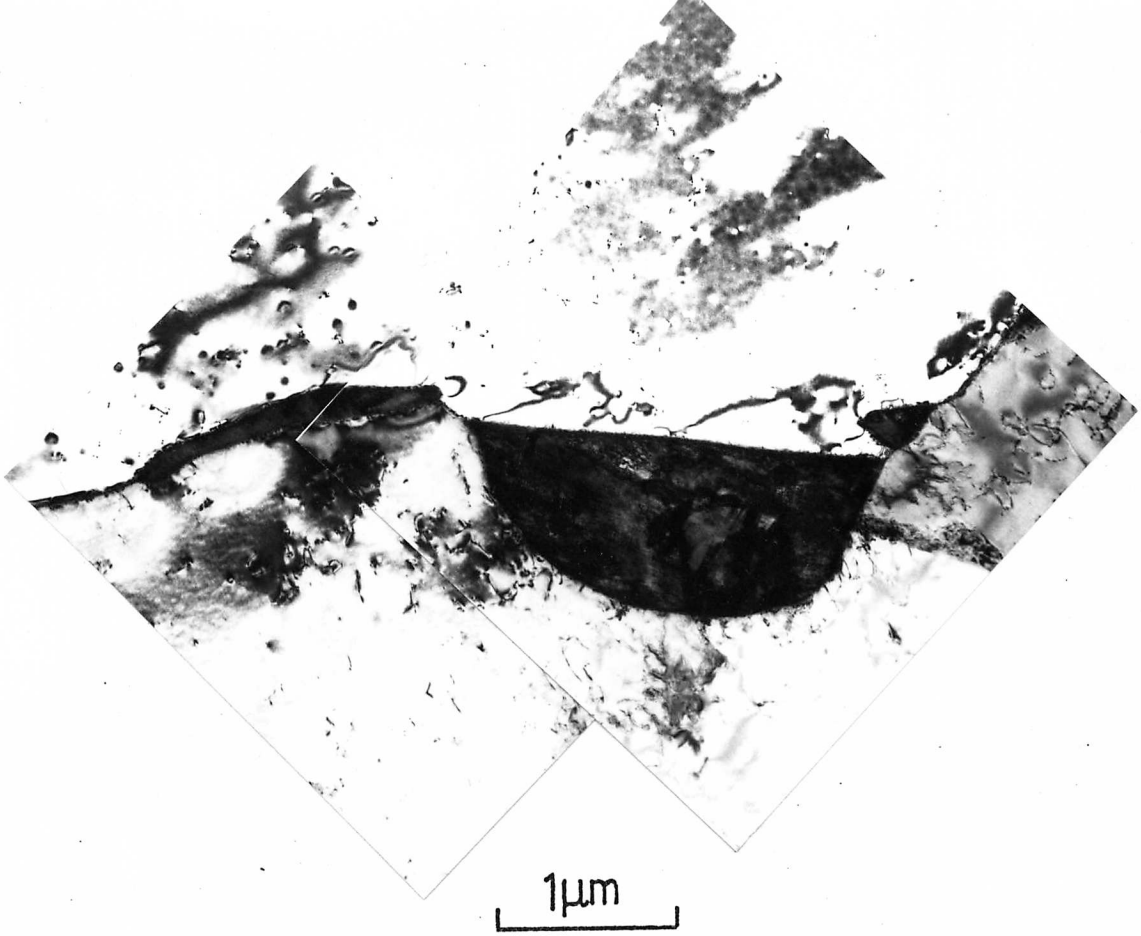

Fig 3.10: Austenite (now martensite) growing at a ferrite grain boundary, showing (left to right) film, allotriomorph and saw-tooth morphologies. Transformed 2s 800°C.

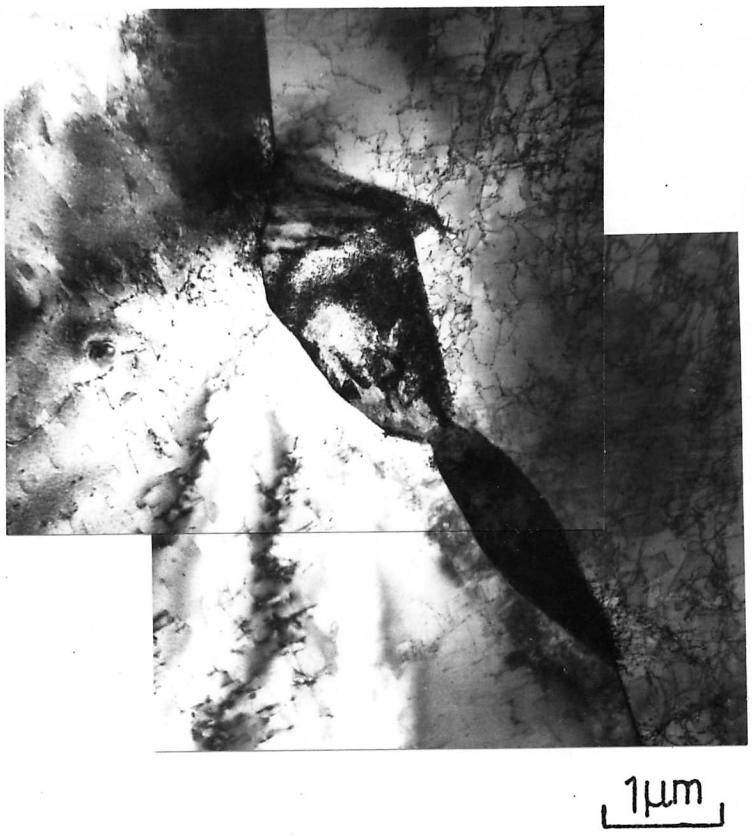

Fig 3.11: Austenite growing at a ferrite grain boundary showing partly facetted interfaces. Transformed 100s 750°C.

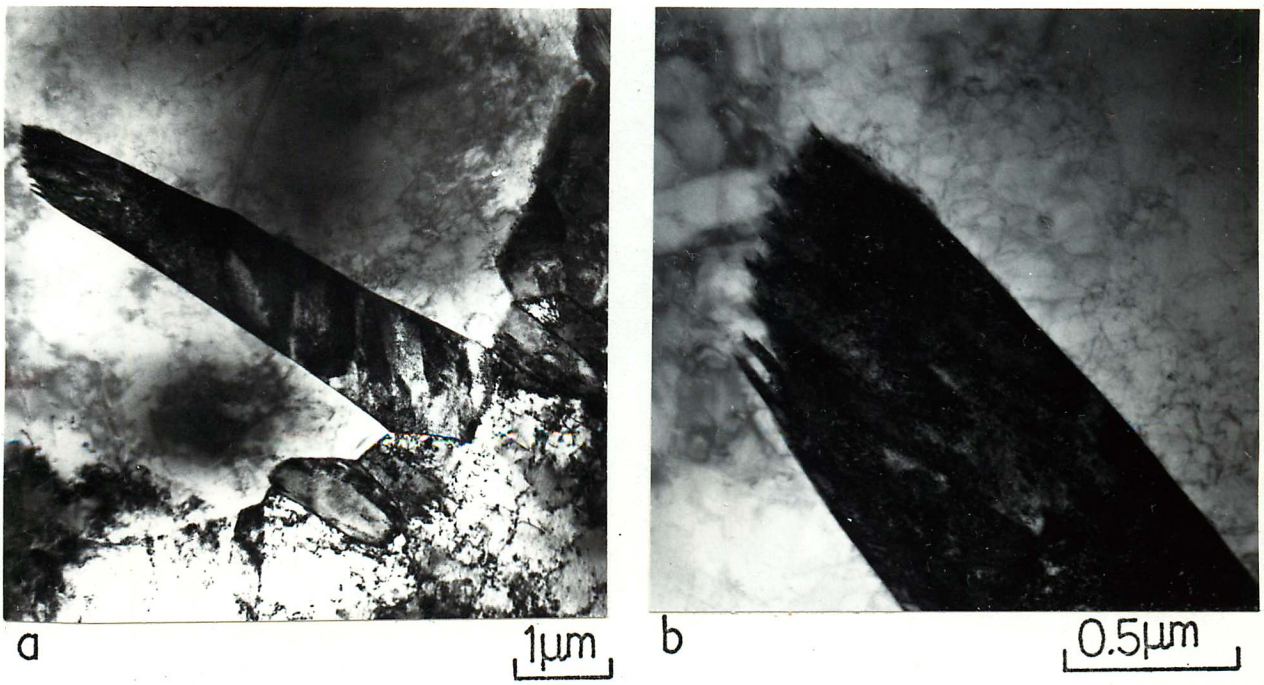

Fig. 3.12: a) Widmanstätten austenite sideplates at a ferrite grain boundary.
b) Higher magnification image of the tip of the large plate.
Transformed 100s 750°C.

Fig. 3.13: Perturbations at a ferrite-austenite (now martensite) interface. Finer starting structure, transformed 30s 750°C.

boundaries, such that small grain boundary austenite precipitates are rare. Widmanstätten austenite morphologies are rarely observed, although interfacial instabilities (as described in chapter 2, section 2.6) are often seen, particularly towards the end of the reaction. Fig. 3.13 shows perturbations at an austenite-ferrite interface, which will lead to relatively coarse sideplates, while Fig. 3.12b shows finer sideplates such as were occasionally seen at austenite interfaces in the coarser structure.

3.3.3 Discussion

The morphology of grain boundary austenite, and the austenite-ferrite interface type, can be understood in terms of driving forces and carbon diffusion paths.

For nucleation of austenite at ferrite grain boundaries, there must be sufficient driving force available, and hence grain boundary austenite is more likely to form at higher temperatures. During the early part of the grain boundary reaction, dissolution of grain boundary carbides and subsequent diffusion of carbon along the boundary or within the austenite occurs, providing carbon for further transformation, and leading to the formation of roughly parallel-sided austenite films. This morphology is predominant in the finer structure because of the high density of grain boundary carbides. When the grain boundary carbon source is depleted, the films are expected to grow out into the ferrite. These conditions occur in the coarser structure at long times or high temperatures. Austenite growth into ferrite implies that carbon must be reaching the interface by diffusion through ferrite, and that the ferrite must therefore be supersaturated. The presence of fine carbides on dislocations, as seen for instance in Fig. 3.11, is evidence that the ferrite was supersaturated with respect to carbon at the austenitisation temperature, carbides precipitating out during the quench. This supersaturation must arise initially from dissolution of cementite.

Under these conditions, interfacial instability would be expected (see section 2.6). Grain boundary austenite films are unlikely to have semi-coherent, low energy interfaces with ferrite, as the position of the interface is determined simply by the flux of carbon from the boundary. The interfaces are thus likely to be high energy interfaces which are prone to instability. On the other hand, austenite which is growing out into ferrite, as is often the case in the coarser structure

(eg. Fig. 3.11), can more readily adopt low energy interfaces, which are less likely to break down. In the coarser structure, interfacial instability was rare, and was indeed only observed on the incoherent curved sections of otherwise low energy interfaces, as in Fig. 3.12.

The difference in scale of the instabilities in the two starting structures, the finer starting structure generally exhibiting coarser protrusions, is diff icult to explain, but may perhaps be due to a difference in interface velocities.

3.4 Austenite - Ferrite Crystallography

In chapter 2 (section 2.5.3), the relationship between the original ferrite and the martensitic ferrite was considered, for cases when both the ferrite to austenite transformation and the austenite to martensite transformation obeyed the KS orientation relationship, and involved the same austenite $\{111\}$ plane. The treatment was able to describe the relationship between certain ferrite and martensite crystals, showing that the forward and reverse transformations indeed involved the same $\{111\}_\gamma$ plane. A similar treatment proved inadequate for the description of relationships between grain boundary nucleated austenite and ferrite in the present system, and thus a more general treatment, allowing any two KS variants for the forward and reverse reactions is needed.

3.4.1 Method

The Kurdjumov-Sachs orientation relationship relating austenite to ferrite is

$$\{111\}_\gamma \,||\, \{110\}_\alpha \;;\; \langle 1\bar{1}0\rangle_\gamma \,||\, \langle 1\bar{1}1\rangle_\alpha$$

As noted in section 2.6, there are six possible KS variants involving the same $\{111\}_\gamma$ plane, and since there are four distinguishable $\{111\}$ planes in the face centred cubic structure, there are 24 possible variants of the KS orientation relationship. In the present case, we are considering the transformation of ferrite to austenite by one KS variant, and the transformation of austenite to ferrite (martensite) by another variant. The number of possible relationships between the two ferrite grains is thus 24^2 (=576). In order to show that the ferrite transforms to austenite with a KS relationship, assuming that austenite always transforms to martensite with a KS relationship, it is thus necessary to show that the original ferrite and the martensitic ferrite are related in any one of 576 ways. Fortunately, symmetry reduces the

number of possibilities considerably, and Bhadeshia (1979) has listed the possible relationships.

The relationship between any two ferrite lattices can be described by an axis-angle pair or a rotation matrix. For this work it was found to be more convenient to use rotation matrices. Bhadeshia (1980) has shown that the relationship between two ferrite crystals which obey a KS relationship with the same austenite, can be described by just 24 rotation matrices, each of which may have its elements in any order. These matrices are listed in appendix A3. The problem in the present case is thus reduced to finding the rotation matrix describing the experimental ferrite-ferrite relationship, and comparing it with the 24 calculated matrices. An agreement for a ferrite-martensite pair then indicates that the austenite was KS with the ferrite, and also transformed to martensite with a KS relationship (ignoring agreements which occur by chance).

In this analysis, it is assumed that if any orientation relationship exists, it is the Kurdjumov-Sachs relationship. Another possibility is that suggested by Nishiyama-Wasserman (1935). Since the two relationships are within a few degrees of each other, and accuracy of better than a few degrees cannot be expected by this method of analysis, it is expected that the two relationships will be indistinguishable, and that this analysis will thus identify all pairs of ferrite crystals which are rationally related to a common austenite.

Crystallographic analysis was carried out on grain boundary nucleated austenite (now martensite) which had formed during reaustenitisation of the coarse ferrite-pearlite structure at 750°C for 100s. In each case, electron diffraction patterns were obtained from the ferrite on either side of the boundary, and from the martensite. Analysis of the diffraction patterns allowed the relationship of any pair of ferrite crystals to be fully described by two crystallographic vectors in each crystal, and the angle between two of the vectors, one from each crystal. The rotation matrix describing the relationship between the two crystals was then computed by a method due to Bhadeshia (1980) and compared with the 24 matrices describing ferrite grains which are KS related to a common austenite.

Inaccuracies in measurements of the orientation of the two crystals are unavoidable, since it is not possible to measure angular rotations

on diffraction patterns to accuracies better than one degree or so. Also, the relationship between the diffraction pattern and the crystal is exact only when the foil normal is accurately parallel to the zone axis of the pattern, a condition which is not always easy to achieve. Thus, exact agreement between the elements of the measured rotation matrices and the calculated ones is unlikely. However, agreement corresponding to differences of only a few degrees in all elements of the matrices was often found; in these cases, the ferrite grains were taken to be KS related to a common austenite.

3.4.2 Results

The results of analysis of eight separate areas are summarised in table 3.1. For each ferrite-ferrite or ferrite-martensite pair, two $\underline{g}$ vectors from each crystal and the angle between one pair of vectors (one from each crystal) are given. Rotation matrices computed from these data are given in appendix A3. The last column of table 3.1 gives the result of comparison of the computed rotation matrix with the matrices calculated for a common KS austenite. Table 3.2 relates the crystallographic data with the metallographically observed growth and interfacial behaviour.

In seven out of the eight cases, the austenite was KS (or close to KS) with one or both ferrite grains. This behaviour is similar to that of proeutectoid ferrite growing at an austenite grain boundary, proeutectoid ferrite nucleating such that it obeys a KS orientation relationship with one or more austenite grains, as suggested by Smith (1953) and experimentally verified by Ryder et al (1967) and King and Bell (1975). The observation of one area in the present work in which the martensite and ferrite do not appear to be related to a common austenite, does not conclusively show that the growing austenite was not related to any ferrite in that case, as a) the austenite may not have transformed to martensite with a KS variant, b) the KS martensite variant may have given a weak diffraction pattern which was not analysed or c) the austenite may have nucleated KS with a ferrite grain above or below the plane of section. The bulk of the evidence therefore indicates that grain boundary austenite always nucleates with a KS orientation relationship with one or both ferrite grains.

In cases where the austenite nucleated KS with both ferrite grains, the ferrite grains themselves were related to a common austenite. In

TABLE 3.1: Crystallographic analysis of ferrite-ferrite and ferrite-martensite pairs, in partially reaustenitised and quenched Fe-1.2%Mn-0.1%C.

Area Number	Crystal pairs Ferrite-A,B... Martensite-M		Diffraction Pattern Analysis					KS with common austenite
			i		j			
	i	j	$\underline{g}_1$	$\underline{g}_2$	$\underline{g}_1$	$\underline{g}_2$	$\underline{g}_2^i : \underline{g}_2^j$	
1	A	B	305	222	110	020	27°	No
	A	M	123	305	020	110	20°	No
	B	M	020	110	020	110	0°	Yes
2	A	B	305	222	110	020	27°	No
	M	A	112	301	123	305	10°	No
	M	B	301	211	110	200	24°	Yes
3	A	B	011	200	211	123	6°	Yes
	M	A	112	301	211	200	20°	Yes
	B	M	123	112	301	112	24°	Yes
4	A	B	101	110	101	110	48°	Yes
	A	M	101	110	101	110	0°	Yes
	M	B	101	110	101	110	48°	Yes
5	A	B	411	420	402	411	4°	Yes
	A	M	011	402	011	301	18°	Yes
	M	B	011	301	011	402	8°	Yes
6	A	B	011	411	011	301	29°	No
	A	M	011	411	200	031	16°	No
	M	B	031	231	301	310	4°	No
7	B	A	101	110	411	011	60°	No
	B	M	101	110	101	110	0°	Yes
	M	A	101	110	411	011	60°	No
8	A	B	123	132	233	011	7°	No
	A	M	132	011	310	011	30°	No
	B	M	011	211	310	011	49°	Yes
	A	C	123	132	110	011	49°	No
	B	C	011	211	011	101	49°	No
	C	M	110	121	301	310	13°	No

TABLE 3.2: Relationship between Crystallography and Growth Characteristics.

Area Number	Ferrite grains that austenite is K-S related to.	Ferrite grains that austenite grows into.	Ferrite grains that austenite has partly facetted interface with.
1	one	one (K-S related)	both
2	one	one (not K-S related)	both
3	both	both	both
4	both	one	both
5	both	one	both
6	neither	both	both
7	one	both	neither
8	one	both	one (K-S related)

other words, adjacent ferrite grains which initially grew with a KS relationship to a common prior austenite grain, lead to the formation of an austenite grain at their boundary which is KS related to both ferrites, and thus likely to be in the same orientation as the prior austenite. The adoption of this orientation by the new austenite then allows the formation of planar low energy interfaces with both ferrite grains, and facetting of some part of the interfaces is indeed always observed, as in Fig. 3.12 (which illustrates area no.3 from tables 3.1 and 3.2). Growth does not always occur into both grains, which is consistent with the generally low mobility of low energy interfaces.

Austenite which nucleates with a KS relationship with only one ferrite grain grows into that grain, into the other grain, or into both grains. Since only a few analyses were made, it is impossible to say which growth mode is most likely to occur.

In most cases, parts of the austenite interfaces with both ferrite grains were facetted (on a scale visible in the electron microscope), whether a KS relationship existed or not. This indicates that many interfaces can relax to low energy planar configurations, as suggested by Honeycombe (1976), even when no rational orientation relationship exists between austenite and ferrite.

3.5 Kinetics in the Two Phase Austenite-Ferrite Region

A Quantimet electronic image analyser was used to determine the volume fraction of austenite (martensite) in polished and etched specimens of partially reaustenitised and quenched material. The results for the finer starting structure are given in Fig. 3.14a, and for the coarser starting structure in Fig. 3.14b.

As is to be expected, the final volume fraction of austenite obtained increases with increasing temperature, as does the rate of transformation, due to both increased driving force and increased rate of carbon diffusion. The austenitisation reaction is seen to be very rapid; for instance, after 10s, the reaction was over 50% complete at all temperatures.

Considering first the finer structure, Fig. 3.14a, it appears that a stable volume fraction of austenite is reached more quickly at both low and high temperatures than at an intermediate temperature. Although

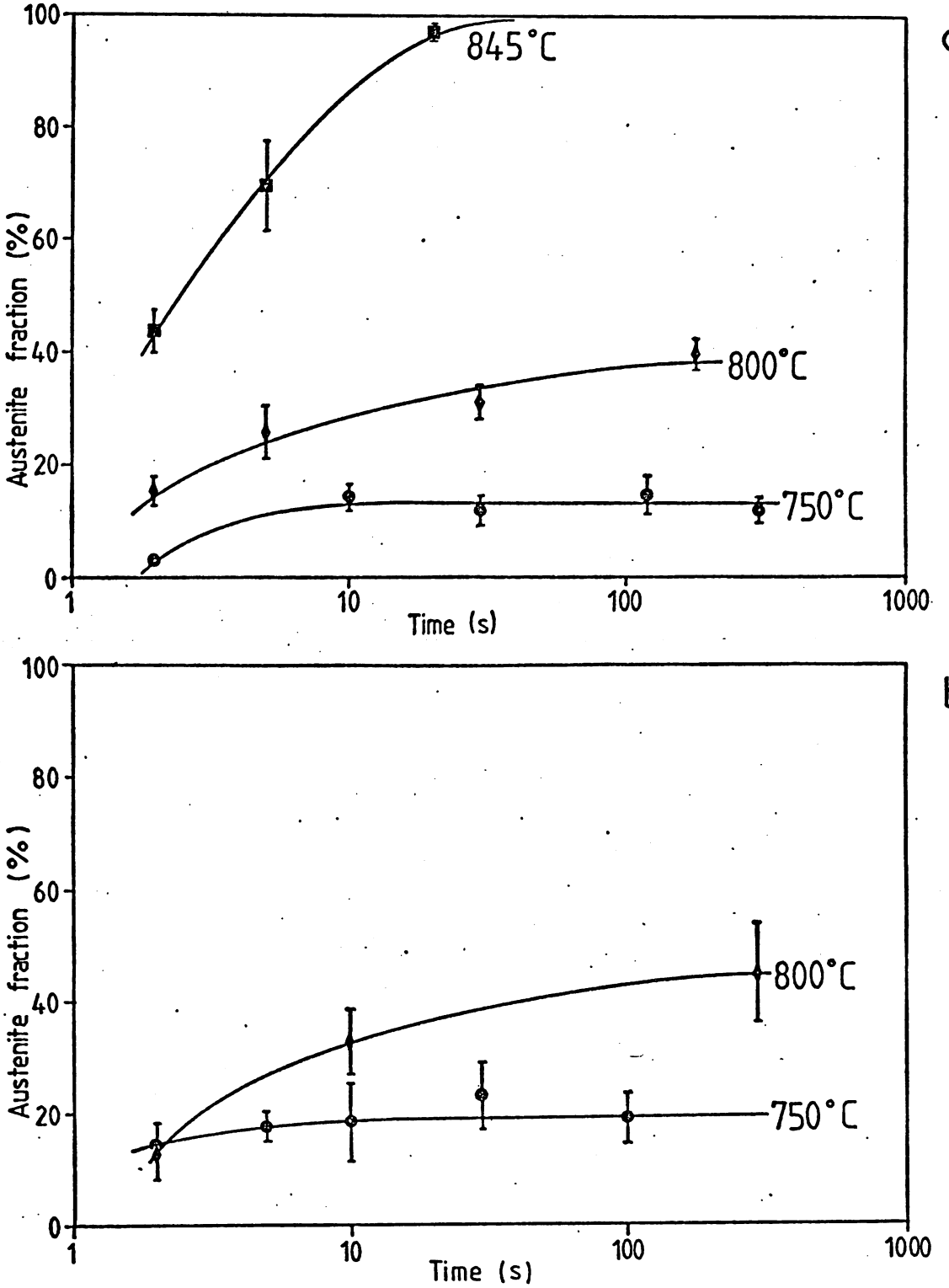

Fig. 3.14: Fraction of austenite formed as a function of time at different temperatures.
a) Finer ferrite-pearlite starting structure.
b) Coarser ferrite-pearlite starting structure.

the evidence is scanty, this behaviour could readily be explained by considering the interplay of reaction rate and equilibrium volume fraction at different temperatures. As the temperature rises, the effects of increased driving force and diffusion rate are offset by the increased equilibrium volume fraction of austenite which must form, and associated impingement. Also, above a critical temperature, at which the austenite volume fraction reaches the initial pearlite volume fraction, longer range diffusion is necessary to complete the transformation, and the growth rate after the pearlite has been consumed will be low. Thus, at an intermediate temperature, a longer time would be necessary to complete the reaction than at higher or lower temperatures.

The coarser starting structure exhibits similar behaviour (Fig. 3.14b), but no high temperature data are available, as difficulties in delineating the ferrite-martensite boundaries were encountered in the high temperature specimens.

The kinetics of reactions in the two-phase austenite plus ferrite region, and the effect of substitutional alloying elements such as manganese, will be considered in more detail in chapter 6.

In the finer structure, the cementite (whether as pearlite or as grain boundary carbides) had disappeared by 10s, 5s and 2s at 750°C, 800°C and 845°C respectively (as determined by electron microscopy). Above 750°C, therefore, it is obvious that a substantial part of the reaction occurs during the time after all cementite has dissolved. Similarly, pearlite had disappeared by 5s, 2s and 2s at 750°C, 800°C and 845°C in the coarser structure. Subsequent transformation must therefore involve the redistribution of dissolved carbon through austenite or ferrite. Since the austenite which forms at pearlite nodules rapidly consumes the pearlite, it seems likely that it initially inherits the full carbon content of these regions and thus contains excess carbon. Redistribution of this carbon to the interface then allows more austenite to form. At the later reaction stages, redistribution of carbon in ferrite also occurs.

The finer starting structure does not display a higher transformation rate, despite having a higher density of nucleation sites. Since the volume fractions formed in the two structures differ, it is deduced that the difference in composition of the two alloys has a

significant effect, and thus that a direct comparison of the kinetics of transformation in the two alloys cannot be made.

3.6 Concluding Remarks

The reaustenitisation of two ferrite-pearlite microstructures has been investigated at temperatures in the two phase austenite plus ferrite region in a low carbon, low manganese steel. Austenite first forms at a temperature a little below 700°C, and carbides become unstable at a slightly higher temperature, between 700°C and 725°C. Full transformation to austenite occurs at a little above 845°C.

In this low carbon alloy, containing pearlite colonies at ferrite grain corners, austenite forms first at pearlite-ferrite boundaries, as observed by previous workers (eg. Digges and Rosenberg 1943). The current work also shows that austenite can form at a ferrite grain boundary, particularly when the driving force is high, and when there are many carbides in the boundary.

3.6.1 Austenite at pearlite colonies

Nucleation at a pearlite colony occurs in several places on the boundary, but is never observed to occur inside the colony. Initial growth is along the boundary, followed by growth both into the pearlite and the ferrite. Pearlitic cementite dissolves in the advancing interface, and carbides in austenite are rarely observed in this system. This behaviour differs from that observed in higher carbon alloys, such as those investigated by Rose and Strassburg (1956), in which carbides remain in the austenite for long times. In the low carbon alloy used in this work, a considerable proportion of the transformation occurs after all pearlite and other carbides have disappeared, indicating that redistribution of carbon, particularly in austenite, is occurring.

3.6.2 Austenite at Ferrite Grain Boundaries

Austenite at ferrite grain boundaries nucleates at carbide particles, which dissolve rapidly. When carbon is available at the boundary, either as carbides in the boundary or as excess carbon in the austenite, the austenite forms grain boundary films. Only when the boundary carbon source is depleted does the austenite grow out into the ferrite, which is supersaturated with carbon at this stage. Under conditions of growth into supersaturated ferrite, curved high energy

interfaces, such as the austenite film boundaries, often become unstable (as described in chapter 2, section 2.6), and many such interfaces develop sideplates.

Crystallographic analysis showed that grain boundary austenite obeys a Kurdjumov-Sachs (or close to Kurdjumov-Sachs) orientation relationship with at least one ferrite grain. When both ferrite grains are themselves KS related to a common prior austenite, the new austenite forms KS related to both ferrites, and is likely to be in the same orientation as the prior austenite. The boundary between austenite and KS related ferrite nearly always exhibits facets at some part of the interface. Such planar sections of boundary are also observed when there is no KS relationship across the interface. Most interfaces, therefore, are able to adopt low energy configurations, whether a rational orientation relationship exists or not.

It is not clear from this work whether austenite prefers to grow into ferrite with which it has an orientation relationship or into ferrite with which it is unrelated.

3.6.3 Kinetics

The rate of austenite growth in the two phase region increases with temperature, but the time taken to complete the reaction depends also on the equilibrium volume fraction to be attained, and on carbon distribution and impingement effects. The reaction appears to reach completion most quickly at high and low temperatures in the two phase region, the process taking longer at intermediate temperatures.

3.6.4 Relevance to Dual Phase Steels

Intercritical annealing and quenching of low carbon ferrite-pearlite systems leads to large areas of martensite replacing prior pearlite colonies, and finer martensite areas at ferrite grain boundaries. Low volume fractions of martensite (20%), as required in dual phase steels, are best obtained by reaustenitising at temperatures low in the two-phase temperature range, where a stable, low volume fraction is rapidly attained. Ferrite which is initially fine grained leads to finer more closely spaced martensite nodules. However, each pearlite colony nucleates several austenite nodules which rapidly impinge, and produce one large martensite area on quenching. The inhomogeneous distribution of carbides in a ferrite-pearlite system is

therefore less efficient at producing finely dispersed martensite than is a homogeneous carbide distribution. The most finely dispersed martensite, and hence the best dual phase steel microstructures, are thus produced from microstructures containing a homogeneous distribution of nucleation sites, such as fine grained spheroidite, and not from ferrite-pearlite.

CHAPTER 4

PREPARATORY STUDIES OF AN Fe-10%Cr-0.2%C ALLOY STEEL

4.1 Introduction

The previous two chapters have described the reaustenitisation of various microstructures in low carbon, low alloy steels. The reaction was studied in the temperature regime in which austenite and ferrite coexist, and in all cases austenitisation was rapid, accompanied by rapid dissolution of carbides. The aims of the present investigation of a high alloy steel, of nominal composition Fe-10%Cr-0.2%C, (alloy E, appendix A1) are:

a) to study reaustenitisation when relatively stable carbides are present, and

b) to monitor the distribution of the substitutional alloying element throughout the reaction.

A vertical section through the Fe-Cr-C ternary equilibrium phase diagram at 0.2%C, taken from Bungardt et al (1959), is given in Fig. 4.1. It can be seen that at low temperatures, an alloy containing 10%Cr consists of ferrite and $M_{23}C_6$ type carbide. On raising the temperature above 800°C, some austenite forms, and the three phases are in equilibrium. Above about 840°C, all ferrite disappears, and both austenite and carbides exist up to about 910°C. Above this temperature only austenite is stable. There is thus a considerable temperature range (about 800°C - 910°C) in which reaustenitisation does not involve complete dissolution of carbides. It is therefore possible to investigate the effect of such carbides on moving interfaces, to study the dissolution of carbides in austenite as well as in ferrite, and to observe the effect on undissolved carbides of the austenite to martensite transformation during quenching.

In iron alloys, carbon is much more mobile than substitutional alloying elements. During phase transformations, redistribution of both carbon and alloying elements is generally necessary in order to achieve equilibrium. However, in some systems the free energy of the system can be lowered by a reaction which does not require redistribution of alloying elements; the reaction occurs relatively rapidly and

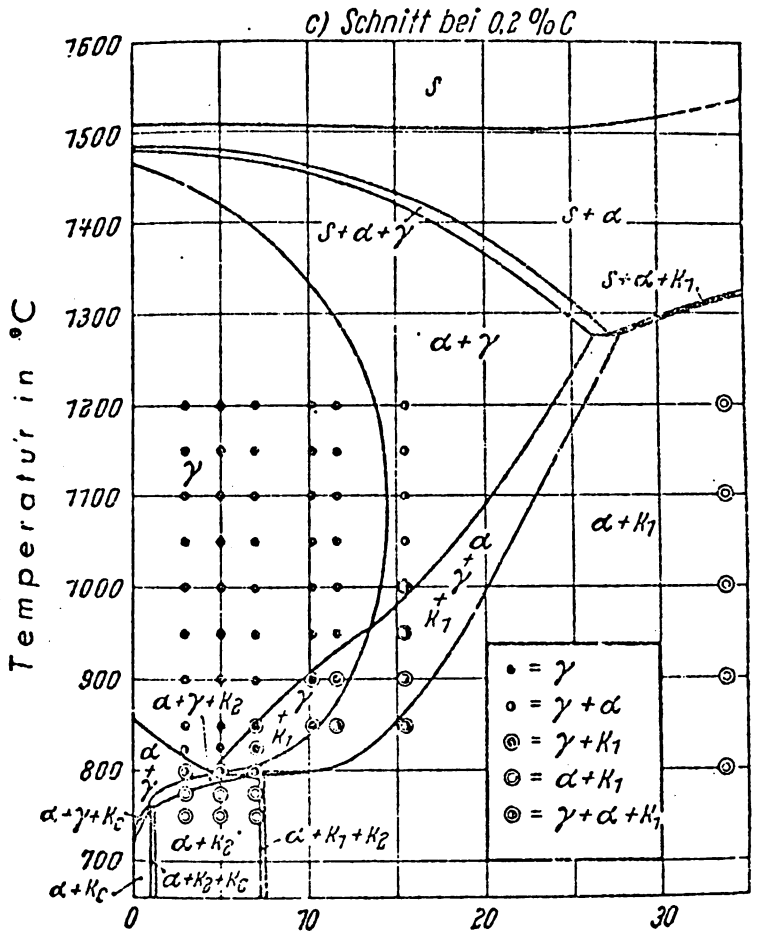

Fig. 4.1: Section through Fe-Cr-C ternary equilibrium diagram at 0.2%C (Bungardt, Kunze and Horn, 1958).

where $K_1 = M_{23}C_6$

$K_2 = M_7C_3$

$K_3 = M_3C$

metastable phases with non-equilibrium compositions are formed.

In order to investigate the movement of chromium during reaustenitisation of the Fe-10%Cr-0.2%C alloy, energy dispersive X-ray analysis in conjunction with both transmission electron microscopy (TEM) and scanning transmission electron microscopy (STEM) was employed. Quantitative analysis of small areas (less than 0.1μm) was thus possible, enabling both the initial ferrite-carbide microstructure and the partially reaustenitised and quenched microstructures to be characterised with respect to the chromium content. Unfortunately, the distribution of carbon cannot be determined by this technique, as X-ray intensities produced by elements of such low atomic number are small (see eg. Reed 1975).

This chapter describes preparatory work on the Fe-10%Cr-0.2%C system, dealing with the Ac_1 and Ac_3 temperatures, the ferrite-carbide microstructure and microanalysis. Chapter 5 then describes the reaustenitisation of the ferrite-carbide microstructure in this alloy.

In section 4.2, the determination by dilatometry of the Ac_1, Ac_3 and A_2 temperatures in Fe-10%Cr-0.2%C is presented. The development and characterisation of the ferrite-carbide microstructure, which acts as a starting structure for reaustenitisation, is described in section 4.3.

Section 4.4 outlines the basis of electron probe microanalysis, and in particular, reviews the literature on quantitative microanalysis of thin film samples. This technique is then used to determine the chromium distribution in the ferrite-carbide structure, and subsequently in the partially reaustenitised and quenched structures (chapter 5, section 5.3). The technique will later be used to determine the manganese distribution in a manganese steel (chapter 6).

The results of the preparatory work on the Fe-10%Cr-0.2%C alloy are summarised in section 4.5.

4.2 Determination of Ac_1, Ac_3 and A_2 Temperatures

In order to define the limits of the reaustenitisation reaction, the temperature at which austenite first forms (Ac_1), and the temperature at which all ferrite transforms to austenite (Ac_3) were determined, by continuous heating in a dilatometer. Using this method

it was not possible to determine the temperature at which all carbides dissolve, as dissolution occurs very slowly, but the magnetic change temperature or Curie point (A_2), was detected, and is included here for completeness.

Experimental details and methods of interpreting the results are given in section 4.2.1, and the results are presented in section 4.2.2.

4.2.1 Methods

A Theta Industries High Speed Dilatometer was used in this study. The Fe-10%Cr-0.2%C alloy specimens were in the form of cylinders, 15mm in length and 2.9mm in diameter. They were heated from room temperature to over 1000°C at various rates, from about 1°C/min to about 3000°C/min. Extrapolation of the results to zero heating rate then gave the equilibrium change temperatures (Ac_1, Ac_3, A_2).

Austenite has a more close packed crystal structure than ferrite, and thus the transformation from ferrite to austenite involves a decrease in volume. This is observed in the dilatometer as a reduction in specimen length. Typical dilatometer temperature and length traces, obtained during programmed continuous heating, are shown in Fig. 4.2. Thermal expansion occurs throughout the experiment, while transformations appear as changes in slope of the length trace. The Ac_1 is taken as the temperature at which the specimen length reaches a maximum, point A in Fig. 4.2. The Ac_3 is taken as the temperature at which no further change in slope of the length trace occurs, point B in Fig. 4.2.

The changes in slope before point A did not follow the same pattern at all heating rates. It was found, however, that the temperature trace always showed a slope change in this region. It was thought that these changes may by caused by the transition from magnetic to non-magnetic ferrite, rather than by the ferrite-plus-carbide to austenite transformation, and arguments to support this will now be given.

The specific heats of non-magnetic metals increase smoothly with temperature, the increase generally being small at temperatures above room temperature. Magnetic materials become non-magnetic at a well-defined temperature known as the Curie point, T_c, and the entropy change on heating through this point appears as an anomaly in the specific heat. A sharp rise in specific heat occurs just below the Curie

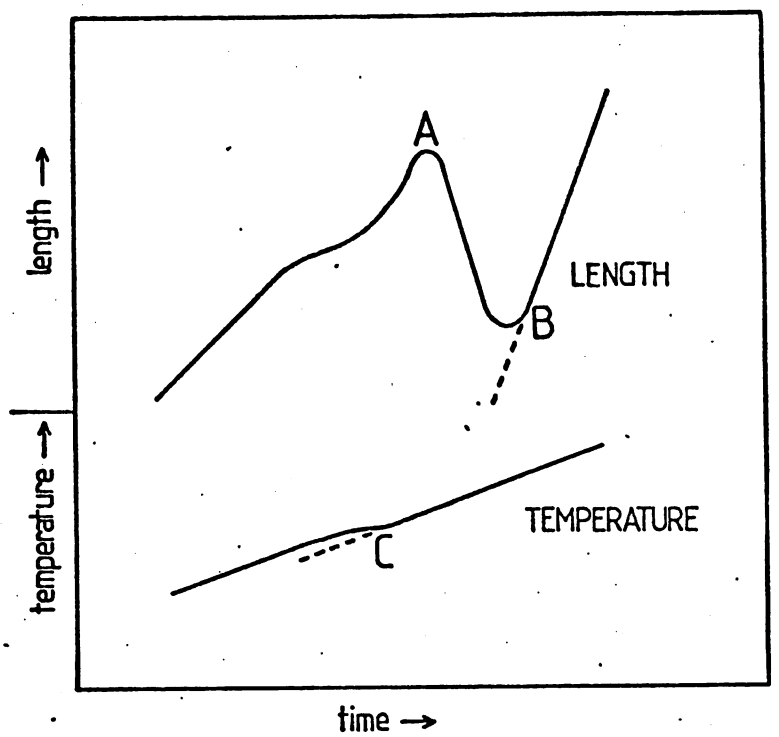

Fig. 4.2: Dilatometer length and temperature traces during continuous heating (schematic).

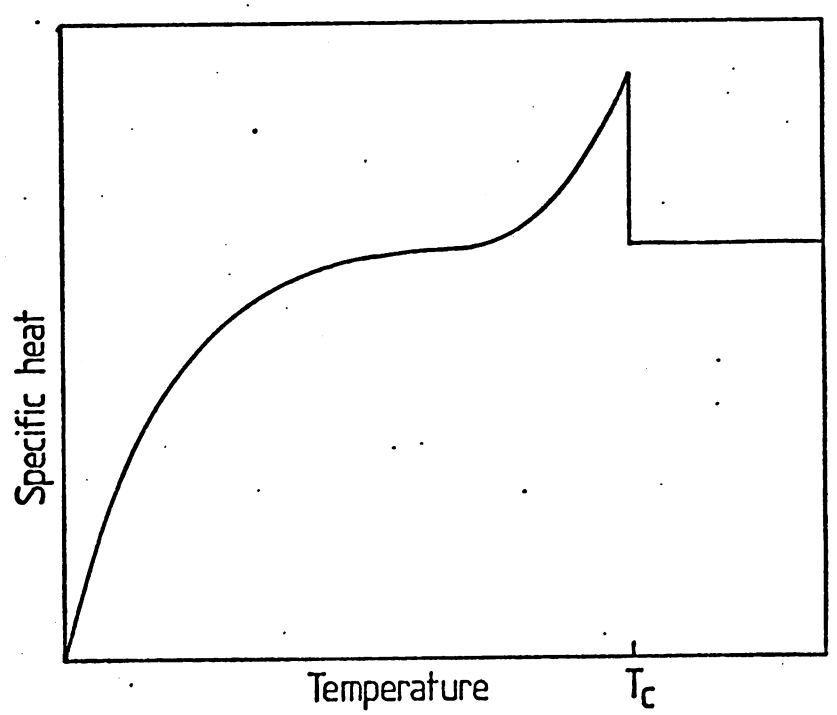

Fig. 4.3: Variation of specific heat with temperature for a magnetic material (schematic). T_c is the Curie temperature.

temperature, and at T_c itself, the specific heat falls back to a value similar to that obtained by extrapolating the smooth specific heat curve from lower temperatures (see eg. Bleaney and Bleaney 1976). Fig. 4.3 illustrates this behaviour schematically.

In the dilatometer, the rise in specific heat below T_c causes the temperature rise per unit of power input to fall as the Curie temperature is approached. The slope of the temperature curve therefore falls in this region. At T_c, the specific heat falls to its previous value, and the temperature curve resumes its previous slope, as at point C in Fig. 4.2. This point is therefore taken as the A_2 temperature.

It should be noted that changes in specific heat are accompanied by changes in thermal expansion behaviour, and the two changes together have a complicated effect on the specimen length during continuous heating. It is therefore better to obtain the A_2 value directly from the dilatometer temperature trace than from the length trace.

4.2.2 Results

The Ac_1, Ac_3 and A_2 temperatures determined during continuous heating experiments are plotted as a function of heating rate in Fig. 4.4. It can be seen that the Ac_1 and Ac_3 temperatures increase with increasing heating rate, as expected, showing that the reactions involved are thermally activated and time dependent. The A_2 temperature is almost constant with heating rate, showing that demagnetisation is complete almost instantaneously at a well defined temperature.

The Ac_1 and Ac_3 temperatures obtained by extrapolating the curves to zero heating rate are found to be 772±5°C and 815±5°C respectively. These are lower than those predicted by Bungardt et al (1958) (see Fig. 4.1), probably because of slight differences in composition. The A_2 temperature is found to be 757°C, which is in fair agreement with that quoted by Hansen (1958) for a binary iron alloy containing 10%Cr (about 740°C).

4.3 Development of the Ferrite-Carbide Microstructure

The starting structure for reaustenitisation of the Fe-10%Cr-0.2%C alloy consisted of ferrite and $M_{23}C_6$ carbides, which were in the form of fibres, plates or particles, as described by Bee et al (1979). This microstructure was obtained by isothermal transformation from austenite

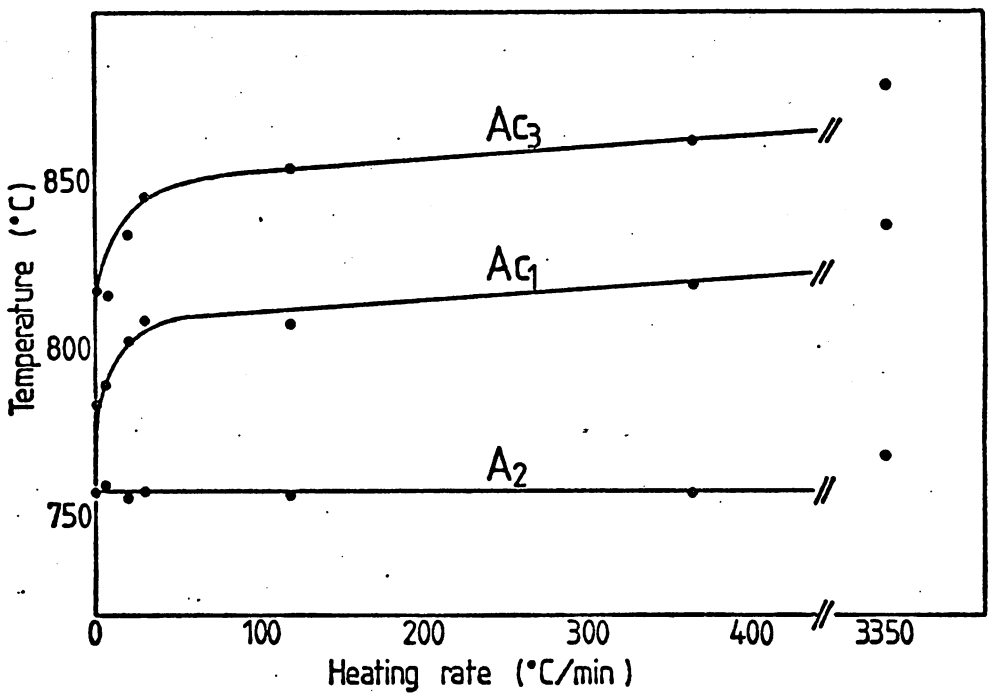

Fig. 4.4: Variation of Ac_1, Ac_3 and A_2 temperatures with heating rate.

at 700°C for one hour, and metallographic observations on the development of the ferrite-carbide microstructure are presented in section 4.3.1. Determination of the chromium distribution in both ferrite and carbides will be reported in section 4.4.

4.3.1 Isothermal Transformation at 700°C

In order to understand the final ferrite-carbide microstructure, it was necessary to follow the progress of the transformation by partial transformation and quenching. After allowing austenite to transform for 5 minutes at 700°C, ferrite had been nucleated at austenite grain boundaries, which were generally decorated with coarse $M_{23}C_6$ carbides. Fig. 4.5 shows ferrite during a very early stage of growth around a carbide in an austenite grain boundary, while Fig. 4.6 shows a later stage of growth in which ferrite has grown considerably into one austenite grain. The line of the prior austenite grain boundary in Fig. 4.6 is delineated by coarse $M_{23}C_6$ particles, and the ferrite immediately on either side of the boundary is seen to be precipitate free. This may well be due to chromium depletion in the vicinity of coarse grain boundary carbides (see section 4.4.4). Subsequent growth of ferrite is accompanied by the precipitation of carbides, and occurs predominantly into one grain, presumably that which allows lower energy interfaces due to crystallographic relationships between ferrite, austenite and carbide (Howell et al 1979). Electron diffraction showed that all carbides were $M_{23}C_6$, and that carbides in one particular area were often all in the same orientation relative to the ferrite.

The earliest carbides to form were generally in the form of discrete particles, and were very fine. As the reaction proceeded, a higher proportion of fibrous and plate-like carbides formed, as shown in Fig. 4.7 (fully transformed), and coarsening occurred.

The fully transformed microstructure then consists of coarse ferrite grains with large carbides both at ferrite grain boundaries and at prior austenite grain boundaries, and with fibrous, plate-like and equiaxed particulate carbides within the grains. Narrow precipitate free zones occur at prior austenite grain boundaries, and large precipitate free zones at some ferrite grain interiors were also found.

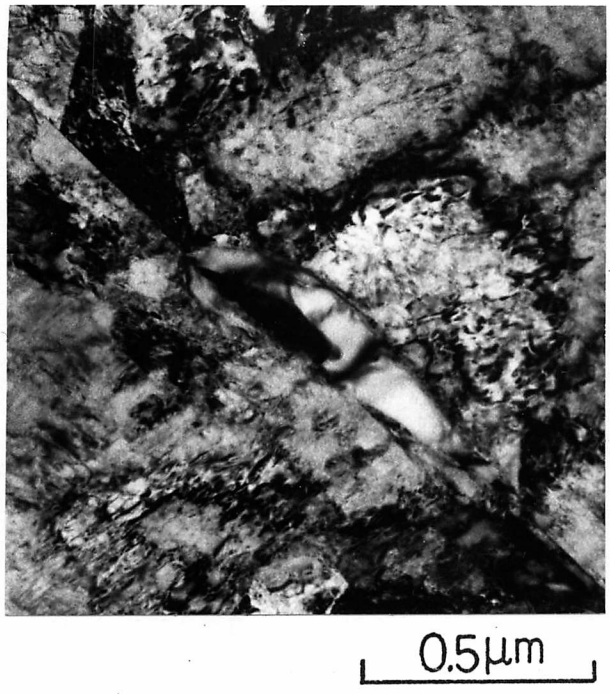

Fig.4.5: Ferrite nucleated at a carbide (dark) in an austenite (now martensite) grain boundary. Transformed from austenite, 5 minutes 700°C.

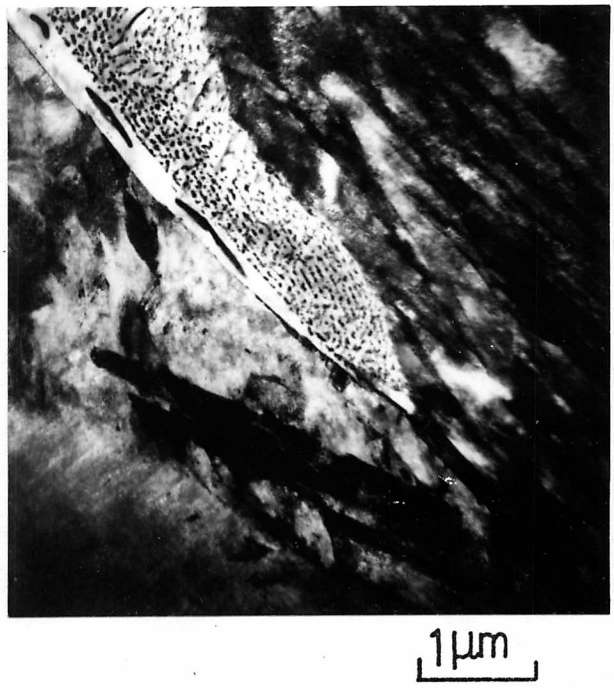

Fig.4.6: Ferrite and fine carbides growing at an austenite grain boundary (delineated by coarse carbides). Transformed 10 mins. 700°C.

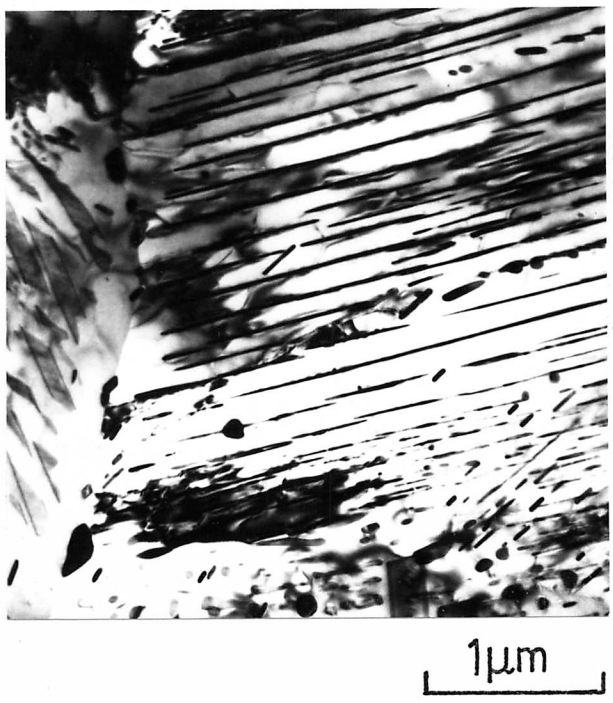

Fig.4.7: Ferrite-carbide microstructure. Transformed 1 hour 700°C.

4.4 Microanalysis

Electron probe microanalysis provides a means of chemically analysing small areas of solid samples. When a focussed electron beam irradiates the sample, the atoms emit characteristic X-rays. The emergent X-rays can be monitored by either a wavelength dispersive or an energy dispersive analyser. The X-ray energies indicate which elements are present, and a comparison of X-ray intensities can provide some idea of the relative proportions of the elements present.

The electron probe microanalyser has long been used for the analysis of bulk samples. The penetration of an electron beam in metals is of the order of a few microns, as is the amount of beam spreading which occurs over this distance. The spatial resolution of the technique can therefore never be better than a few microns. Examination of the detailed behaviour of the electrons and X-rays as they travel through the specimen has made quantitative, as well as qualitative, analysis possible. Quantitative microanalysis of bulk specimens, by application of ZAF (atomic number, absorption and fluorescence) correction factors to intensity ratios, is a well established technique, and details can be found in standard texts eg Reed (1975).

Recently, attempts have been made to improve the spatial resolution of microanalysis by using thin (about 100nm) samples, in which beam spreading occurs to a much lesser degree, and resolutions of about 10nm can be obtained. The microanalysis system is generally incorporated in a TEM or STEM. The problems inolved in quantitative analysis of thin samples are similar to those encountered in bulk specimens, except that the magnitude of the various interactions between specimen, electrons and X-rays, now depends on specimen thickness. In general, quantitative analysis of thin samples is not as well understood as analysis of bulk samples, and a review of the technique will now be given.

4.4.1 Quantitative microanalysis of thin specimens

In quantitative analysis, the ratio of concentrations of two elements is taken to be proportional to the ratio of intensities of their characteristic X-rays, ie:

$$\frac{I_A}{I_B} = k_{AB} \frac{C_A}{C_B} \qquad (4:1)$$

where I_A, I_B are the measured intensities of K_α X-rays of elements A,B; C_A, C_B are the concentrations (weight fractions) of elements A,B; k_{AB} is the constant of proportionality for elements A,B.

k_{AB} is a function of atomic number and absorption, but is a constant for a given instrument, and can be calculated. For an energy dispersive system, the effect of analyser characteristics such as window thickness and detector material can be taken into account. This effect is generally small when elements of relatively high atomic number are being analysed, and need not be further considered here. The proportionality between intensities and concentrations breaks down when fluorescence is occurring.

a) Atomic Number Correction

The atomic number correction is independent of thickness, and the constant of proportionality, k_o, is given (eg. Goldstein et al 1977) by:

$$k_o = \frac{A_A(Q_K w_K a)_B}{A_B(Q_K w_K a)_A} \qquad (4:2)$$

where A is the atomic weight, Q_K is the K shell ionisation cross section, w_K is the fluorescence yield, and a is the ratio of $K\alpha$ radiation to $(K\alpha+K\beta)$ radiation.

k_o values have been calculated by eg. Goldstein et al (1977), and determined experimentally by eg. Lorimer et al (1977). The best agreement between experimental and calculated data was found when the ionisation cross-sections (Q) were calculated from a formula given by Green and Coslett (1961);

$$Q_K = 7.92 \times 10^{-20} \frac{1}{U} \ln U \frac{1}{E_K^2} \ (cm^2) \qquad (4:3)$$

where $U = E_o/E_K$, E_o = accelerating voltage, E_K = energy of K_α radiation.

b) Absorption

The k_o value obtained so far is effectively for an infinitely thin film, in which no absorption occurs. The k value which takes account of absorption, k_{AB}, is given (eg. by Goldstein et al 1977) as:

$$k_{AB} = k_0 \exp\left[-\left(\left(\frac{\mu}{\rho}\right)^{B}_{AB} - \left(\frac{\mu}{\rho}\right)^{A}_{AB}\right) \operatorname{cosec}\alpha \left(\frac{\rho t}{2}\right)\right] \qquad (4:4)$$

where $(\mu)^{A}_{AB}$ is the mass attenuation coefficient of A X-Rays in a thin film consisting of elements A and B, etc., ρ is the density of the specimen, α is the X-ray take-off angle and t is the film thickness.

The $(\mu/\rho)^{A}_{AB}$ vary with concentration, and it is found (eg Mirkin 1964) that

$$\left(\frac{\mu}{\rho}\right)^{A}_{i} = \sum_{i} c_i \left(\frac{\mu}{\rho}\right)^{A}_{i} \qquad (4:5)$$

where the summation is carried out over the different elements, i (in the present case, A and B). Thus k_{AB} can be readily calculated for any two component system.

It follows that the effect of absorption will be important if the film thickness is large (greater than about 50nm) or if the difference in mass absorption coefficients, $\left(\left(\frac{\mu}{\rho}\right)^{A}_{AB} - \left(\frac{\mu}{\rho}\right)^{B}_{AB}\right)$, is large.

c) Fluorescence

Fluorescence occurs when X-rays of one element are excited by higher energy X-rays. The higher energy X-rays may be $K\alpha$, $K\beta$ or L radiation from elements of higher atomic number, or may be continuum background radiation. The overall effect of fluorescence is to increase the emergent intensity of lower energy X-rays, and to decrease the intensity of higher energy X-rays.

Philibert and Tixier (1975) consider the fluorescence of element A by $K\alpha$ radiation of element B in a thin film, and give the intensity of A due to fluorescence, I_f, as a fraction of the primary A radiation, I_A as:

$$\frac{I_f}{I_A} = 2w_B C_B \frac{(r_A - 1)}{r_A} \frac{A_A}{A_B} \mu^{B}_{A} \mu^{B}_{AB} \frac{\nu_A}{\nu_B} t^2 \qquad (4:6)$$

where r is the absorption edge jump ratio, and ν_A is the characteristic frequency of A radiation, etc. The fluorescence correction is small if $\mu^{B}_{AB} t \ll 1$, and is often negligible for thin metal foils (Philibert and Tixier 1975). The fluorescence due to continuum X-radiation and radiations other than $K\alpha$ are also often negligible.

d) Beam broadening

Assuming that the effective X-ray source size is that within which 90% of the electron trajectories lie, Goldstein et al (1977) give the beam spreading, b, as

$$b = 6.25\times10^{5}\frac{Z}{E}\left(\frac{\rho}{A}\right)^{\frac{1}{2}}t^{3/2} \qquad (4:7)$$

where Z is the atomic number. The beam broadening, b, must be added to the initial beam diameter, and is generally a significant proportion of the final beam diameter. The resolution which can be achieved is thus a function of beam spreading.

4.4.2 Accuracy

The accuracy of microanalysis is limited by

a) the accuracy with which intensities can be measured (counting statistics),

b) machine factors (such as detector materials, noise levels) and

c) the uncertainties in the correction factors which are applied to the results.

It is felt that the technique of microanalysis of thin films is not sufficiently advanced to enable absolute quantitative microanalysis. However, within any one system the results are consistent, and relative compositions can be treated with a high degree of confidence.

4.4.3 Methods of Microanalysis in Fe-10%Cr-0.2%C

a) Experimental details

Microanalysis was carried out in the present work using either an EDAX or a Link Energy Dispersive System, attached to a Philips 400 electron microscope which was operated both in the TEM and STEM mode. All results reported in this chapter were obtained from the EDAX system.

The two phases present, ferrite and $M_{23}C_6$, were analysed separately, and the results are reported in sections 4.4.4 and 4.4.5 respectively. It was possible to analyse the ferrite between carbides in a thin film sample (about 100nm thick) without interference from the carbides. The carbides, however, had to be extracted from the bulk sample before analysis, to avoid interference from the ferrite. A standard extraction replication technique was used (as described in appendix A2).

For each analysis, several thousand X-ray counts were obtained from the elements iron and chromium, such that there were at least one thousand counts of the less abundant element. Correction factors (see following section) were applied, and the error in the final composition of each analysis, including counting errors and errors introduced by the correction procedure, was generally of the order of 4% of the composition. The average composition of a particular type of area was obtained from several measurements, usually 10 to 20, and the error in the average value is taken to be the standard deviation of the mean. During microanalysis, the presence of carbon was ignored, and the results are in the form of relative proportions of Fe and Cr.

b) Correction Factors for Cr and Fe

Using the formulae quoted in section 4.4.1, and data from standard texts (eg Reed 1975), the correction factors for microanalysis of thin films containing Cr and Fe were calculated. k_o was calculated as 1.064, and all intensity ratios were corrected by this factor.

Microanalysis was carried out both on the ferrite, which had a chromium content of the order of 10%, and on extracted carbides which contained 50-80%Cr. The difference in mass attenuation coefficients $\left(\left(\frac{\mu}{\rho}\right)^{Cr}_{FeCr} - \left(\frac{\mu}{\rho}\right)^{Fe}_{FeCr}\right)$ varies with composition, and calculated values are given in Table 4.1. The value can be seen to reach a minimum near 10%Cr, and thus absorption effects in the ferrite are very low. The fluorescence of Cr X-rays by Fe X-rays was calculated to be negligible in thin films of ferrite.

Extracted carbides were often relatively thick (>100nm), and more care had to be taken with their microanalysis. The thickness of the carbides was taken to be similar to their width, which could be readily estimated in the electron microscope. The absorption effect is large at high chromium levels (see table 4.1), and microanalyses of carbides of all thicknesses were corrected for absorption. The fluorescence effect is again found to be negligible in most cases, although it becomes significant for carbides which are more than about 1μm thick.

During analysis of a particular area, care was taken to ensure that beam spreading did not cause interference from surrounding areas. A beam diameter of 10nm was generally used, and for a foil thickness of about 100nm, beam spreading was calculated to be 20nm.

TABLE 4.1: Fe and Cr mass attenuation coefficients as a function of composition, x.

x_{Fe}	x_{Cr}	$x_{Fe}\left(\frac{\mu}{\ell}\right)^{Cr}_{Fe}$	$x_{Cr}\left(\frac{\mu}{\ell}\right)^{Cr}_{Cr}$	$\left(\frac{\mu}{\ell}\right)^{Cr}_{FeCr}$	$x_{Fe}\left(\frac{\mu}{\ell}\right)^{Fe}_{Fe}$	$x_{Cr}\left(\frac{\mu}{\ell}\right)^{Fe}_{Cr}$	$\left(\frac{\mu}{\ell}\right)^{Fe}_{FeCr}$	$\left(\frac{\mu}{\ell}\right)^{Cr}_{FeCr} - \left(\frac{\mu}{\ell}\right)^{Fe}_{FeCr}$
1.00	0.00	115.0	0.0	115.0	72.8	0.0	72.8	42.2
0.95	0.05	109.3	4.5	113.8	69.2	24.5	93.7	20.3
0.90	0.10	103.5	9.0	112.5	65.5	49.0	114.5	-2.0
0.85	0.15	98.0	13.5	111.5	61.9	73.5	135.4	-23.9
0.80	0.20	92.0	18.0	110.0	58.2	98.0	156.2	-46.2
0.75	0.25	86.3	22.5	108.8	54.6	122.5	177.1	-68.3
0.70	0.30	80.5	27.0	107.5	51.0	147.0	198.0	-90.5
0.65	0.35	74.8	31.5	106.3	47.3	171.5	218.8	-112.6
0.60	0.40	69.0	36.0	105.0	43.7	196.0	239.7	-134.7
0.55	0.45	63.3	40.5	103.8	40.0	220.5	260.9	-157.1
0.50	0.50	57.5	45.0	102.5	36.4	245.0	281.4	-178.9
0.45	0.55	51.8	49.5	101.3	32.8	269.4	302.3	-201.1
0.40	0.60	46.0	54.0	100.0	29.1	294.0	323.1	-223.1
0.35	0.65	40.3	58.5	98.8	25.5	318.5	344.0	-245.2
0.30	0.70	34.5	63.0	98.5	21.8	343.0	364.8	-267.3
0.25	0.75	28.8	67.5	97.5	18.2	367.5	385.7	-289.2
0.20	0.80	23.0	72.0	95.0	14.6	392.0	406.6	-311.6
0.15	0.85	17.3	76.5	93.8	10.9	416.5	427.4	-333.6
0.10	0.90	11.5	81.0	92.5	7.3	441.0	448.3	-355.8
0.05	0.95	5.8	85.5	91.3	3.6	465.5	469.1	-377.9
0.00	1.00	0.0	90.0	90.0	0.0	490.0	490.0	-400.0

4.4.4 Chromium Distribution in Ferrite

Microanalysis of ferrite was carried out in three distinct areas, namely:

a) in large precipitate free areas,

b) in precipitate free areas associated with coarse carbides at prior austenite grain boundaries, and

c) in ferrite between fibrous or particulate carbides.

The bulk precipitate free areas were found to have an average composition of 10.4±0.1%Cr (the quoted error is the standard deviation of the mean), close to the overall chromium content of the alloy, which wet chemical analysis showed to be 9.9%Cr. The discrepancy between these values indicates that microanalysis results cannot be taken as absolute values. The lack of carbide precipitation in these areas is therefore deduced to be due to a local carbon depletion, and not to a lack of chromium (see also Howell et al 1980). The areas must therefore represent the last austenite regions to transform, the ferrite forming after all the carbon has precipitated elsewhere as carbides.

The precipitate free areas at prior austenite grain boundaries, on the other hand, were found to be low in chromium, at 8.4±0.2%Cr, showing that these areas are chromium (and probably carbon) depleted due to heavy carbide precipitation on the grain boundary.

Ferrite between carbide fibres and particles was also found to have a lower than bulk chromium content, the average composition being 8.3±0.2%Cr, showing that the formation of carbides drains chromium from the surrounding areas. Fig. 4.8a shows an example of the results obtained from a partially transformed specimen (10 minutes at 720°C). A series of microanalyses were taken across the ferrite-martensite interface, the ferrite analyses being taken midway between parallel fibres, in an area similar to that shown in Fig. 4.9. Considerable scatter of the data occurs, which is thought to reflect a real scatter of chromium content, as variations are larger then the expected errors (which include counting errors, and errors introduced by application of correction procedures). It can be seen that the chromium content of the austenite (now martensite) is considerably higher than that in the ferrite, and that no long range chromium concentration gradient in the ferrite exists. Redistribution of chromium therefore seems to occur predominantly in the vicinity of the interface.

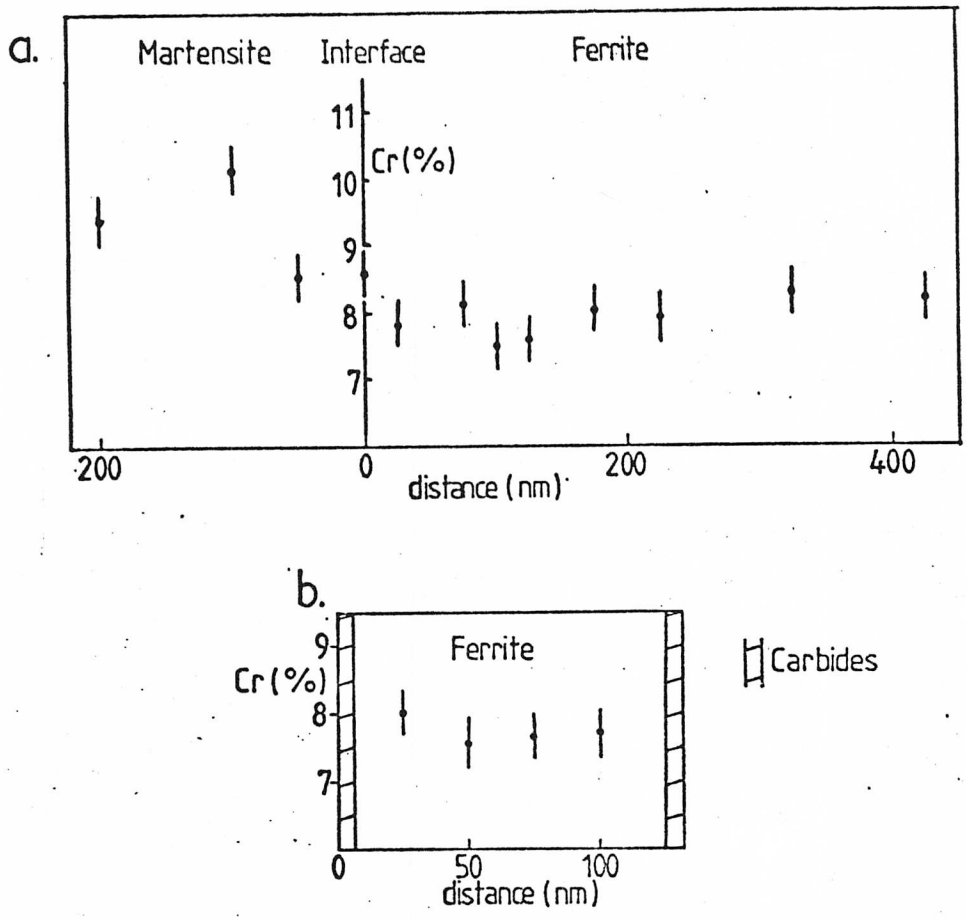

Fig. 4.8: Microanalysis of ferrite and martensite.
a) Midway between parallel fibrous carbides. 10 mins 700 C.
b) Perpendicular to fibres. 1 hour 700°C.

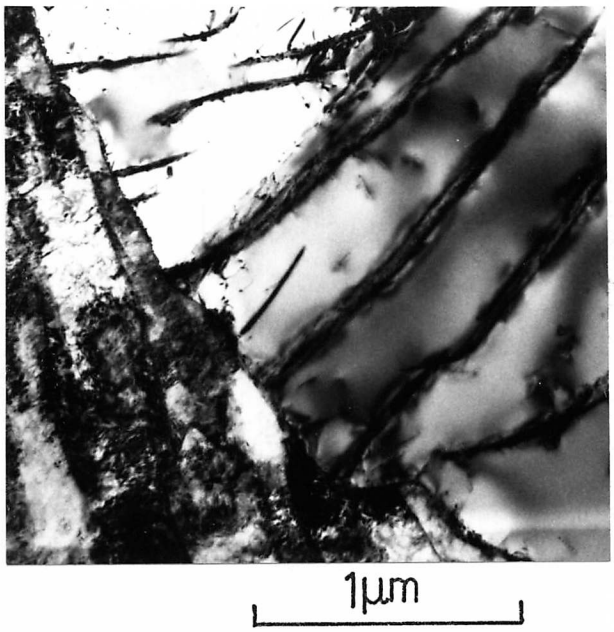

Fig. 4.9: Ferrite and fibrous carbides at an interface with austenite (now martensite). 10 mins 700°C.

Fig. 4.8b shows a series of microanalyses taken perpendicular to two fibrous carbides in a fully transformed specimen. No significant trend in variation of chromium content with distance from carbides was detected in any such area.

It was also noted that the average chromium content of ferrite between fibres changed little with time of transformation.

4.4.5 Chromium Content of Carbides

Carbides were successfully removed from the ferrite by the carbon extraction replication technique. The replicas obtained in this way confirmed that the carbides were in the form of fibres, plates or roughly equiaxed particles, and electron micrographs of the carbides in such replicas are given in Fig. 4.10. The average chromium content of each type of carbide in partially and fully transformed specimens was obtained by microanalysis.

It was found that the chromium content of fine particles and fibres (of the order of 0.1μm wide) was consistently higher than that of coarse grain boundary carbides, (about 1μm wide) and plates. After partial transformation for 5 minutes at 700°C, the fine carbides contained 67±2%Cr while the coarser carbides contained 56±1%Cr. After 10 minutes transformation, the chromium content of the carbides had increased a little, and after complete transformation (1 hour at 700°C) the chromium content of the fine carbides had increased to 79±2%Cr, while that of the coarse carbides had also increased to 68±4%Cr.

The increase in chromium content with time is interpreted as being due to the early carbides forming rapidly with insufficient time to allow full chromium partitioning; during further time at temperature further partitioning of chromium to the carbides can occur. The lower chromium content of the coarser carbides is attributed to the longer distance over which diffusion is necessary within a carbide in order to change its composition.

Assuming that all the carbon in the alloy is taken up as carbides, and having measured the chromium content of the carbides, it is possible to estimate the expected chromium level of the ferrite. This is calculated to be about 7.8%Cr, which is in fair agreement with the measured value of 8.4%Cr (see previous section).

Concentration gradients in fibres or plates were never detected,

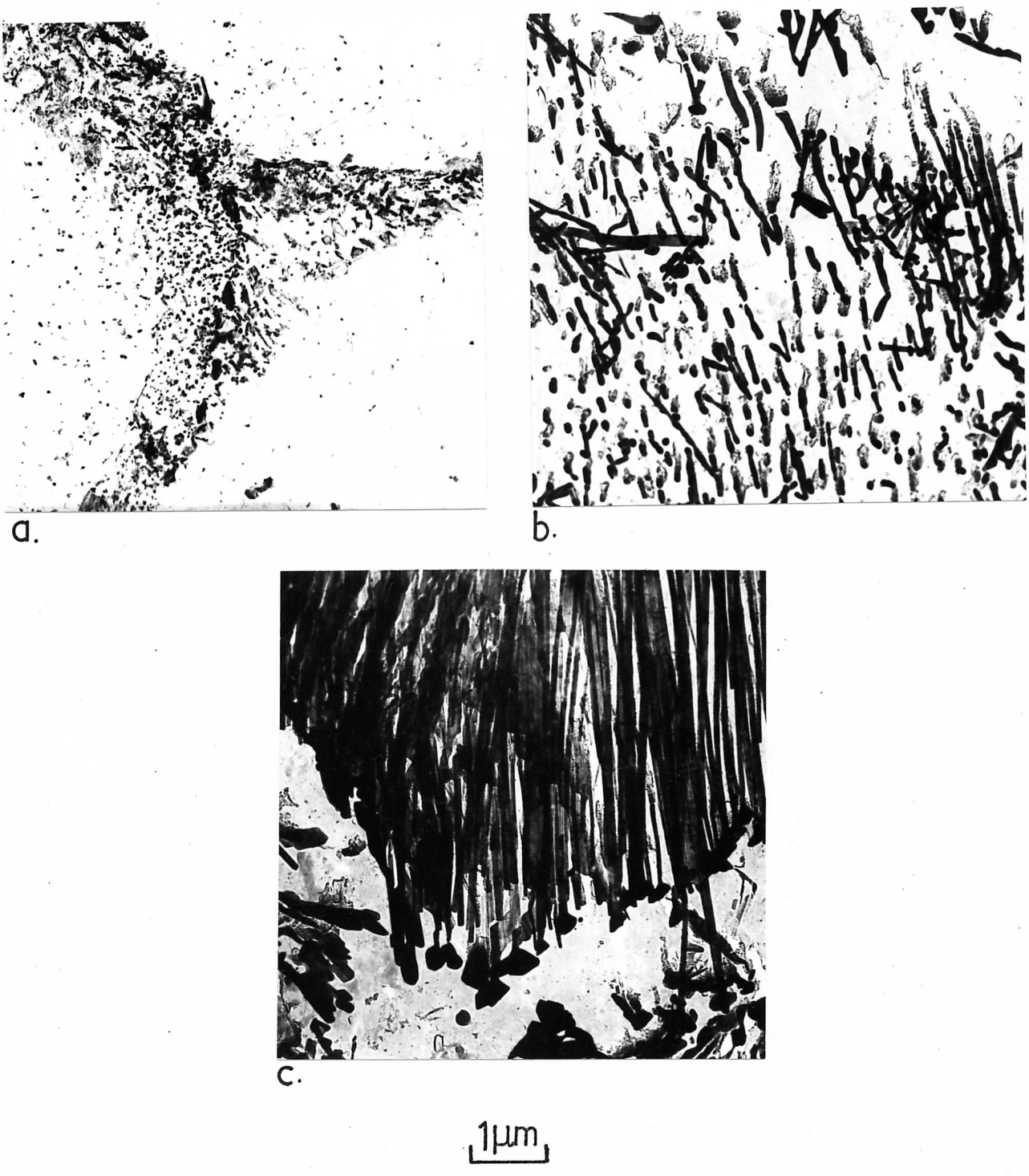

Fig. 4.10: Extraction replicas of $M_{23}C_6$ carbides.
a) 10 mins 700°C. Fine carbides, from ferrite at prior austenite grain boundaries.
b) 1 hour 700°C. Fibrous and particulate carbides.
c) 1 hour 700°C. Plate-like and coarse grain boundary carbides.

either in partially transformed specimens behind the transformation front, or in fully transformed specimens.

4.5 Summary

In an Fe-10%Cr-0.2%C alloy, the Ac_1 and Ac_3 temperatures have been found to be 772°C and 815°C respectively. The Curie temperature is 757°C.

During the decomposition of austenite in an Fe-10%Cr-0.2%C steel, ferrite nucleates and grows preferentially in the chromium (and carbon) depleted regions around carbides in the austenite grain boundaries. The ferrite at the prior austenite boundary is therefore carbide free, but ferrite growth is generally accompanied by precipitation of $M_{23}C_6$ type carbides. The first carbides to form are mostly fine and equiaxed, while at later stages of transformation, fibrous and plate-like carbides become predominant. The ferrite between carbides, and that near prior austenite grain boundaries, has a chromium content lower than the alloy composition. Coarse carbides exist at grain boundaries; these and plate-like carbides contain less chromium than the finer carbides. All carbides coarsen with time at the transformation temperature, and considerably increase their chromium content. The corresponding decrease in chromium content of the ferrite with time is not detected. The last austenite to transform does so after all the carbon has precipitated elsewhere as carbides; the last ferrite regions are therefore carbide free, and contain high levels of chromium. Concentration gradients in ferrite or carbides were never detected, either behind the transformation front or in fully transformed material.

The starting structure for reaustenitisation therefore consists of ferrite of composition 8.3±0.2%Cr containing a distribution of fibrous and particulate carbides of composition 79±2%Cr and plate-like carbides of composition 68±4%Cr. Coarse carbides, of composition similar to that of the plate-like carbides, exist at prior austenite and at ferrite grain boundaries, and the ferrite in these regions contains 8.4±0.2%Cr. Large precipitate free ferrite regions, containing high chromium levels (10.4±0.1%Cr) are also present.

CHAPTER FIVE

REAUSTENITISATION OF AN Fe-10%Cr-0.2%C ALLOY STEEL

5.1 Introduction

In order to understand the complicated reaustenitisation reaction in the Fe-10%Cr-0.2%C alloy, it was necessary to characterise the ferrite-carbide starting structure, as described in the previous chapter, and to employ several separate techniques to investigate the transformation to austenite. Electron metallography of partially reaustenitised and quenched samples is described in section 5.2, while the results of energy dispersive X-ray analysis, which was used to determine the chromium contents of small regions, are given in section 5.3. Kinetic data were obtained by isothermal dilatometry, and these are presented in section 5.4. The conclusions drawn from the results of all techniques are given in section 5.5.

5.2 Metallography of Reaustenitisation

The starting material for reaustenitisation was the Fe-10%Cr-0.2%C alloy with the ferrite-carbide microstructure described in chapter 4, section 4.3. Specimens were made from 3mm diameter rod, and were partially reaustenitised in a salt pot before being water quenched. Reaustenitisation was carried out at temperatures in the range 790°C to 905°C, for times of 2s to 200s.

Although many etching techniques for optical metallography were tried, it proved impossible to distinguish reliably between martensite and ferrite, probably because both phases contain a distribution of fine carbides. Metallographic examination was therefore restricted to transmission electron microscopy.

The general characteristics of the reaustenitisation reaction were as follows:

a) Nucleation was slow, and growth rapid, at all temperatures in the range investigated, such that partially reaustenitised and quenched samples always contained few large martensite areas, rather than many small areas.

b) The transformation to austenite occurred much more rapidly than the dissolution of carbides.
c) The carbides impeded the motion of austenite-ferrite interfaces, and subsequently dissolved and spheroidised in austenite.
d) Towards the end of the transformation, the ferrite which had not transformed was often carbide free, and was always heavily dislocated as a result of transformation stresses.

Several aspects of the reaustenitisation reaction, as observed by TEM, will now be considered in more detail in sections 5.2.1 to 5.2.6.

5.2.1 Extent of the Reaction

A reaustenitisation Time-Temperature-Transformation (TTT) diagram, determined by electron metallography, is presented in Fig. 5.1. It can be seen that nucleation is generally slow, but that after nucleation growth occurs rapidly. At a temperature just above the Ac_3 (815°C), complete transformation of ferrite to austenite occurs in a little over 100s, and the nucleation incubation time and time to austenite reaction finish decrease with increasing temperature. Thus, even in a highly alloyed steel, the reaustenitisation reaction is seen to occur very rapidly, as in low alloy steels. The dissolution of alloy carbides, however, occurs much more slowly in this steel than does the dissolution of cementite in plain carbon steels; some carbides were present in all the samples of Fig. 5.1.

It should be noted that the data for the TTT curve were obtained from thin foil TEM samples, and as in general only one foil was prepared and examined for each heat treatment, the results may not always be representative of the bulk samples. No attempt was made to extend the TTT curve to the three phase austenite-ferrite-carbide temperature regime below 815°C, nor was the dissolution of carbides monitored. These problems were investigated dilatometrically and will be discussed in section 5.4.

5.2.2 Nucleation

Because of rapid growth, austenite in the early stages of growth after nucleation was difficult to observe. Fig. 5.2 shows the only example of an austenite nodule less than a few microns in size which was seen during investigation of a large number of samples. Here, nucleation is seen to have occurred at a ferrite grain boundary. Even

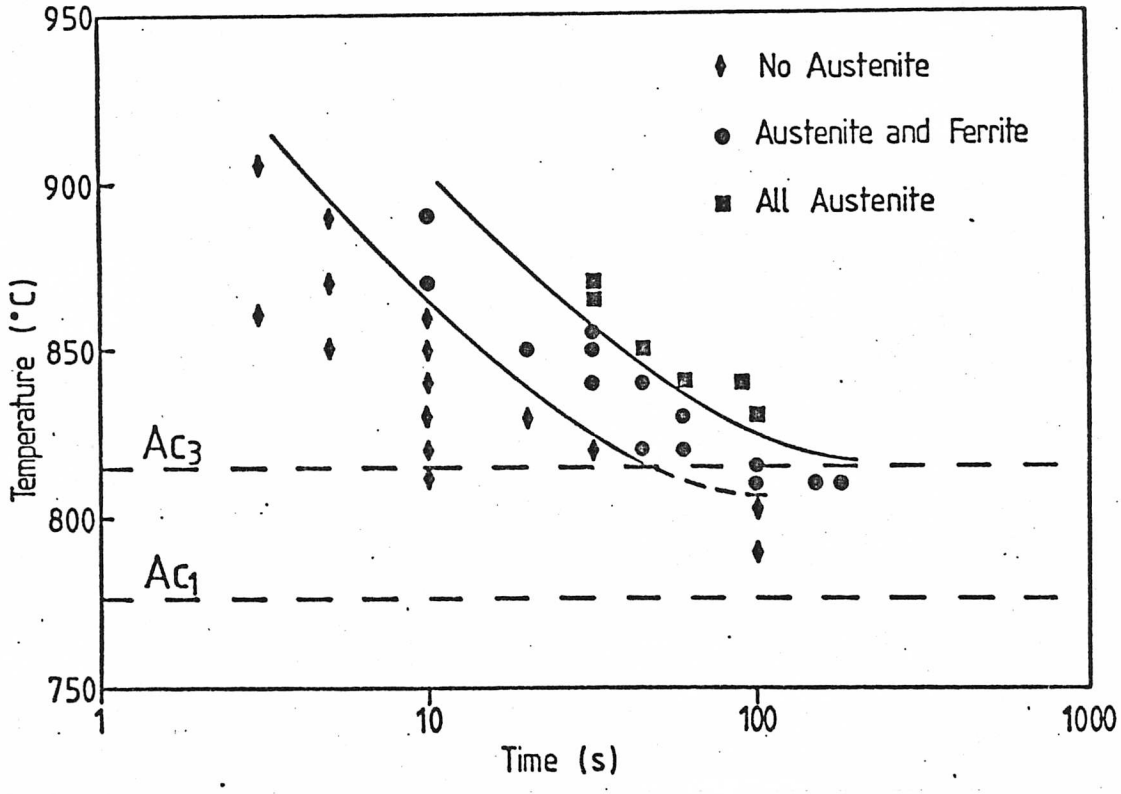

Fig. 5.1: Reaustenitisation TTT curve, determined by electron metallography. Regions of no transformation, some transformation and complete transformation are shown.

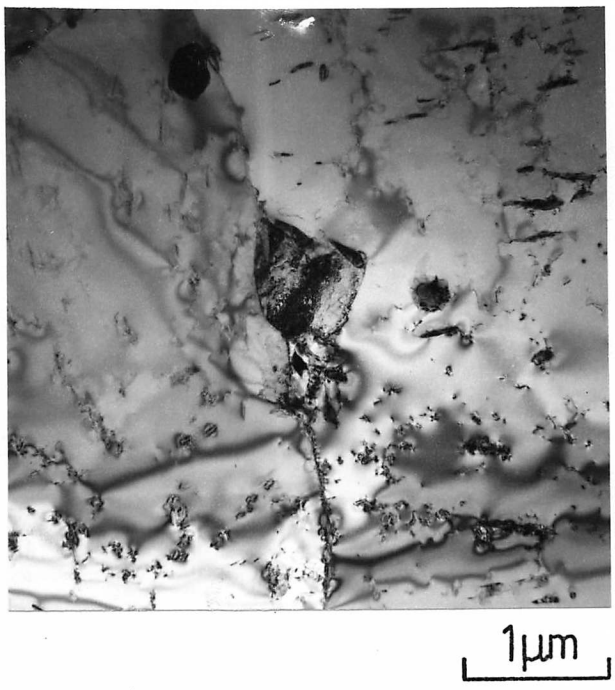

Fig. 5.2: Early stages of growth of austenite (now martensite) at a ferrite grain boundary. (1 minute 830°C.)

at late reaction times, however, many grain boundaries had not nucleated austenite.

5.2.3 Interaction of Fine Carbides with the α-γ Interface

In the Fe-10%Cr-0.2%C system, carbides do not dissolve in the early stages of reaustenitisation. It was found that the fibrous and plate-like carbides have a considerable effect on the movement of the austenite-ferrite interface. Figs. 5.3 and 5.4 show the interaction of the interface with fibres or laths which are approximately perpendicular to and parallel to the interface respectively, while Fig. 5.5 shows an interface which is at an angle to carbide laths.

In some cases the interface appears to be attracted to the carbide, as in Fig. 5.4, indicating that a favourable composition gradient of chromium or carbon may exist around the carbide. It was not possible to measure carbon concentration gradients with the techniques available. Direct measurements of chromium contents are discussed in section 5.3.

It is clear from Figs. 5.3 to 5.5 that carbides also act as physical barriers to growth. When the austenite-ferrite interface is perpendicular to, or at an angle to, the carbides, the interface itself is sometimes relatively flat and sometimes curved, either towards the ferrite or towards the austenite. Examples of each can be seen in Figs. 5.3 and 5.5. The curvature of the austenite-ferrite interface between carbides may be due to surface tension effects, the exact shape of the interface depending on the local geometry of the carbide distribution. The possible effect of composition fluctuations will be discussed in section 5.3.

The action of carbides as physical barriers to growth indicates that they are likely to be lath or plate-like rather than fibrous, as austenite would more readily be able to grow around fibres. Fine equiaxed particulate carbides have little effect on the movement of the interface.

5.2.4 Interaction of Coarse Carbides with the α-γ Interface

As well as fine fibrous and particulate carbides, the starting structure contained coarse carbides at prior austenite grain boundaries and at ferrite grain boundaries. These carbides were able to pin the interface.

Fig. 5.3: Interaction of lath-like carbides with a ferrite-austenite (now martensite) interface. 1 minute 830°C. Fibres predominantly perpendicular to interface.

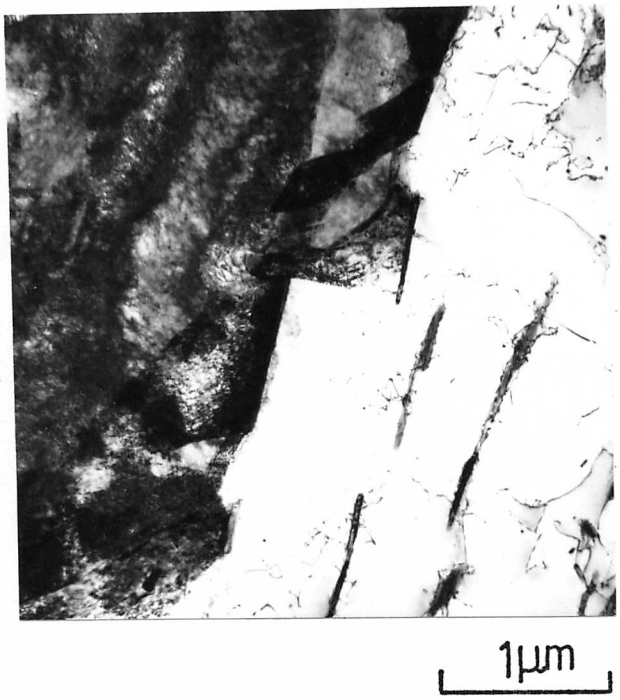

Austenite
growth direction

Fig. 5.4: Interaction of carbides with a ferrite-austenite interface. 30s 850°C. Fibres approximately parallel to interface.

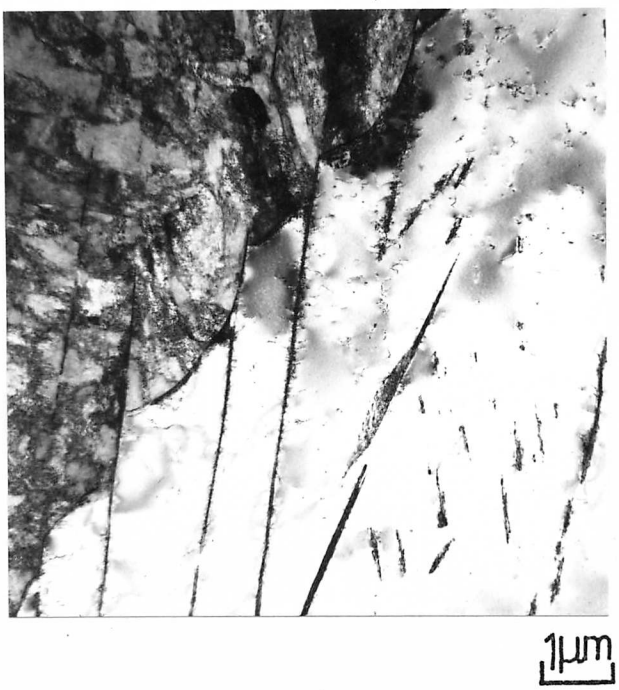

Austenite
growth direction

Fig. 5.5: Interaction of carbides with a ferrite-austenite interface. 30s 850°C. Fibres at an angle to interface.

Fig. 5.6 shows an area in which austenite is attempting to grow past a ferrite grain boundary containing coarse carbides. The closely spaced carbides at the top of the micrograph have pinned the interface, preventing further growth. However, the interface has been able to bow between the more widely spaced particles lower in the micrograph, and growth has continued between fibres in the next ferrite grain. The pinning by coarse carbides in boundaries is more effective than that by fine matrix carbides, showing that the coarser particles exert a larger drag force.

5.2.5 Dissolution of Carbides

During reaustenitisation, and on further holding at temperature, dissolution of carbides occurs. Carbides in ferrite showed little evidence of dissolution, although occassionally some breakdown and spheroidisation of fibres was observed.

The dissolution of carbides in austenite occurs much more readily. Partial dissolution of fibrous carbides in austenite occurs rapidly, leaving discrete particles. Fig. 5.7 shows an area of austenite which initially contained fibrous carbides, quenched from 835°C a few seconds after the reaustenitisation reaction had started. That fibres were initially present is obvious from the enhanced contrast in the electron micrograph, which may be due to composition differences (see later) or to higher dislocation densities caused by dissolution, along the line of the carbide. The fibres have broken down into discrete particles, which have spheroidised. At longer times, only a few spheroidal carbides remain in the austenite.

Little evidence of carbide dissolution in the austenite-ferrite interface was found, fibres often being continuous across the interface.

5.2.6 Effect of the Austenite to Martensite Transformation on Carbides

Since $M_{23}C_6$ carbides have a crystal structure closely related to that of austenite, it is interesting to investigate the effect of the austenite to martensite transformation on carbides embedded in austenite. Fig. 5.8 is an electron micrograph showing austenite growing into ferrite containing short fibrous carbides which continue into the austenite (the diagonal carbides in Fig. 5.8). It was possible to image the fibres in the ferrite and some parts of the fibres in the martensite

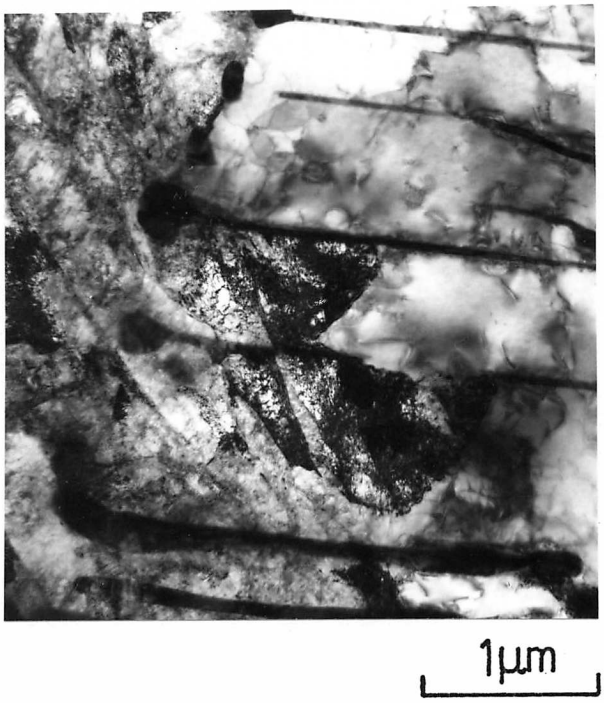

Fig. 5.6: The ferrite-austenite interface in the vicinity of a prior ferrite grain boundary containing coarse carbides. 1 min 830°C.

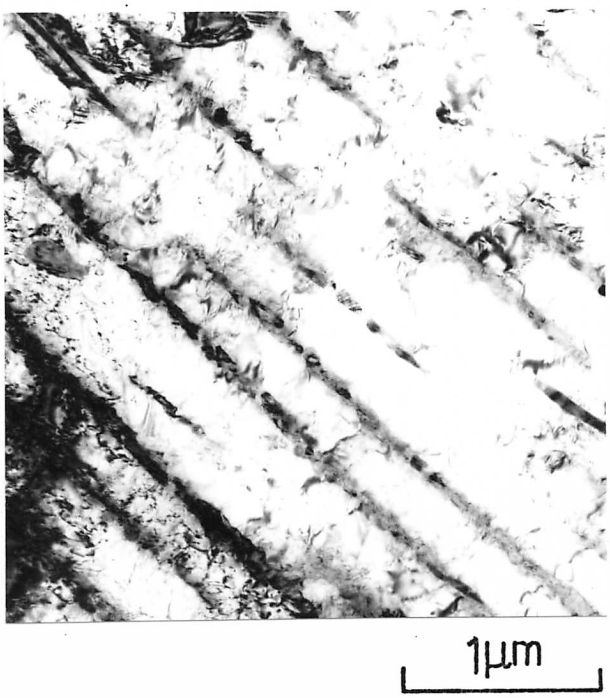

Fig. 5.7: Fibrous carbides dissolving in austenite leaving spheroidal carbides. A few seconds at 835°C.

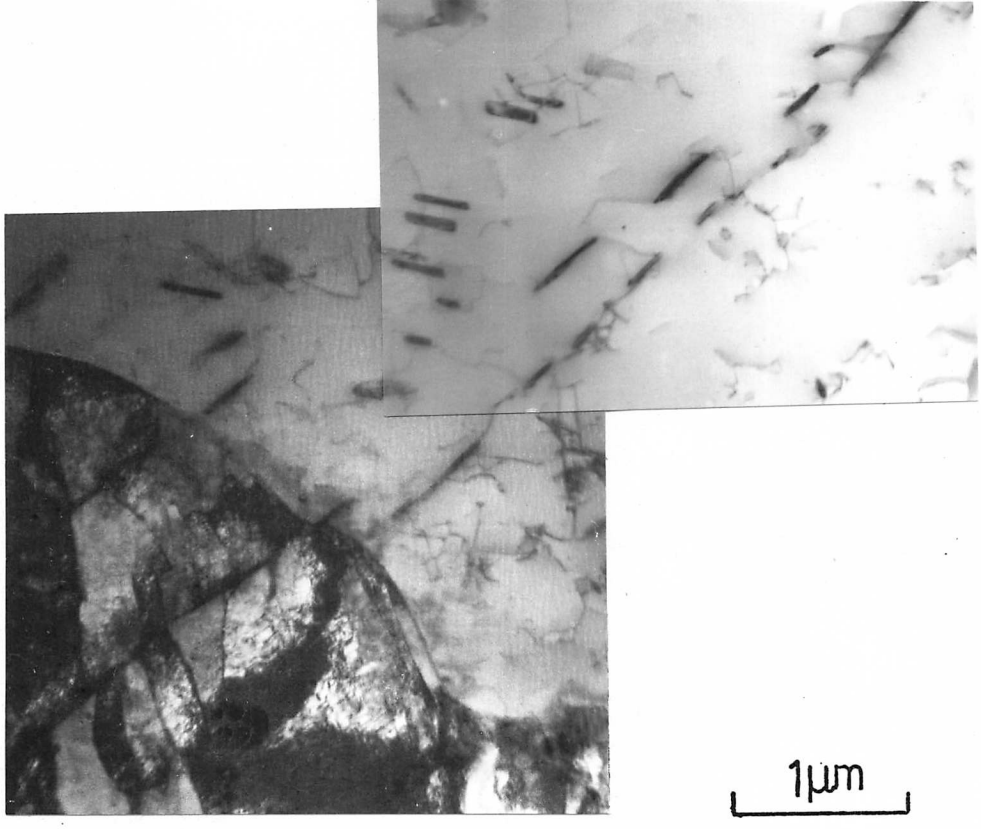

Fig. 5.8: Fibrous carbides on either side of a ferrite-austenite (now martensite) interface. Transformed 3s at 855°C.

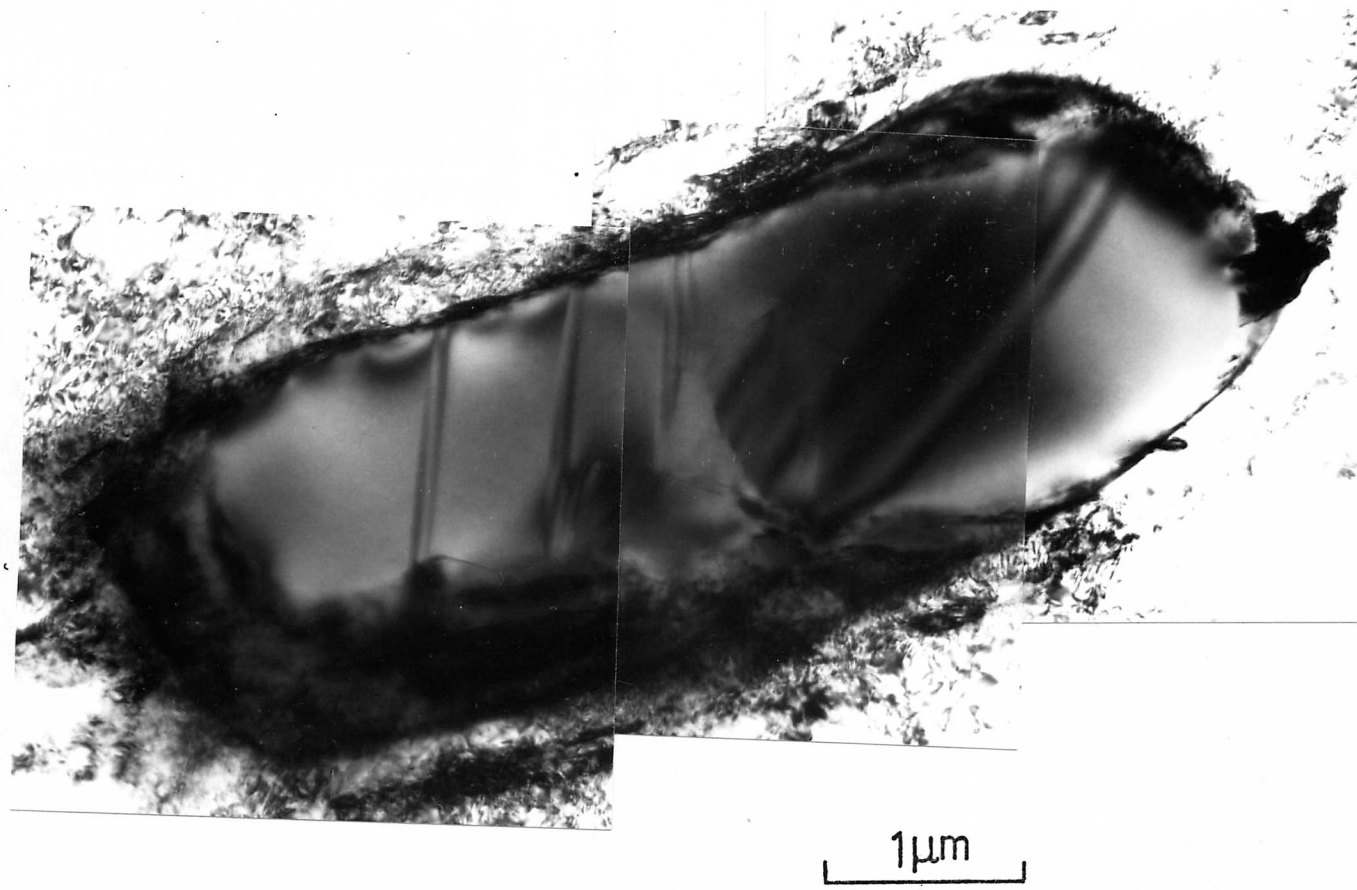

Fig. 5.9: Coarse carbide containing faults after reaustenitisation and quenching. Carbides coarsened at 750°C for 60 hours, reaustenitisation at 900°C, about 1 min.

in dark field using an $M_{23}C_6$ reflection. Slight tilting of the specimen caused the fibres in the ferrite to go out of contrast, and brought other parts of the fibres in the martensite into contrast. Different parts of the carbides lit up progressively as the specimen was tilted to about 1° from the position in which the carbides in ferrite were in contrast.

There seems little reason to expect the ferrite to austenite reaction to have any effect on the carbides, so the misorientations of the fibres must be due to the transformation from austenite to martensite. It was not possible to examine the internal structure of the fine carbides in this structure, so specimens in which the carbides had been allowed to coarsen in the ferrite (by holding at 750°C for 60 hours) were reaustenitised and quenched. Electron microscopy showed that, after reaustenitisation and quenching, the undissolved carbides contained many faults. An example is shown in Fig. 5.9. A more detailed analysis of the faulting was not carried out, but it is possible that the faults are due to the passage of the martensitic shear during the transformation of the surrounding austenite to martensite. The observed misorientation of the fibrous carbides in the finer structure is attributed to similar faulting.

5.3 Distribution of Chromium during Reaustenitisation

Microanalysis of specimens which had been partially or fully reaustenitised at temperatures of 810°C, 830°C and 870°C, was carried out. A Link energy dispersive analysis system was used, and the techniques and correction procedures employed were as described in chapter 4, section 4.4.

The work on the ferrite-carbide starting structure described in sections 4.4.4 and 4.4.5 established:

a) that no concentration gradients exist in ferrite,

b) that ferrite between carbides and at grain boundaries is depleted in chromium compared to bulk carbide free ferrite, and

c) that the carbides are very rich in chromium, the finer carbides containing somewhat more chromium than the coarser ones.

Microanalysis of reaustenitised specimens aimed to establish firstly, whether compositions in the ferrite (and carbides) altered during the reaction, and secondly, how the chromium content of the austenite

differed from that of the ferrite, and how it varied with time and temperature.

5.3.1 Chromium Distributions near an α-γ Interface

Most of the interfacial studies were carried out on a sample which had been partially reaustenitised for 60s at 830°C and water quenched. Since 830°C is above the Ac_3 temperature, the austenite reaction goes to completion, given time. In a partially transformed sample, therefore, the austenite interface has not reached equilibrium and is advancing. Microanalytical data should therefore represent true chromium compositions at moving interfaces.

In order to determine the concentration profile near an austenite-ferrite interface, a series of microanalyses was taken at approximately 0.2μm intervals across the interface. Several such series were taken parallel to the fibrous carbides illustrated in Fig. 5.3, midway between them. One example of the concentration profiles obtained is given in Fig. 5.10a. In this case there is a slight rise in concentration near the interface, but this feature did not appear in all such series. In all cases the scatter of data was fairly large (more than 1% chromium), but no significant trends emerged. It therefore seems that local composition fluctuations exist, but that long range concentration gradients in, and composition differences between, the austenite and ferrite on either side of austenite-ferrite interfaces do not occur.

Another series of data was taken perpendicular to the carbides depicted in Fig. 5.3, in a region in which the boundary between austenite and ferrite lay along a fibrous carbide. The data from austenite and martensite are presented in Fig. 5.10b. Again, the scatter is large, but no trend is obvious, and no concentration gradients are detected.

Similar series of microanalyses were taken parallel to the fibres and between the coarse boundary carbides illustrated in Fig. 5.6. Analyses were taken midway between the fibres both across the austenite-ferrite interface and across the prior ferrite grain boundary. The results are given in Fig. 5.11. Figs. 5.11a and b again show that there are no concentration gradients at the austenite-ferrite interface, and no compositional difference at the prior ferrite grain boundary is detected.

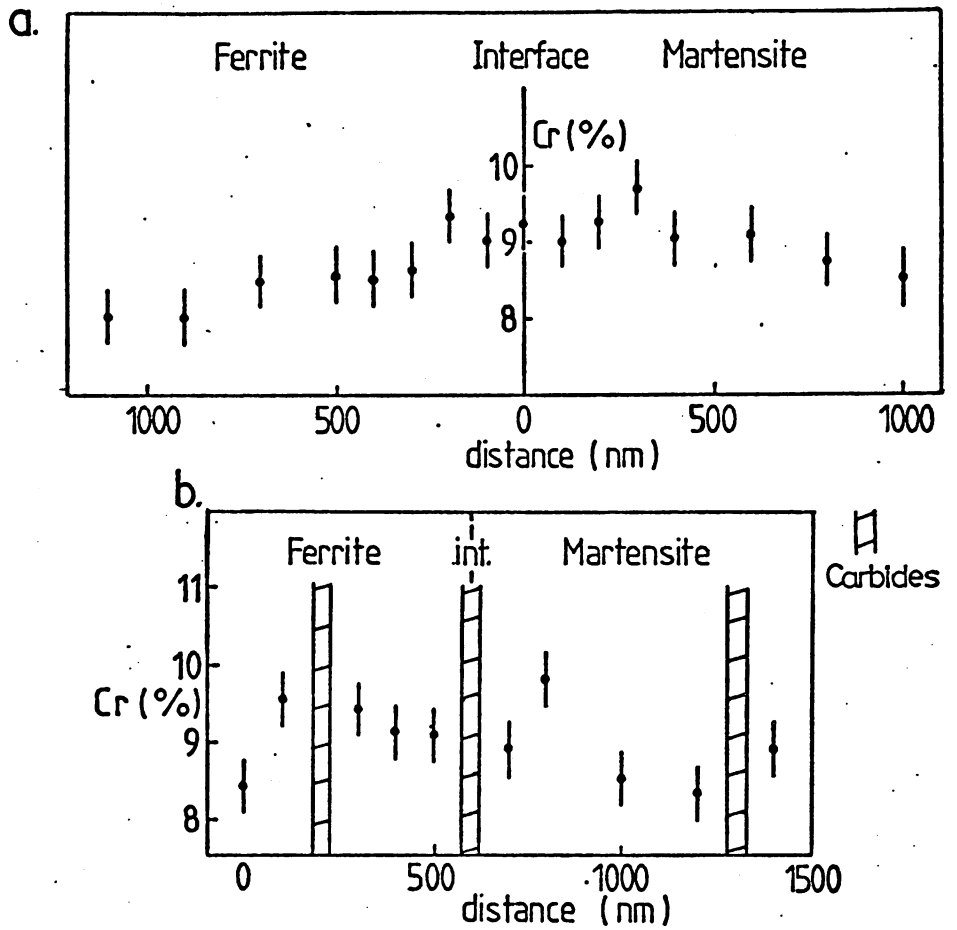

Fig. 5.10: Chromium content of ferrite and martensite (previously austenite) between carbides in Fig. 5.3
a) parallel to fibres
b) perpendicular to fibres.

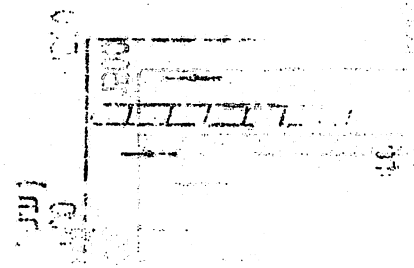

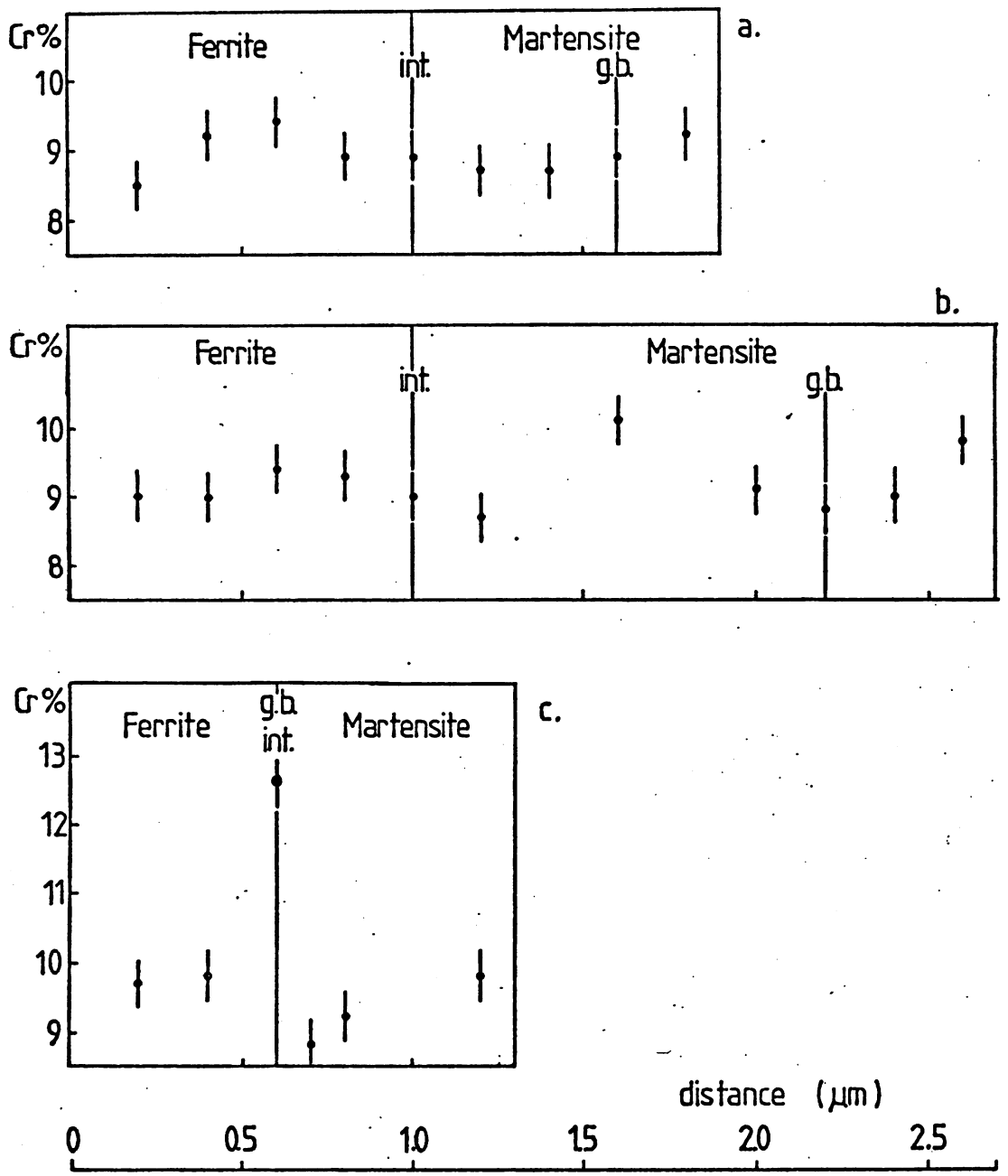

Fig. 5.11: Chromium content of ferrite and martensite between the carbides in Fig. 5.3. Position of ferrite-austenite interface (int.) and prior ferrite grain boundary (g.b.) shown.

Fig. 5.11c gives a concentration profile across the interface in a case when the interface is coincident with the prior ferrite grain boundary. In this case, there is a marked peak in chromium concentration at the interface. It therefore seems that when the austenite-ferrite interface is stationary, in this case due to pinning, carbides dissolve in the interface and the boundary chromium content increases. In the absence of pinning, the austenite interface moves rapidly and dissolution of carbides in the interface does not occur.

In all the above series, measurements were taken at 0.2μm intervals, and no concentration gradients were seen. It should be noted that smaller scale concentration gradients would not have been detected. Such concentration gradients, if present, would be too close to boundaries (such as austenite-ferrite or ferrite-carbide interfaces) to allow reliable microanalysis.

Some measurements of chromium content between fibrous carbides on both sides of an austenite-ferrite interface were also carried out after partial reaustenitisation at 810°C and 870°C. Again, no difference in composition between austenite and ferrite was found. Concentrations on either side of austenite-ferrite interfaces in carbide-free regions were also found to be similar in austenite and ferrite at all temperatures.

5.3.2 Chromium Distributions away from an α-γ Interface

Measurements of chromium content away from interfaces were made on samples which had been partially reaustenitised for 150s at 810°C (below the Ac_3 temperature) and for 10s at 870°C (above the Ac_3 temperature), and on samples which had been fully reaustenitised by holding at 870°C for 30s. For each sample, the mean of several (usually five to ten) measurements of chromium content in particular areas was obtained. Carbide free ferrite and martensite, and ferrite and martensite between carbides, were analysed in this way, enabling comparison between different areas in the same specimen, and between different specimens.

a) Partially Transformed Samples

In specimens partially transformed at 810°C and 870°C, no significant difference in chromium content between ferrite and martensite regions was detected, the austenite inheriting the chromium content of the ferrite. For instance, at 810°C;

1) in carbide free areas, the chromium level in ferrite was 11.2±0.2%Cr, and that in the martensite was similar at 11.0±0.1%Cr, and

2) in areas between fibrous or particulate carbides, ferrite and martensite contained 9.8±0.1%Cr and 9.8±0.2%Cr respectively (the quoted error is the standard deviation of the mean).
It therefore appears that during these heat treatments no significant movement of chromium between austenite and ferrite, or dissolution of carbides releasing chromium, has occurred.

It may be noted that the chromium contents measured here are consistently higher than those measured in the ferrite-carbide starting structure (chapter 4, section 4.4.4). These discrepancies are attributed to the fact that different X-ray analysing systems were used, due to unavoidable circumstances, for the two sets of measurements.

b) Fully Transformed Samples

Microanalyses of martensite between carbides were carried out in the sample fully transformed at 870°C for 30s. Midway between carbides, the chromium concentration had not changed significantly from that of similar areas in the partially transformed sample (10s transformation). However, microanalysis at sites where a carbide had obviously dissolved during the transformation, such as the breaks in the fibres illustrated in Fig. 5.7, yields higher chromium levels. In such areas, the chromium content was 11.0±0.2%Cr, whereas midway between fibres the composition was 9.7±0.2%Cr.

5.3.3 Discussion

A correlation between metallographic and microanalytical data can now be made. No net movement of chromium occurs during the early stages of the reaustenitisation reaction at any of the temperatures investigated, and no detectable concentration gradients exist in the starting structure, or arise during reaustenitisation. The apparent attraction of the austenite-ferrite interface to carbides ahead of the interface can thus not be attributed to long range chromium gradients. It therefore seems likely that higher carbon concentrations near carbides may be responsible for enhanced growth. This situation can arise if some dissolution of carbides occurs, a flux of carbon through ferrite to the austenite interface being set up. After diffusion away of the carbon, the remaining chromium can dissolve in the ferrite.

The shape adopted by the austenite-ferrite interface in contact with fibres as it moves through carbide colonies also cannot be controlled be long range chromium gradients. However, microanalysis has

shown that considerable differences in chromium concentrations occur, and local fluctuations may well be partly responsible, along with surface tension and carbon concentration gradient effects, for the particular shape and curvature of any interface.

It has been observed that coarse carbides pin the austenite growth front more effectively than do fine carbides. It was shown in section 4.4.5 that coarse carbides contain less chromium than do fine carbides, but this seems unlikely to provide an explanation for the pinning. Enhanced pinning is attributed to the high drag force exerted by large particles, the pinning being even more effective when these are closely spaced.

Dissolution of carbides in austenite has been shown to involve the breakdown and spheroidisation of carbides, and the diffusion away of much of the chromium. Since the austenite contains dissolved carbon, it cannot tolerate large amounts of chromium in solution; the chromium must therefore diffuse away before further carbide dissolution can take place. Dissolution is therefore likely to be volume diffusion controlled, and to be slow. An $M_{23}C_6$ carbide contains about 79%Cr, while austenite which replaces dissolved carbides (after 30s at 870°C) contains only 11.0%Cr, which is somewhat more than the chromium content of the surrounding austenite (9.7%Cr). Long holding times at such austenitisation temperatures should therefore result in an increase in chromium content of the austenite as carbides dissolve. The austenite directly replacing dissolved carbides should not contain much more chromium than does the bulk austenite, and thus large concentration gradients will not arise. Therefore, after complete dissolution of carbides the composition of all austenite should be close to that of the bulk alloy.

5.4 Kinetics of Reaustenitisation

Having established that the austenite reaction in the Fe-10%Cr-0.2%C alloy does not involve the movement of chromium, but that dissolution of carbides in austenite does, it now remains to elucidate the rate controlling factors of reaustenitisation and carbide dissolution respectively, and to determine the time scales over which these reactions take place. Isothermal dilatometry was used to do this.

5.4.1 Dilatometry of Fe-Cr alloys

a) Experimental Details

The specimens for dilatometry were made from 3mm diameter rod, and had the ferrite-carbide microstructure described in section 4.3.2. Specimens 15mm in length were cut from the rod, and after grinding the ends flat, the rod was hollowed out, leaving a tube of wall thickness 0.5mm. A Theta Industries high-speed dilatometer, which employs an R.F. coil to heat the specimen, was used. With hollow specimens, a rapid heating rate is achieved (several hundred degrees per second) and the temperature stabilises out rapidly (one or two seconds) at the preset isothermal hold temperature. Temperatures stable to within ±1°C can be maintained for many hours. The specimen length is monitored continuously and is recorded on a chart recorder.

b) Calculation of length changes during transformation

The starting structure consists of ferrite and $M_{23}C_6$ carbides, and during reaustenitisation various mixtures of austenite, ferrite and carbide exist, until at high temperatures only austenite remains. In order to understand the length changes recorded by the dilatometer it was found necessary to calculate the expected length changes on (1) thermal expansion of ferrite from room temperature to a typical reaustenitisation temperature, (2) transformation of ferrite plus carbide to austenite plus carbide, without any dissolution of carbide and (3) dissolution of all carbides in austenite. Lattice parameters for austenite and ferrite were obtained from Pearson (1967) and for $Cr_{23}C_6$ from the X-ray Powder Diffraction File. The expansion of the austenite and ferrite lattices by addition of 10%Cr was estimated from data given by Pearson (1967) and the increase in austenite lattice parameter (in Å) due to carbon was taken to be the weight percent of carbon multiplied by 0.044 (Roberts 1953). The thermal expansion coefficients of ferrite and austenite were taken from Austin and Pierce (1934, 1935).

(1) Neglecting the presence of carbides, the length increase on heating ferrite from 0°C to 800°C was found to be 1.17% of the initial specimen length.

(2) Again neglecting carbides, the length decrease on transforming ferrite to austenite (both containing about 10%Cr) at 800°C was found to be 0.34% of the length of the ferrite specimen at 800°C.

(3) Assuming that initially all carbon is in the form of $M_{23}C_6$ carbides

and that finally it is all dissolved in the austenite lattice, the length decrease on dissolving all the carbides was found to be 0.11% of the length of the austenite plus carbide specimen.

5.4.2 Isothermal Transformation Results

Isothermal transformations were carried out at several temperatures in the range 772°C to 907°C. At all temperatures in this range, the transformation to austenite begins immediately the preset temperature is reached, and at most temperatures, some transformation cannot be avoided during heating. The beginning of the length trace obtained on isothermal transformation at 808°C is shown at the top of Fig. 5.12, in which the preset temperature is reached at time zero (the length change due to expansion on heating is actually much larger than that shown). It can be seen that a rapid decrease in length occurs immediately, showing that there is no detectable nucleation incubation time. This is rather surprising, as considerable nucleation incubation times were observed metallographically (section 5.2). However, the specimens for metallographic examination were heated by immersion in baths of hot salt, while specimens in the dilatometer are heated by an R.F. coil which induces currents in the specimen surface. It therefore seems possible that the rapid nucleation in dilatometer specimens is a surface phenomenon caused by the method of heating. The technique of dilatometry can thus provide information only about austenite growth and not about austenite nucleation.

After the initial rapid length decrease, the length continues to fall gradually for a considerable time, often several hours, before a steady value is reached. It was found that plotting the length against the square root of time always yielded two straight line sections, the first having a steeper gradient than the second. Examples are given in Figs. 5.12 and 5.13, in which length is plotted in arbitrary linear units. Curved sections on such a plot always occurred at the beginning of the reaction, and sometimes at the cross-over of the straight lines (as at A in Fig. 5.12), and towards the end of the reaction (as in Fig. 5.13). It was always possible, however, to define two straight lines and the point at which they crossed (the points marked A in Figs. 5.12, 5.13), and the time at which no further length change occurred (point B in Fig. 5.13). The end of the reaction (B) was not recorded at the lower temperatures, where a steady value of length was not reached in less than 10,000s.

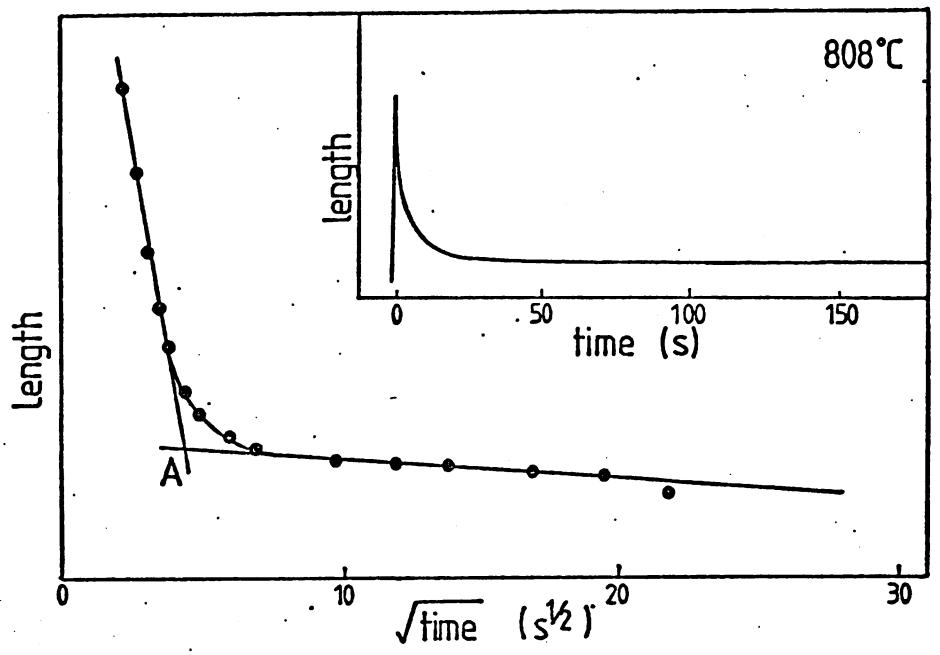

Fig. 5.12: Plot of length against the square root of time during reaustenitisation at 808°C, from a dilatometer length trace.
Inset: beginning of dilatometer length trace.

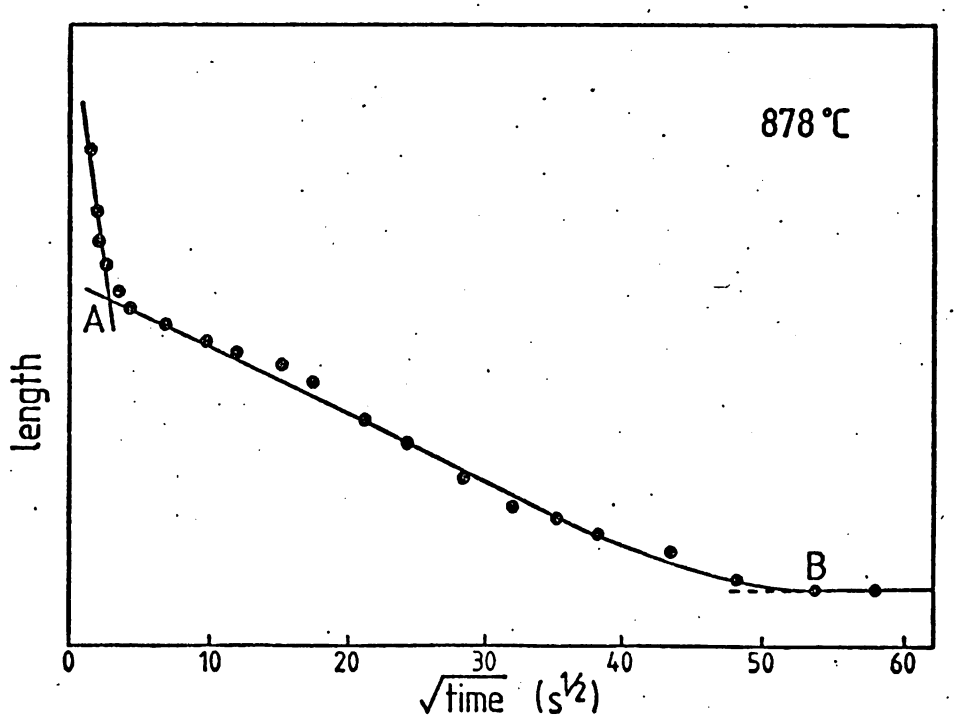

Fig. 5.13: As above, reaustenitisation at 878°C.

It was found to be impossible to calibrate the observed length changes in terms of actual lengths, due to difficulties in accurate measurement of the initial specimen length, and in accurate calculation of the expected length at temperature. It was also not possible to relate length changes during transformation to the length of the untransformed specimen at that temperature, as this length could not be recorded, mainly because transformation occurs before the temperature is reached. Uncertainties are also caused by instabilities in temperature just after the preset temperature is reached, and by overshoot of the length pen. Thus it was not possible to relate observed length changes directly to fractions of transformation.

5.4.3 Interpretation

In a volume diffusion controlled transformation, the fraction transformed varies as $t^{3/2}$ (where t is time). Thus the volume change caused by the transformation also varies as $t^{3/2}$, and the length change in one dimension varies as $t^{1/2}$ (see eg Christian 1975). Thus, the dilatometric results in this alloy indicate that two volume diffusion controlled reactions occur, the first proceeding more quickly than the second. It is suggested that:

a) the first reaction is the transformation to austenite and the second is the dissolution of carbides, and

b) the first reaction is carbon diffusion controlled and the second is chromium diffusion controlled.

This hypothesis will now be explored.

a) Sequence of Reactions

In section 5.4.1, the length changes which should occur during the complete transformation of ferrite to austenite, during the complete dissolution of carbides in austenite and, for comparison, during thermal expansion from room temperature to an austenitising temperature, were calculated. From these calculations, if the first reaction involves only austenitisation and the second only carbide dissolution, then the length change during the first reaction should be about one third of that during thermal expansion, and the length change during the second reaction should be about one third of that during the first reaction, at temperatures at which both reactions go to completion. Since the transformation begins before the isothermal hold temperature is reached, particularly at high temperatures, exact comparison of length changes cannot be made. However, on the whole, the relative length changes are

qualitatively consistent with the first reaction being austenitisation and the second, carbide dissolution.

Electron metallography of solid dilatometer specimens, which had been isothermally transformed and He gas quenched in situ in the dilatometer, was carried out. Partial reaustenitisation had occurred in even the specimens held for the shortest times (a few seconds) showing that nucleation occurred rapidly in these specimens.

Examination of specimens which had been transformed for times before the end of the first reaction (before A) and times during the second reaction (after A) showed that austenite formed during the first reaction, and above the Ac_3 temperature (as determined in chapter 4, section 4.4) austenitisation was complete at the onset of the second reaction.

Evidence of carbide dissolution in austenite was found in most specimens, and at temperatures below 900°C carbide dissolution was found to be incomplete even after the end of the second reaction.

b) Rate Controlling Factors

As noted above, length changes proportional to $t^{1/2}$ are consistent with volume diffusion controlled reactions. The deviations from linearity in a length v. $t^{1/2}$ plot can readily be explained. Firstly, the length trace at the beginning of the isothermal reaction is affected by transformation during heating, temperature instability and overshoot of the length pen, and continuing nucleation in the first few seconds is also expected to cause deviation from $t^{1/2}$ behaviour. Secondly, impingement of growing particles, or of diffusion fields, is known to decrease the rate of transformation (see eg. Christian 1975). Thus deviations from $t^{1/2}$ behaviour are also expected towards the end of both the austenitisation and the dissolution reactions. Deviations at the cross-over may also be due to a gradual change from one reaction to the other.

If the first reaction is carbon diffusion controlled, and the second reaction chromium diffusion controlled, the activation energies should vary accordingly. However, attempts to determine activation energies from the dilatometric data were unsuccessful, because the austenite reaction started before the transformation temperature was reached, and insufficient data for complete carbide dissolution times were collected.

The $t^{1/2}$ kinetics of both reactions show that they are volume diffusion controlled. Microanalysis (section 5.3) showed that no partitioning of chromium is detectable during the early part of the reaction. Consequently, it is concluded that the first reaction is carbon diffusion controlled. Carbon diffuses from carbides through ferrite to the advancing austenite interface; thus diffusion through ferrite is rate controlling.

During the second reaction, carbides dissolve in the austenite and chromium diffuses away through austenite; thus chromium diffusion through austenite is rate-controlling.

5.4.4 The Austenitisation TTT Curve

The austenitisation TTT curve obtained by dilatometry is shown in Fig. 5.14. The austenitisation curves at short time, labelled A, are the locus of points at which the reaction rate changes (ie. points similar to those marked A in Figs. 5.12 and 5.13). The carbide dissolution curves, labelled B, are the locus of points at which no further reaction occurs (ie. points similar to B in Fig. 5.13). The phase fields are marked in accordance with the interpretation presented in section 5.4.3, and phases which have reached their equilibrium proportions are underlined. Between the Ac_1 and Ac_3 temperatures, austenitisation is not complete; the curve defines the times at which the austenite volume fraction reaches equilibrium and no further austenitisation occurs (see also paragraph 6 below). Similarly, below about 900°C, carbide dissolution is incomplete, and the curve defines the times at which no further carbide dissolution occurs.

Several points should be noted.

1. No reaction start times are given, as nucleation occurs too rapidly to be measured under the experimental conditions used.
2. The austenitisation finish curve between the Ac_1 and Ac_3 temperatures is in the form of a C-curve. As the temperature increases, both driving force and diffusion rate, and hence growth rate, increase. However, the volume fraction which must be formed also increases with increasing temperature, and at the higher volume fractions, impingement slows down the growth rate. The result of the interaction of all these factors can be a reaction finish curve which is in the form of a C-curve. This concept is discussed further in chapter 6.
3. Above the Ac_3, the time to complete austenitisation decreases with

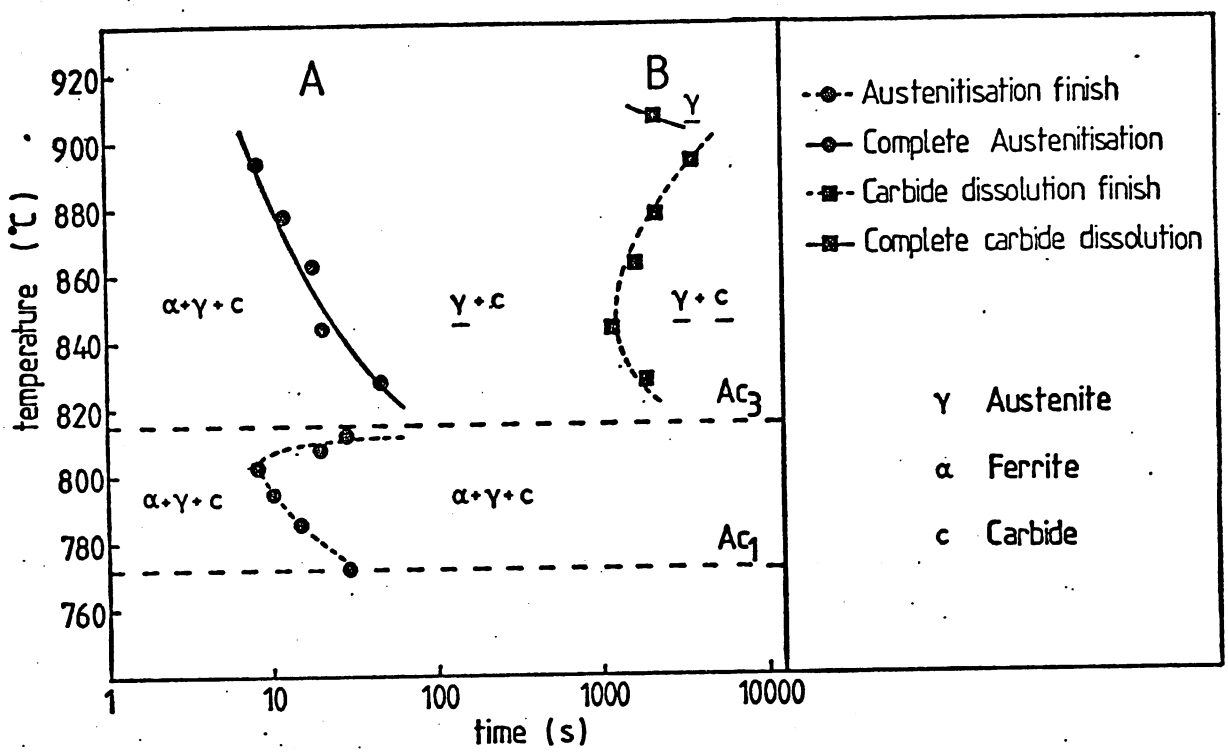

Fig. 5.14: Reaustenitisation TTT curve for the Fe-10%Cr-0.2%C alloy, ferrite-carbide starting structure. Determined by dilatometry.

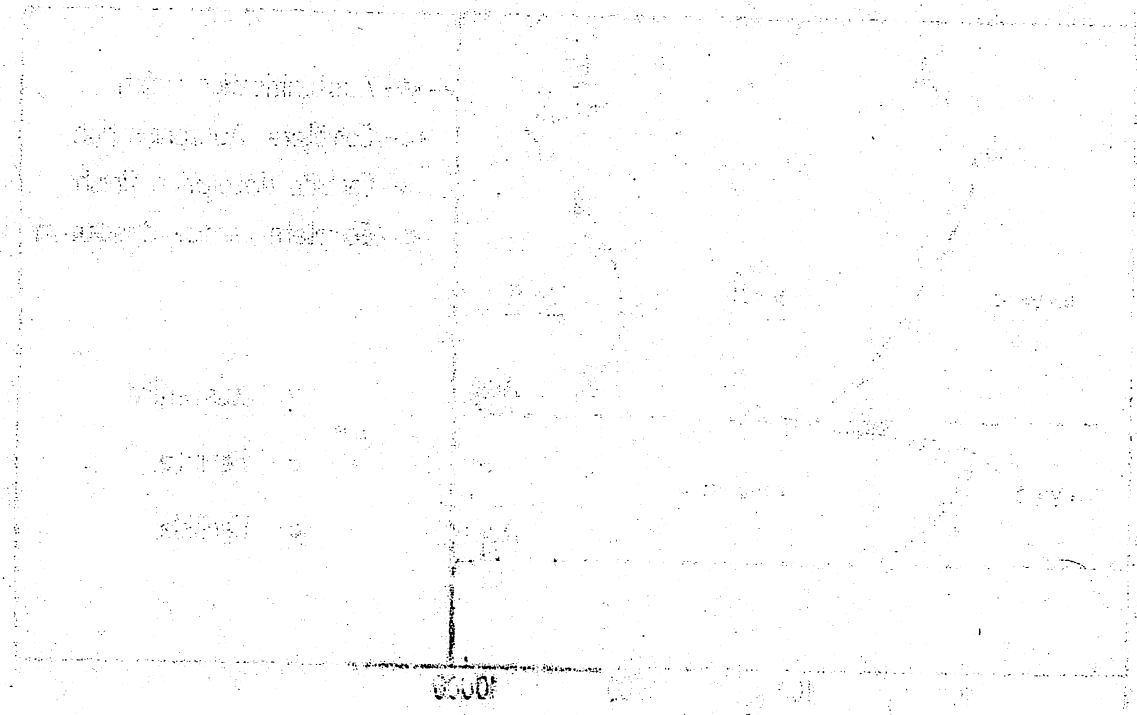

increasing temperature as the driving force and diffusion rate increase.
4. The carbide dissolution finish curve is also a C-curve, for reasons similar to those given in paragraph 2.
5. Above 900°C, the time taken to finish the carbide dissolution reaction has decreased from its value below 900°C, indicating that above about 900°C complete carbide dissolution occurs. This is in fair agreement with the carbide dissolution temperature given by Bungardt et al (1959), 910°C.
6. No evidence is available to indicate that the austenite and ferrite in the region after the "austenitisation finish" curve between the Ac_1 and Ac_3 temperatures have attained their final equilibrium proportions. The curve is better regarded as the "carbon diffusion controlled austenitisation finish" curve, as the chromium diffusion controlled dissolution of carbides, and consequent change in composition of the austenite and ferrite, may well lead to a change in relative proportions of the phases.

5.5 Conclusions

Investigation of reaustenitisation in an Fe-10%Cr-0.2%C alloy by metallography, microanalysis and dilatometry have led to the following conclusions:

1. On heating, austenite first begins to form at 772°C, all ferrite disappears at 815°C, and all carbides dissolve above about 900°C.
2. During isothermal transformation to austenite at temperatures above 772°C, a sequence of two reactions occurs, the first proceeding more rapidly than the second.
3. The first reaction is austenitisation, and is controlled by carbon diffusion through ferrite.
4. The second reaction is dissolution of carbides in austenite, and is controlled by chromium diffusion through austenite.
5. Under normal heating conditions, considerable nucleation incubation times occur.
6. Direct R.F. heating causes rapid nucleation of austenite throughout the austenitisation temperature range.
7. Growth of austenite occurs very rapidly, such that complete austenitisation occurs within about 100s at all temperatures above the Ac_3 (815°C).
8. The combination of low nucleation rate and high growth rate leads to

a distribution of a few large areas of martensite in partially transformed and quenched samples.

9. Carbides do not dissolve substantially in the austenite-ferrite interface during reaustenitisation.

10. The shape of the austenite-ferrite interface is determined by interaction with carbides (a surface tension effect), by local fluctuations in chromium content, and possibly by carbon concentration gradients.

11. Coarse carbides pin the austenite-ferrite interface more effectively than do fine carbides.

12. Dissolution of carbides in austenite is slow, but no large chromium concentration gradients should exist after dissolution is complete.

CHAPTER SIX

TRANSFORMATIONS IN THE TWO PHASE AUSTENITE-FERRITE REGION

6.1 Introduction

Previous chapters have considered reaustenitisation in a number of systems. It has become apparent that the kinetics of the reaction in the two phase austenite plus ferrite region are not straightforward, particularly when substitutional alloying elements are present. In view of the applications of intercritical annealing to the production of dual phase steels, it was felt worthwhile to study the transformation in the two phase region in more detail.

In chapter 3, some kinetic data, obtained metallographically, for the reaustenitisation of ferrite-pearlite aggregates in the two-phase austenite-ferrite region were presented. Indications that the inhomogeneous distribution of carbides had a dominating effect on the kinetics were found. In chapter 5, the results and interpretation of a dilatometric investigation of the kinetics of an alloy containing 10%Cr were presented. In this system, carbides are present in the region in which austenite and ferrite coexist, and the effect of the dissolution of carbides, and subsequent redistribution of chromium on the austenite reaction at temperatures between the Ac_1 and Ac_3 was unclear.

In order to understand the kinetics of reaustenitisation in the austenite-ferrite region, it was therefore felt to be necessary, in the first instance, to investigate the reaction in a system in which a carbide-free austenite-ferrite regime exists, and in which the starting structure is homogeneous in microstructure and in distribution of alloying elements. An Fe-1.2%Mn-0.1%C alloy (alloy D, as in the ferrite-pearlite work, chapter 3) was used, the starting structure being martensite, obtained by quenching austenite after homogenisation. It was hoped that the distribution of alloying elements would be homogeneous, and that, on rapid heating to the reaustenitising temperature, carbon would remain in solution, or that such finely dispersed carbides would form that they would have little effect on the austenite reaction.

Isothermal dilatometry forms the basis of the investigation, and

the dilatometric results are presented in section 6.2. Metallography and microanalysis results follow in section 6.3. Interpretation of the experimental results involves consideration of thermodynamics and kinetics (section 6.4), impingement (6.5) and recrystallisation (6.6). Conclusions are presented in section 6.7.

6.2 Dilatometry

6.2.1 Experimental Details

Specimens of the Fe-1.2%Mn-0.1%C alloy were prepared in the form of 3mm rod, and those for use in the dilatometer were hollowed out and accurately finished. All specimens were austenitised at 1050°C for ten minutes in evacuated silica capsules, and quenched into water. Optical metallography showed that the specimens were fully martensitic. These specimens were used for all the experimental work reported in this chapter.

In order to determine the Ac_1 and Ac_3 temperatures, continuous heating in the dilatometer at various heating rates was employed. Isothermal reaustenitisation experiments in the dilatometer were then carried out, at temperatures both in the two-phase austenite plus ferrite region between the Ac_1 and Ac_3, and above the Ac_3.

6.2.2 Determination of the Ac_1 and Ac_3

Continuous heating through the transformation range was carried out in the dilatometer, as described in chapter 4, section 4.4, at rates varying from 0.33°C per minute to over 1000°C per minute. The continuous heating curves obtained varied in shape with heating rate, and it was often difficult to pinpoint the change temperatures. No consistent trend in change temperatures with heating rate was obtained, and it was thus impossible to extrapolate to zero heating rate to find the true change temperatures. The values obtained at the lowest heating rate were therefore used. The complicated behaviour shown in the continuous heating curves is attributed to the slow movement of the alloying element, manganese, during the reactions.

The Ac_1 and Ac_3 temperatures were found to be 695±5°C and 847±5°C respectively. The A_2 temperature lay between the Ac_1 and Ac_3 temperatures, at about 748°C.

6.2.3 Isothermal Transformation Curves

The general characteristics of the transformation curves obtained by isothermal reaustenitisation of the martensite specimens were as follows. At all temperatures between 695°C and 1050°C, the reaction started immediately the preset temperature was reached, and in many cases some reaction occurred during heating. At the beginning of the transformation, the specimen length fell rapidly, and a gradual fall in length continued for long times, often several hours. In general, a plot of length against the square root of time yielded two stages, each of which displayed a distinct linear section.

Examples of length v. $t^{1/2}$ plots (where t is time) are given in Figs. 6.1a,b,c for temperatures 760°C, 834°C and 1050°C respectively (length is plotted on a linear scale in unspecified units, which are not necessarily the same in a, b and c). At all temperatures between the Ac_1 and Ac_3 temperatures (695°C-847°C), plots similar to 6.1a and b were obtained, displaying two linear sections, the first having a steeper gradient then the second. The time at which the two straight lines cross is labelled A in Fig. 6.1a,b, and is taken as the beginning of the second stage of the reaction. The time at which no further reaction occurs is labelled B. The relative length changes in the two stages, and the proportion of the plot which was not linear, varied with temperature.

On the whole, a transformation at a temperature low in the two-phase region showed the greater proportion of its total transformation (length change) during the second stage (see Fig. 6.1a). At higher temperatures, the greater proportion of the transformation tended to occur in the first stage (Fig. 6.1b), although often the two stages showed fairly similar amounts of transformation. Similar problems in defining lengths, and thus transformed fractions, as were encountered during dilatometry of the 10%Cr alloy (as described in chapter 5, section 5.4.2) were encountered in this alloy. It was thus not possible to make a more detailed comparison of length changes.

Non-linear portions of the $t^{1/2}$ plot occurred towards the end of the transformation, and at the cross-over of the two straight lines, at most temperatures.

Above the Ac_3 temperature (847°C), reactions accurately proportional to $t^{1/2}$ were generally not found, except at temperatures just

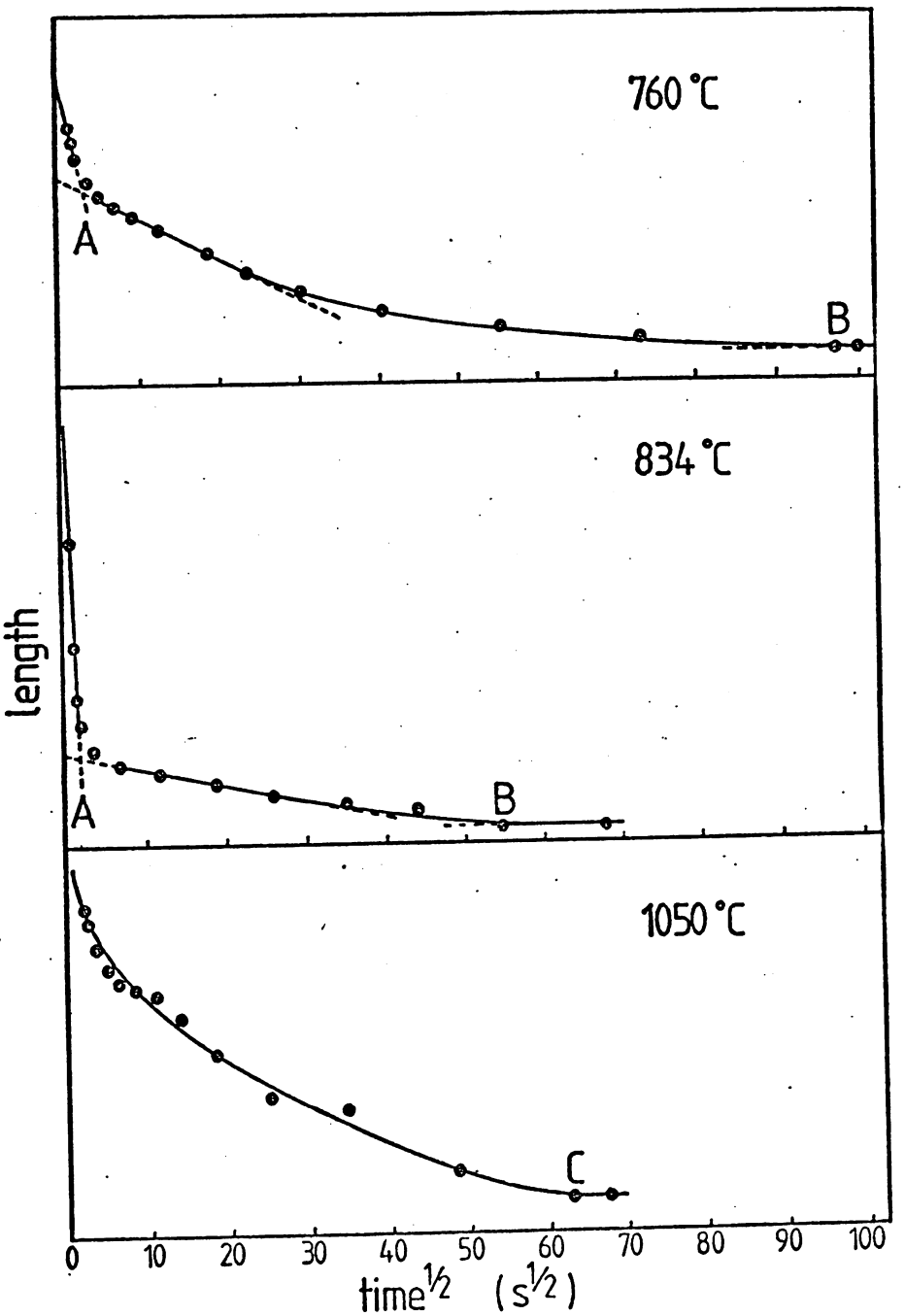

Fig. 6.1: Dilatometer length traces, plotted against the square root of time, for isothermal reaustnitisation at:

a) 760°C
b) 834°C
c) 1050°C

above the Ac_3 (up to about 900°C), where behaviour similar to that at lower temperatures was found. An example of a length v. $t^{1/2}$ plot for 1050°C, a temperature well above the Ac_3, is given in Fig. 6.1c. A rapid initial large length drop occurs, and is followed by a more gradual length change, continuing until the time marked C in Fig. 6.1c. Similar long reaction times were found at all temperatures above the Ac_3.

6.2.4 The Reaustenitisation TTT Curve

The reaustenitisation TTT curve is presented in Fig. 6.2. No reaction start curve is given, as the transformation started too rapidly to allow measurement. The points in the bands labelled A, B and C correspond to points similar to those marked A, B and C respectively in Fig. 6.1, and are taken from length v. $t^{1/2}$ plots at various temperatures. Thus, band A signifies the time at which the reaction rate changes, and bands B and C signify the time at which all reaction finishes.

Between the Ac_1 and Ac_3 temperatures, it can be seen that the points A fall in a band which lies at shorter times at the higher temperatures, while the points B fall broadly on a C-curve. The band A varies from a maximum time of about 30s at the low temperature end of the two phase region, to about 2s at the high end. The minimum time of the band B occurs in the middle of the two-phase temperature range, at a temperature of about 780°C and a time of about 1000s. At higher and lower temperatures, longer times, of up to 100,000s, are recorded. The data shows a lot of scatter.

Above the Ac_3, the final points, C, lie on a smooth curve which decreases in time with increasing temperature, varying from over 10,000s near the Ac_3 to about 3000s at 1050°C.

6.2.5 A Possible Interpretation

A possible interpretation of the dilatometric results will now be given, and will be discussed in subsequent sections.

In the two-phase austenite plus ferrite temperature range, the reaustenitisation reaction takes place in two stages, the length change in each being linearly related to $t^{1/2}$. It is suggested that the first reaction involves the carbon-diffusion-controlled transformation to austenite without redistribution of manganese (the no-partition of Mn reaction), and that the second reaction is manganese diffusion

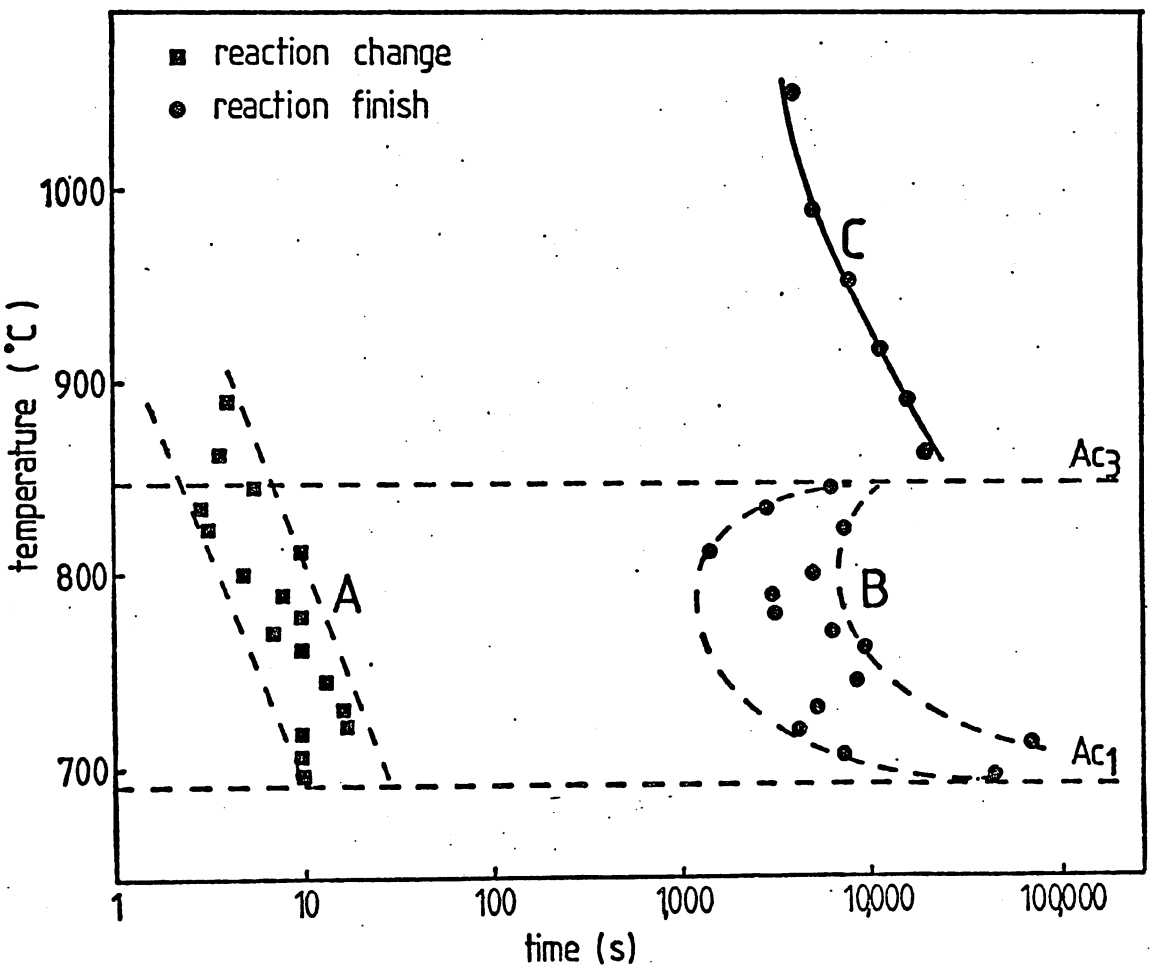

Fig. 6.2: TTT curve for reaustenitisation of martensite in Fe-1.2%Mn-0.1%C, obtained by dilatometry.

controlled and involves further transformation to austenite associated with redistribution of both manganese and carbon (the partition reaction).

If this is the case, it should be possible to show:
a) that some transformation to austenite occurs during the first reaction (before A) and that austenitisation continues during the second reaction (after A), and
b) that during the first reaction, no movement of manganese occurs, while during the second reaction, manganese partitions between austenite and ferrite.
Metallography and microanalysis were the techniques used to investigate this, and the results are reported in section 6.3.

Some thermodynamics of phase equilibria in the two-phase region are considered in section 6.4, in order to test:
i) whether a no-Mn-partition reaction is feasible throughout the temperature range in which the two stage reaction occurs, and
ii) whether the no-partition and partition reactions are expected to produce different volume fractions of austenite.
The kinetics of such reactions are also considered.

It is proposed that the C-shape of the reaction finish curve, at B in the two-phase region (Fig. 6.2), is due largely to impingement, as first put forward in chapter 5, section 5.4.4. This possibiltiy will be considered in more detail in section 6.5.

It is suggested that the long time process above the Ac_3, finishing at C in Figs. 6.1c and 6.2, is the process of recrystallisation. This will be discussed in section 6.6.

Finally, the scatter of the kinetic data in the two-phase region is attributed to inhomogeneity of the starting structure samples, which had not been austenitised for a sufficiently long time to ensure a homogeneous distribution of manganese.

6.3 Metallography and Microanalysis

Specimens for microscopy and microanalysis were heat treated in a conventional tin bath and water quenched, as quenching to martensite in situ in the dilatometer proved unreliable. It was shown in chapter 5, section 5.4.2 that austenite nucleation in a 10%Cr steel was enhanced by

the heating method used in the dilatometer; thus in that system conventionally heated samples could not be directly related to dilatometer results. In the Fe-1.2%Mn-0.1%C alloy, however, nucleation was observed to be very rapid (ie. too rapid to be measured) both in the dilatometer and during conventional heating, and direct comparison was possible.

6.3.1 Metallography of Reaustenitisation of Martensite

Specimens which had been partially reaustenitised from martensite at temperatures low (750°C) and high (825°C) in the two-phase austenite plus ferrite region, were examined after quenching. Etching characteristics of the phases in specimens for optical microscopy were variable, but interpretation was aided by electron microscopy. In general, it was possible to distinguish the original martensite from the final martensite, as the original martensite recrystallised during austenitisation.

a) Optical Microscopy

Fig. 6.3 shows micrographs of specimens which have been reaustenitised at 750°C for 3s, 10s and 4500s. From the TTT curve, Fig. 6.2, it can be seen that 3s lies in the regime in which the first reaction is taking place, 10s is close to the reaction change time (band A) while 4500s is near the reaction finish time (band B). It is clear that considerable transformation has occurred between each of the micrographs illustrated, showing that austenite does indeed form during both the first and the second reactions.

Fig. 6.4 illustrates the sequence of reaustenitisation at 825°C, the specimens having been transformed for 3s (near the change time, A), 100s (in the middle of the second reaction) and 3600s (near the reaction finish time, B). Again, the volume fraction of austenite is seen to increase throughout the second reaction.

The change in morphology from predominantly acicular austenite at 750°C, to predominantly globular austenite at the higher temperature of 850°C, is in accordance with previous observations (eg Matsuda and Okamura 1974), the higher driving force at higher temperatures allowing austenite to grow past the restraining martensite lath boundaries.

Because of the fineness of the structure, and the difficulty in delineating the phase boundaries, no attempt was made to measure volume

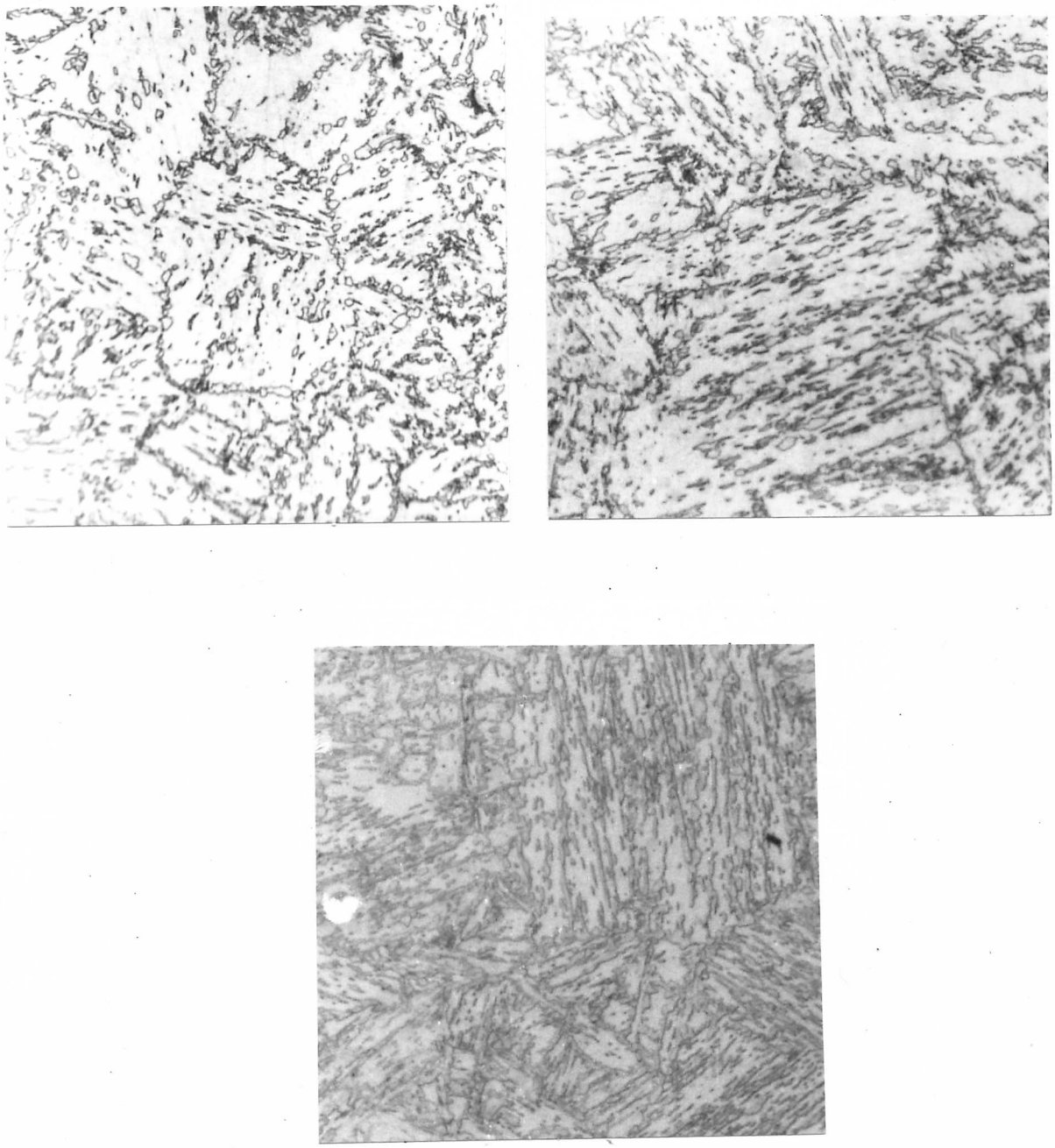

Fig. 6.3: Growth of austenite in martensite. Partial reaustenitisation at 750°C, followed by quenching.

a) 3s. Austenite (now martensite) in fine discrete particles.
b) 10s. As for 3s.
c) 4500s. Austenite (now martensite) is the darker etching constituent.

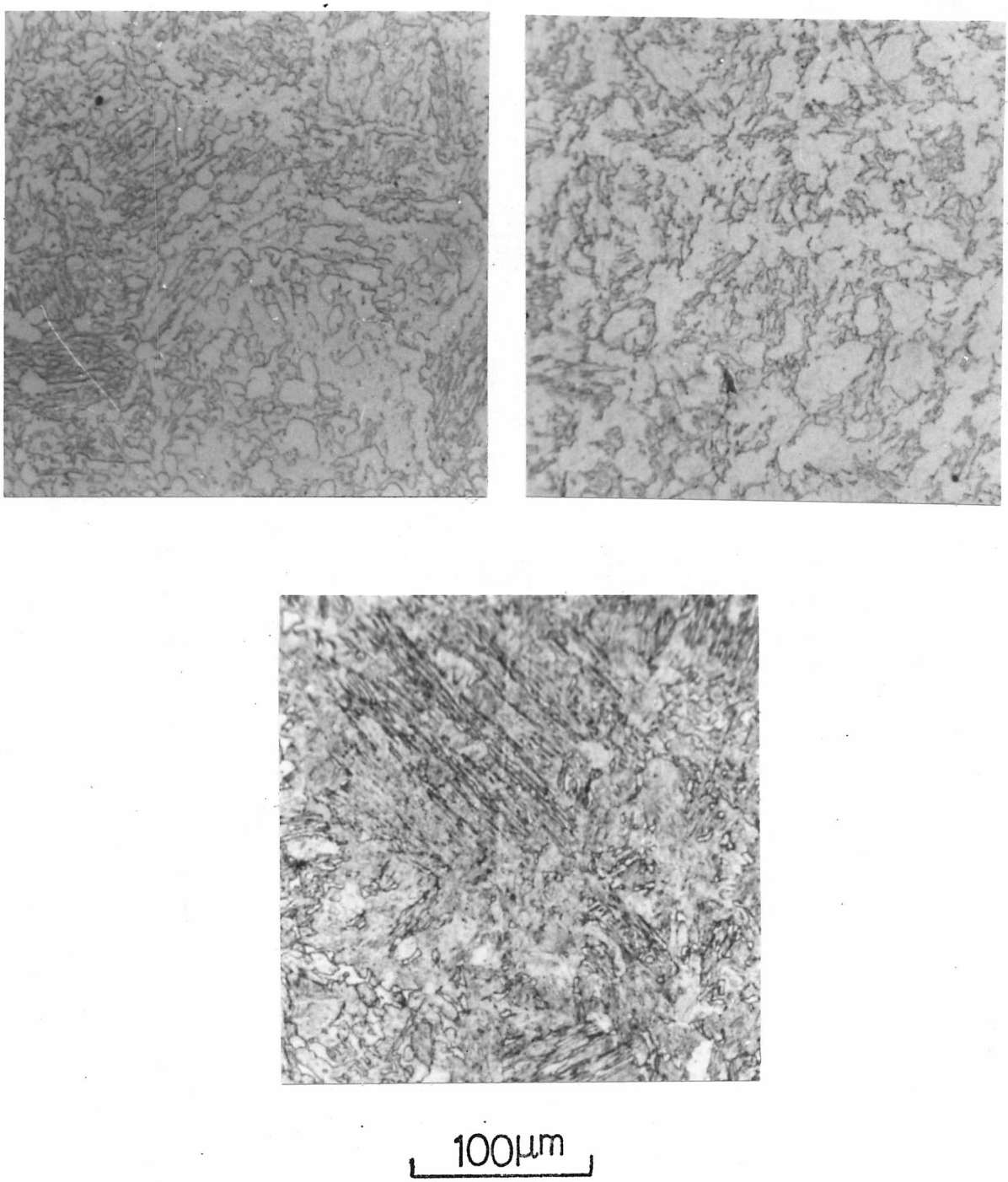

Fig. 6.4: Growth of austenite in martensite. Partial reaustenitisation at 825°C, followed by quenching.

a) 3s. Austenite (now martensite) is the lighter etching constituent.
b) 100s. As for 3s.
c) 3600s. Mostly austenite (now martensite), containing a few small, light etching ferrite areas (from prior martensite).

fractions of transformation in these specimens.

b) Electron Microscopy

The original martensite was observed to recrystallise rapidly with time at temperature, many of the martensite lath boundaries disappearing within a few seconds at the austenitising temperature. Fig. 6.5 is an electron micrograph showing several austenite nodules (now martensite) in a matrix of recrystallised martensite (which is now essentially ferrite) after transformation at 750°C for 900s. Cementite particles were never seen in partially reaustenitised and quenched samples, indicating that the heating rate from room temperature to the two phase austenite-ferrite region was sufficiently rapid to prevent the precipitation of carbides of a detectable size.

In all specimens examined by electron microscopy, the martensite nodules (which were previously austenite) were searched for retained austenite, using a dark field technique. Retained austenite was never observed in specimens which had been reaustenitised for only short times, but was occasionally observed in long time specimens. Fig. 6.6 shows a bright field-dark field pair of electron micrographs, which depict a martensite nodule in a specimen which has been held for a long time (900s) at 825°C, and quenched. The dark field image was produced from an (002) austenite diffraction spot, and retained austenite between the martensite laths has been imaged. Since austenite stabilisers such as manganese are known to encourage the retention of austenite, the occurrence of retained austenite only in specimens which had been reaustenitised for long times is supporting evidence for the partition of manganese to austenite in the latter part of the transformation.

6.3.2 Microanalysis

Specimens for microanalysis were partially reaustenitised at 750°C for 3s, 10s, 100s, 900s and 4500s, and water quenched. Analysis was carried out on thin foils in a Philips 400 electron microscope operating in the TEM mode, using a Link energy dispersive X-ray analysis system.

a) Correction Factors for Fe and Mn

The correction procedures described in chapter 4, section 4.4.1 were used to convert X-ray intensity ratios to compositions. The constant of proportionality for Fe and Mn, k_{FeMn}, was calculated to be 1.0218. The effect of the absorption of X-rays in the specimen was found to be negligible, as the difference in mass attenuation

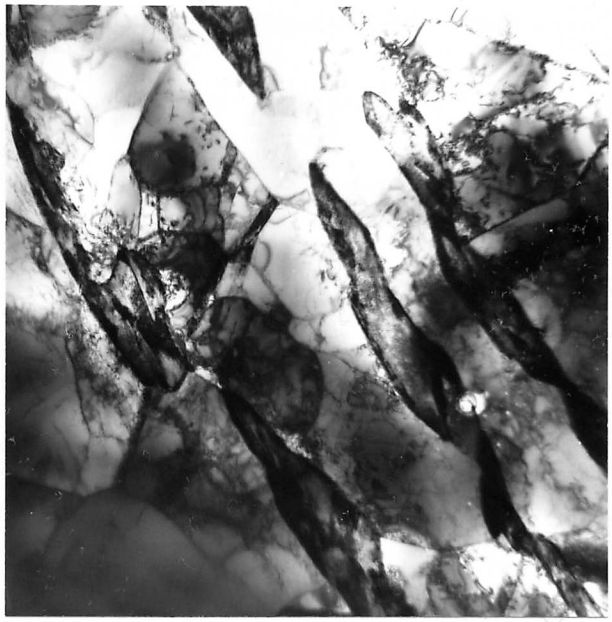

Fig. 6.5: Austenite (now martensite, dark etched) nodules growing in martensite (now ferrite). 15 mins 750 C.

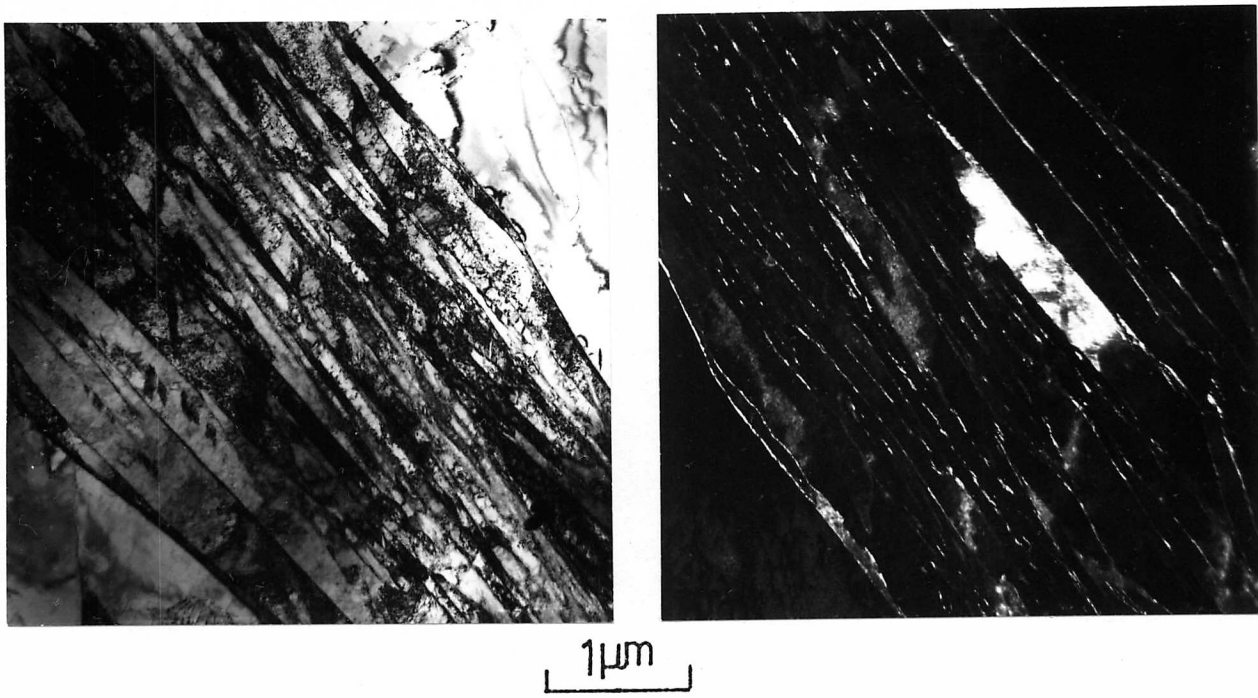

Fig. 6.6: Bright field - dark field pair of an austenite (now martensite) nodule containing retained austenite, imaged in dark field with an (002) diffraction spot. 15 mins 825 C.

coefficients, $\left(\left(\frac{\mu}{\rho}\right)^{Mn}_{FeMn} - \left(\frac{\mu}{\rho}\right)^{Fe}_{FeMn}\right)$ is always less than about 20 (cf. table 4.1 for Fe and Cr). Fluorescence effects were also found to be negligible, and beam spreading was calculated to be about 20nm in a foil of thickness 100nm.

b) Results and Discussion

In each of the specimens, several (10 - 15) measurements of Mn content were made on the ferrite regions and on the martensite (previously austenite) regions. After applying correction procedures, mean compositions were calculated, and measurements which were more than two standard deviations from the mean were discarded (this occurred in less than 10% of cases). The resulting mean compositions of austenite (c_γ) and ferrite (c_α), together with the standard deviations of the means, are given in table 6.1. The difference in manganese content between austenite and ferrite, $c_\gamma - c_\alpha$, in each specimen is also given, and the final column indicates whether this difference is significant within experimental error ie. whether the compositions of austenite and ferrite are the same within one standard deviation of the mean or not.

It can be seen from the austenite-ferrite composition differences in table 6.1 that partitioning of Mn to austenite is not detected in the early stages of the reaustenitisation reaction, but that partitioning occurs during the later stages, and increases with time. This evidence supports the hypothesis put forward in section 6.2.5; ie that the early stages are carbon diffusion controlled (not requiring manganese partitioning) while the later stages are Mn diffusion controlled. Referring to the dilatometrically determined TTT curve of Fig. 6.2, it can be seen that at 750°C, the change in reaction rate at the time when Mn diffusion becomes rate controlling (band A), occurs at around 10s. The microanalytical results given in table 6.1 show that partitioning of Mn is not detectable until after 100s; during the early stages of the Mn-partition reaction partitioning is likely to be too small to be measured. It is therefore concluded that partitioning of Mn occurs during the later stages of the reaction, and it seems likely that partitioning starts at the time at which the reaction rate changes, ie. about 10s.

It should be noted that the overall Mn content of the specimens in table 6.1 varies considerably. This is taken to reflect true variations in Mn content from specimen to specimen, due to inhomogeneity of the stock from which the specimens were made, and explains the broad scatter

Table 6.1: Mn contents of ferrite and martensite after partial reaustenitisation at 750°C and quenching.

Time at 750°C (s)	%Mn in ferrite c_α	St. dev. of the mean	%Mn in martensite c_γ	St. dev. of the mean	$c_\gamma - c_\alpha$	Significance of $c_\alpha - c_\gamma$, within experimental error
3	1.174	0.068	1.185	0.053	0.011	Not significant
10	1.249	0.056	1.343	0.047	0.094	Not significant
100	1.274	0.077	1.269	0.047	-0.005	Not significant
900	1.280	0.059	1.447	0.074	0.167	Significant
4500	1.047	0.051	1.271	0.045	0.224	Significant

of dilatometric data points on the TTT curve, Fig. 6.2.

6.4 Thermodynamics and Kinetics of Reactions in the Two-Phase Region

The aims of this section are to elucidate whether, during reaustenitisation of an Fe-C-X alloy (where X is a substitutional alloying element):

a) it is thermodynamically feasible for a no-partition of X reaction to occur at all temperatures in the two-phase region, and

b) the kinetics are such that an X-partition reaction is likely to follow.

A brief review of some previous work on partitioning will now be given, followed by a consideration of free energy changes during transformations in two-phase regions in three component systems. Calculated values of phase compositions and proportions at temperatures throughout the two-phase region in the Fe-1.2%Mn-0.1%C alloy will then be presented, and finally, comparisons between experimental and theoretical behaviour will be made.

6.4.1 Background

For clarity, three change temperatures relevant to the austenite-ferrite reactions in a ternary Fe-C-X alloy (where X is a substitutional alloying element) will now be defined.

1. Ae_3 temperature: The Ae_3 is the equilibrium $\delta/(\alpha+\delta)$ phase boundary, both α and δ having their equilibrium compositions in C and X.
2. T_o temperature: The T_o temperature is that at which austenite and ferrite with the same composition have the same free energy.
3. Ae_3' temperature (no-partition Ae_3): The Ae_3' is the metastable $\delta/(\alpha+\delta)$ phase boundary, for austenite and ferrite of the same X content, but (in general) different C contents.

Aaronson et al (1966b) obtained thermodynamic expressions for these change temperatures and phase boundaries by developing a theory (Zener 1955) of the effect of alloying elements on phase transformations in binary iron alloys, and combining it with statistical thermodynamic theories of Fe-C alloys (Aaronson et al 1966a). The Ae_3 for Fe-Mn-C alloys, and the Ae_3' and T_o temperatures for Fe-1.2%Mn-C alloys have been calculated (Bhadeshia 1980), and their variation with carbon

content can be seen in Fig. 6.7. Similar curves are found for other Fe-C-X alloys (Aaronson et al 1966b).

Aaronson and Domian (1966) investigated experimentally the growth of proeutectoid ferrite in several Fe-C-X alloys. Partitioning of the alloying element was never observed below the Ae_3', a no-X-partition reaction occurring at these temperatures. In systems in which the Ae_3 and Ae_3' were widely separated, such as those containing over 3%Mn or Ni, the proeutectoid ferrite reaction above the Ae_3' was observed to involve the partition of the alloying element between austenite and ferrite. In other cases, the times used experimentally were insufficient to allow a partition reaction to be observed. The results of Kinsman and Aaronson (1967) (Fe-C-Mn or Mo alloys) and Purdy et al (1964) (Fe-C-Mn alloys) follow the same pattern.

Kogan and Entin (1971) investigated transformations in the two-phase region in Fe-Cr/Ni pseudo-binary alloys (5-8%Cr and 2-3%Ni). They found that no-partition austenite-ferrite and ferrite-austenite reactions occurred below and above the T_o temperature respectively. Also, at temperatures fairly high in the two-phase region, redistribution of alloying elements during reaustenitisation was found to occur.

Thus, no-X-partition reactions have been reported to occur during formation of ferrite below the Ae_3' in Fe-C-X alloys, and during formation of austenite above the T_o in Fe-X alloys. The behaviour to be expected throughout the two-phase region in an Fe-C-X alloy will now be rationalised in terms of free energy.

6.4.2 Free Energy Considerations

The Ac_1 temperature of the Fe-1.2%Mn-0.1%C alloy has been determined as 695°C. Referring to Fig. 6.7, it is obvious that on heating an alloy containing 0.1%C through the two-phase region (between Ae_1 and Ae_3), temperature regions below T_o, between T_o and Ae_3', and between Ae_3' and Ae_3, are traversed. It can also be seen that at any particular temperature, alloys with different carbon contents lie in different temperature regimes; for instance, at 750°C, a low carbon alloy lies below its T_o temperature, a slightly higher carbon alloy lies in the temperature regime between its T_o and Ae_3' temperatures, and higher carbon alloys lie between their Ae_3' and Ae_3 temperatures, or above their Ae_3 temperatures. Thus, the variation in behaviour of

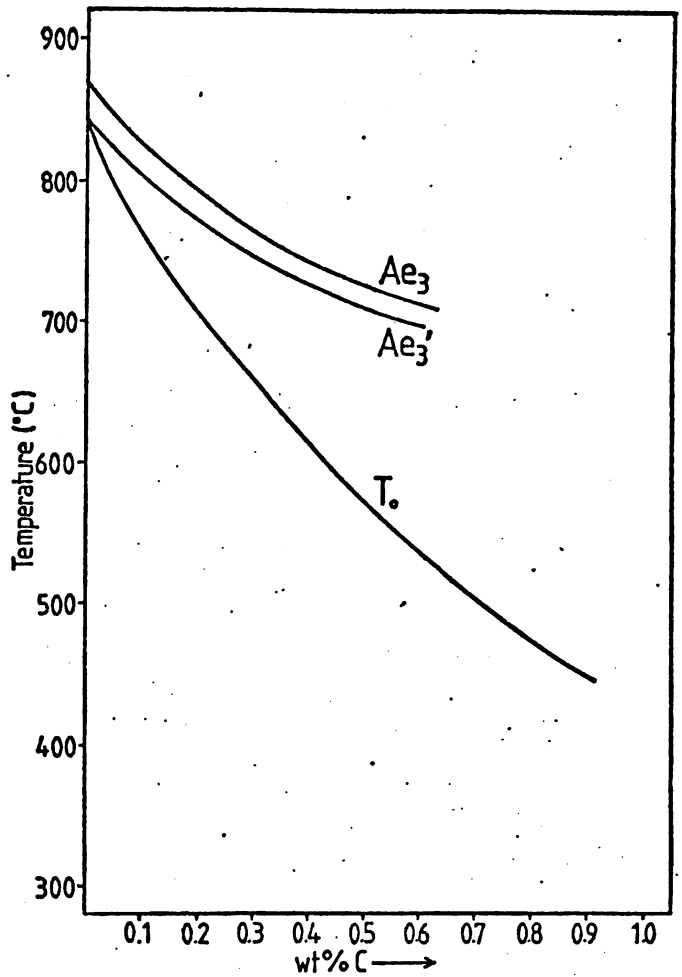

Fig. 6.7: Variation of the Ae_3, Ae_3' and T_o temperatures with carbon content in Fe-1.2%Mn-C alloys (for definitions, see text).

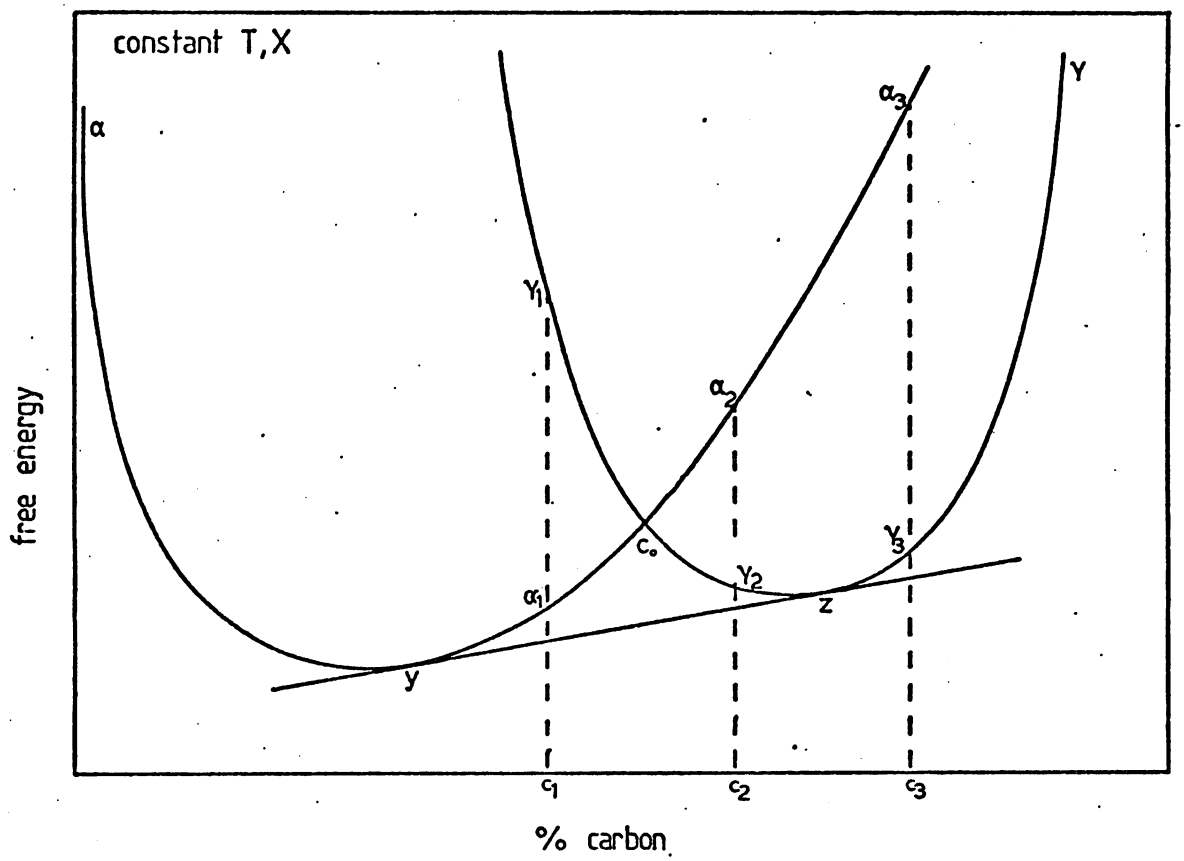

Fig. 6.8: Schematic section through free-energy - composition surface in an Fe-C-X alloy. The section is at constant X (the X content of the alloy) and at constant temperature. Variation of free energy with carbon content is shown.

alloys of different carbon contents at a constant temperature is analogous to the variation in behaviour of a single alloy with constant carbon content at different temperatures.

A schematic section through an Fe-C-X free-energy-composition diagram, at constant temperature and constant X content (the X content of the alloy), showing variation of free-energy with carbon content, is given in Fig. 6.8. The composition c_o is that at which the free energies of austenite and ferrite are the same; thus for an alloy of composition c_o, the temperature of the diagram is T_o. The compos ition z is that at which austenite is in metastable equilibrium with ferrite of the same X content, but of carbon content y. Thus, for alloys with carbon content z, the temperature of the diagram is the Ae_3'. The Ae_3 composition lies outside the plane of the diagram, as it occurs at a different X content; however, it must lie at a higher C content (see Fig. 6.7). Thus alloys of compositions c_1, c_2 and c_3 of Fig. 6.8, correspond to alloys lying in the temperature regimes below T_o, between T_o and Ae_3', and between Ae_3' and Ae_3, respectively.

It can be seen that for ferrite such as α_1 and α_2, with carbon contents c_1 and c_2, a driving force (ie. decrease in free energy) exists for the formation of ferrite and austenite with the same X content, and with C contents y and z respectively. (In fact, for ferrite α_2, a driving force exists for the formation of austenite γ_2 without partitioning of C or X. However, it is thought that this product will not be observed, as ferrite and austenite partitioned in carbon, of compositions y and z respectively, will rapidly form.) Thus, both above and below T_o (corresponding to the right and to the left of composition c_o in Fig. 6.8) no-X-partition reaustenitisation reactions can occur. Similarly, no-X-partion austenite decomposition reactions can occur from austenite such as γ_1 and γ_2 in Fig. 6.8, with carbon contents c_1 and c_2. The driving force for reaustenitisation is greater than for austenite decomposition above T_o, and vice versa below T_o. The redistribution of X (out of the plane of section in Fig. 6.7), and associated redistribution of carbon, will lead to a further reduction in free energy, and finally to the equilibrium phases.

Between the Ae_3' and Ae_3 temperatures (or for alloy compositions to the right of composition z in Fig. 6.8), a reduction in free energy cannot be achieved by redistribution of C without movement of X. Considering firstly austenite decomposition, austenite γ_3 of composition

c_3 in Fig. 6.8 can only decrease its free energy by a reaction involving redistribution of X (out of the plane of the diagram); thus above the Ae_3', decomposition of austenite must involve partitioning of both X and C. During reaustenitisation, however, ferrite α_3 of composition c_3 can decrease its free energy by transforming to austenite of the same composition, γ_3; partitioning of neither C nor Mn is required. The reaction should thus occur very rapidly, as no long range diffusion is required, and may go to completion both above and below the Ae_3. However, below the Ae_3 temperature, the equilibrium product is a partitioned austenite-ferrite mixture; thus any fluctuations in X content should prevent completion (or cause reversal) of the austenite reaction.

To summarise:

(1) During isothermal decomposition of austenite in Fe-C-X alloys-
a) at temperatures between the Ae_3 and Ae_3', both C and X must partition between austenite and ferrite,
b) at temperatures below the Ae_3' (both above and below T_o), a reaction which does not involve redistribution of X is thermodynamically feasible; to reach equilibrium, an X-partition reaction must also occur.
c) at temperatures below T_o, a reaction which does not involve redistribution of C or X is feasible; to reach equilibrium partitioning of both C and X must occur.

(2) During isothermal reaustenitisation-
a) at temperatures between Ae_1 and Ae_3' (both above and below T_o) a reaction which does not involve redistribution of X is thermodynamically feasible; to reach equilibrium, an X-partition reaction must also occur,
b) at temperatures between T_o and the Ae_3', a reaction involving partitioning of neither C nor X is feasible, although transformation involving redistribution of C only is more favourable, and the redistribution of X must also occur to achieve equilibrium,
c) at temperatures between the Ae_3' and the Ae_3, a reaction which involves partition of neither X nor C is feasible; to reach equilibrium redistribution of both X and C must occur,
d) above the Ae_3, no partition of X and C is necessary.

6.4.3 Calculated Phase Equilibria

Using the equilibrium $\gamma/(\alpha+\gamma)$ phase boundaries for Fe-Mn-C alloys determined by Purdy et al (1964), and extrapolating to lower temperatures, isothermal sections of the ternary Fe-Mn-C equilibrium diagram, and $(\alpha-\gamma)$ tie lines, have been calculated for several temperatures throughout the two-phase austenite-ferrite region (Bhadeshia 1980), and are illustrated in Fig. 6.9.

Using these data, the $(\alpha-\gamma)$ tie lines passing through the alloy composition used in the present work (Fe-1.2%Mn-0.1%C) were determined, for both equilibrium partitioning of Mn, and no-partition of Mn (from Ae_3' curve, Fig. 6.7). Examples are given in Fig. 6.10. Applying the lever rule, it can be seen that the volume fractions of austenite and ferrite present at the end of the no-partition reaction and at equilibrium differ substantially, particularly at high temperatures. Volume fractions of austenite and ferrite were calculated for temperatures throughout the two-phase region, and are plotted as a function of temperature in Fig. 6.11. The no-partition volume fractions refer to the proportions of austenite and ferrite with the same X content which would be present if the no-partition reaction were allowed to go to completion (ie. to reach the stage at which no further driving force for a no-X-partition reaction exists); the equilibrium volume fractions refer to austenite and ferrite whose compositions and proportions have reached equilibrium. The curves in Fig. 6.11 apply to both austenite decomposition and reaustenitisation. It is clear that more ferrite exists at equilibrium than at completion of the no-partition reaction; similarly, there is less austenite at equilibrium than at the end of the no-partition reaction.

It should be noted that at temperatures below about 725°C, cementite is thermodynamically stable. The reaction in the three-phase austenite-ferrite-cementite regime is not considered here.

6.4.4 Comparison of Theoretical and Experimental Reaustenitisation Behaviour

a) The Temperature regime between the Ae_1 and Ae_3'

Theoretical considerations involving free energy have shown that at temperatures in the two-phase region below the Ae_3', an austenite reaction involving partition of C but not of Mn is feasible, although Mn must partition to achieve equilibrium. Experimental results of

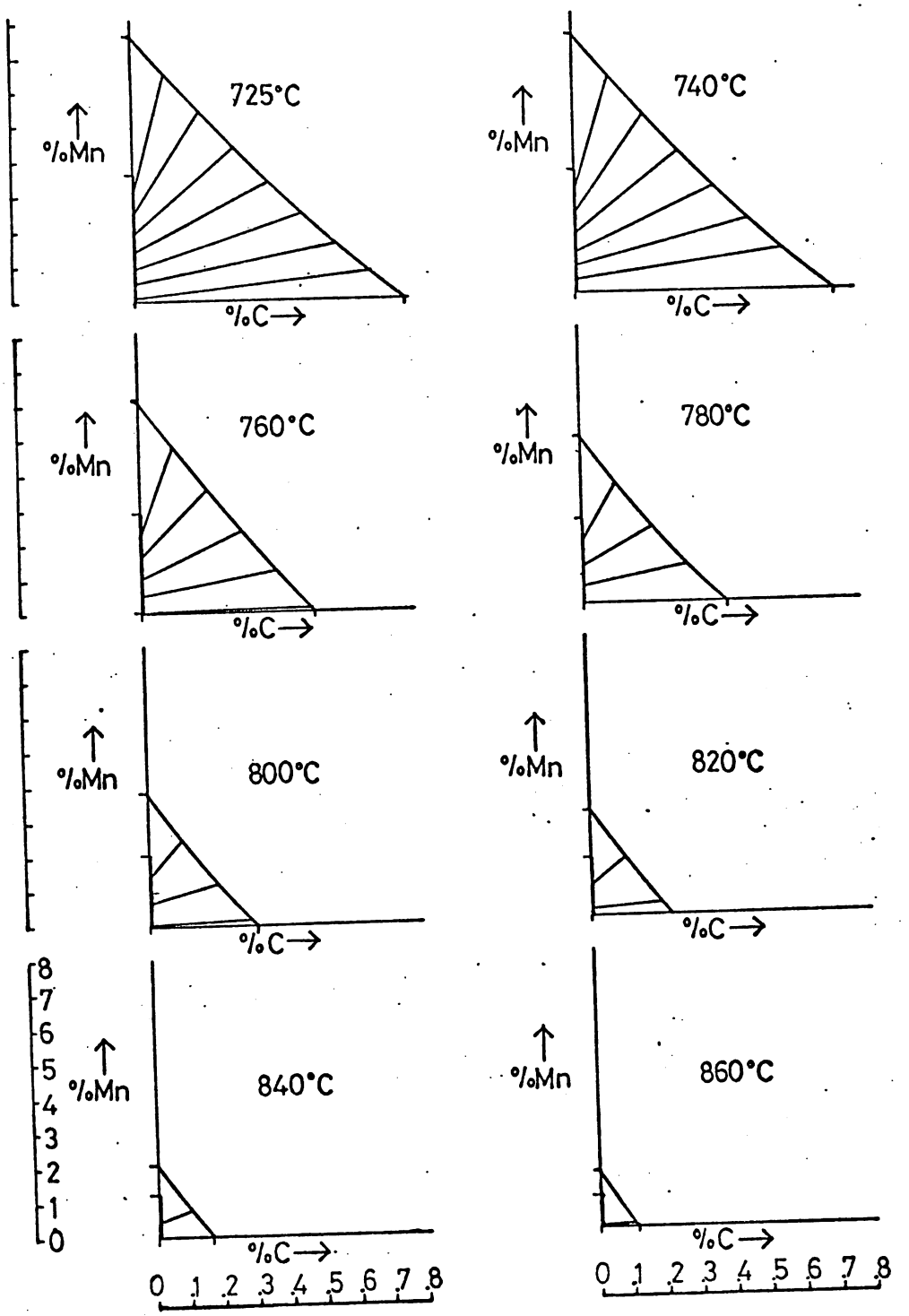

Fig. 6.9: Isothermal sections of the ternary Fe-Mn-C phase diagram, showing two-phase α-γ regions. Calculated tie lines from austenite (on the right) to ferrite (on the left, approximately 0%C) are shown.

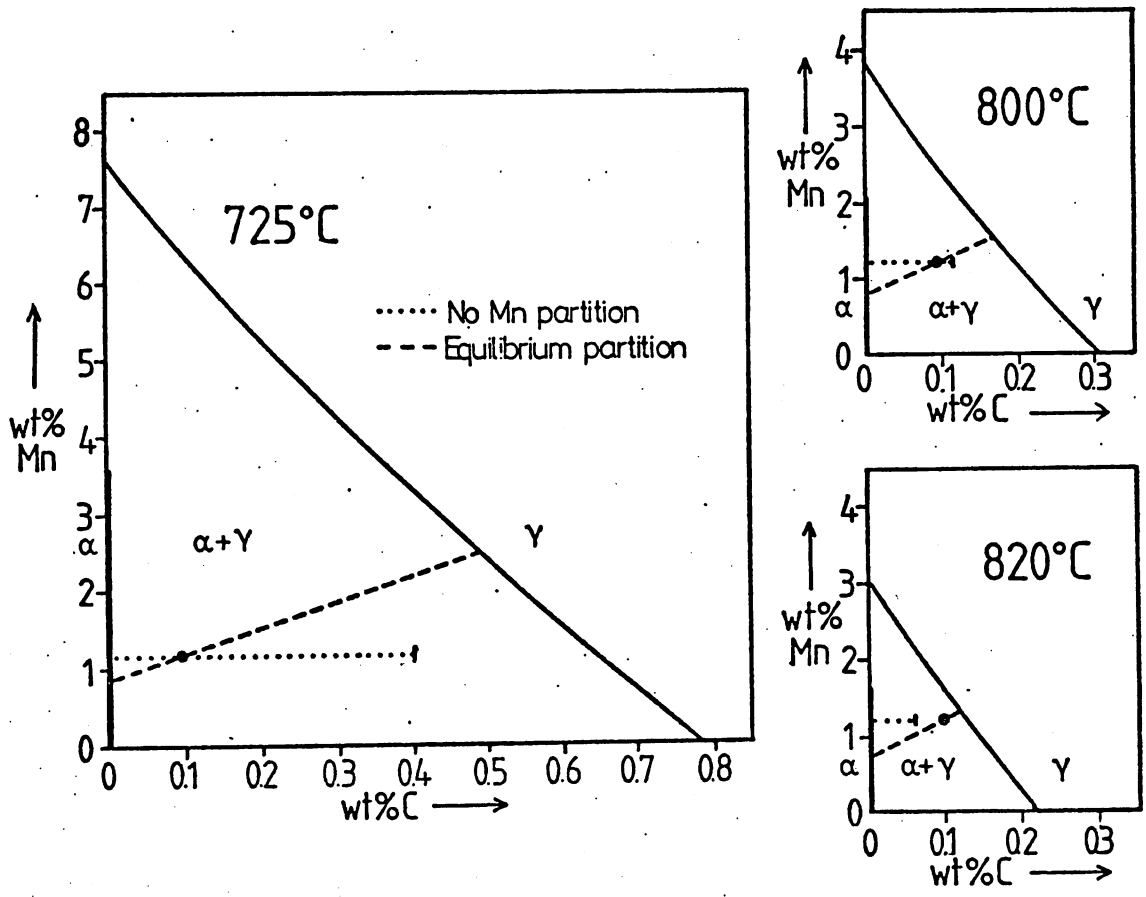

Fig. 6.10: Isothermal sections of the ternary Fe-Mn-C phase diagram, showing equilibrium and no-Mn-partition α-γ tie-lines, passing through the composition Fe-1.2%Mn-0.1%C.

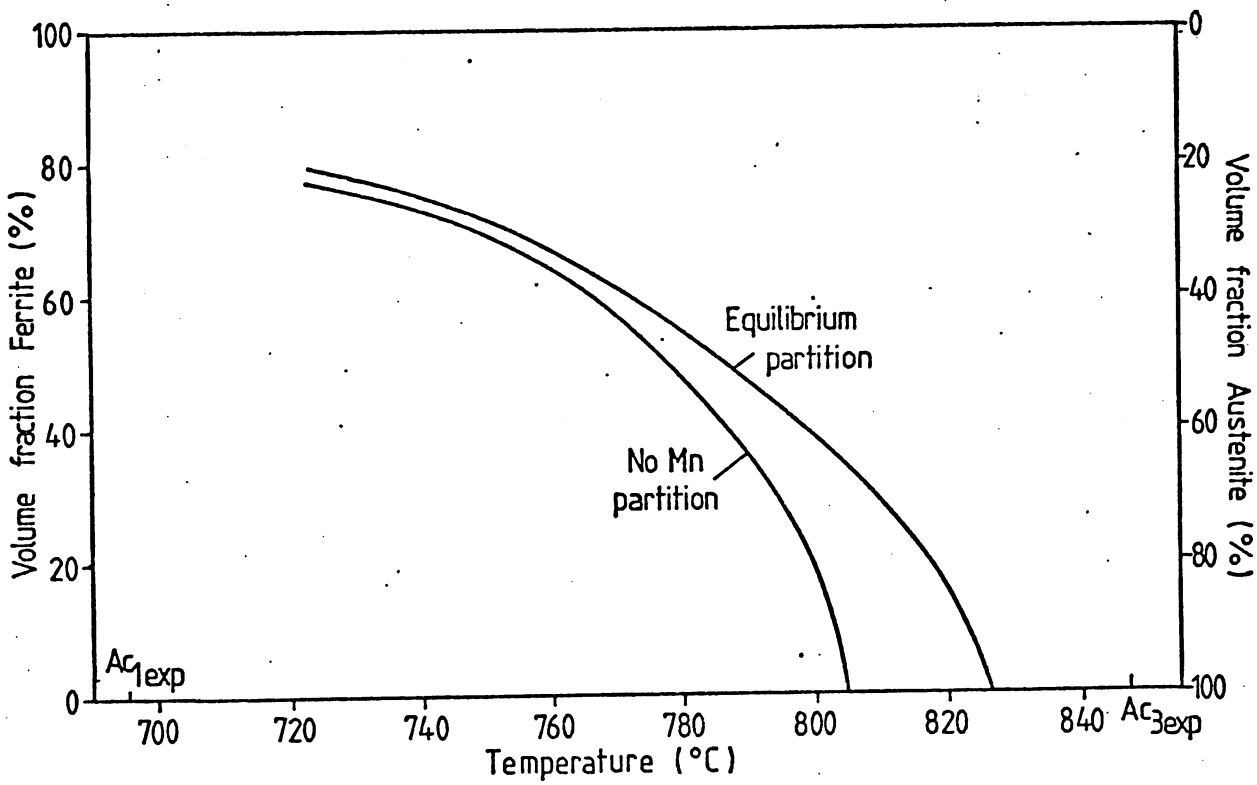

Fig. 6.11: Proportions of austenite and ferrite present at temperatures in the two phase α-γ region at completeion of the no-Mn-partition reaction, and at equilibrium. (For explanation, see text.)

dilatometry showed that at temperatures throughout the two-phase region, isothermal reaustenitisation of an Fe-1.2%Mn-0.1%C alloy occurred in two consecutive stages, the reaction rate in each stage being related to $t^{1/2}$ (indicative of volume diffusion control). It is therefore concluded that in the temperature regime below the Ae_3', the first stage of reaustenitisation is carbon diffusion controlled and does not involve partitioning of Mn, while the second stage is Mn diffusion controlled, involving partitioning of both Mn and C.

Calculations of phase equilibria have shown that at all temperatures throughout the two-phase region, the fraction of austenite attainable by the no-Mn-partition reaction is greater than that at equilibrium (see Fig. 6.10). Experimentally, however, the volume fraction of austenite is found to increase with time until the end of transformation; thus it is seen that the no-Mn-partition reaction does not go to completion. This behaviour can be explained on kinetic grounds, which will now be discussed.

Whether the reaction involving no-partitioning of Mn, or the reaction involving full partitioning of both Mn and C, occurs at any stage is determined by which reaction can decrease the free energy of the system most rapidly. Since carbon diffuses much more rapidly than manganese, the no-partition reaction, which involves only carbon diffusion and releases some free energy, is favoured initially. However, the equilibrium partition reaction, involving diffusion of manganese, is able to release more free energy. Any diffusion controlled reaction slows down with time (as $t^{1/2}$), and as the rate of the carbon diffusion controlled reaction decreases, a critical point is reached, at which a reaction involving the diffusional partitioning of manganese further decreases the free energy of the system more rapidly than does a continuing no-Mn-partition reaction. The reaction then changes from a carbon diffusion controlled no-Mn-partition reaction to a Mn diffusion controlled partition reaction. In the Fe-1.2%Mn-0.1%C system, the change is seen to occur after a few seconds,well before the no-Mn-partition reaction goes to completion.

The time at which the change occurs decreases with increasing temperature (see Fig. 6.2, band A). This is as expected, since the rates of diffusion of both carbon and manganese increase with temperature.

It was noted qualitatively in section 6.2.3, that at a temperature low in the two-phase region, the greater proportion of the two-stage isothermal austenitisation reaction occurs during the second stage of the reaction. At higher temperatures, the greater proportion occurs during the first stage. This is in accordance with the increase in driving force (free energy change) for the first stage no-Mn-partition reaction as the temperature increases (as discussed in section 6.4.2).

b) The Temperature regime between the Ae_3' and Ae_3

The calculated Ae_3 (827°C) is somewhat lower than the experimental Ac_3 (847°C), determined by continuous heating. Since metallographic observations (chapter 3, section3.5) and the shape of the TTT curve (Fig. 6.2) support an Ac_3 of about 850°C, the difference in calculated and experimental change temperatures will be taken as real. As the calculated Ae_3 and Ae_3' temperatures are about 22°C apart, the experimental Ae_3' will be taken as 825°C, 22°C below the experimental Ac_3 (847°C).

From free energy considerations (section6.4.2), a reaustenitisation reaction which is not diffusion controlled is expected to occur at temperatures between the Ae_3' and the Ae_3, although manganese diffusion must take place to attain equilibrium. Isothermal dilatometry, however, shows two diffusion controlled reactions in this temperature range, (see Fig. 6.1b, 834°C) as at lower temperatures. The second stage of the austenitisation reaction is again likely to be the manganese diffusion controlled partition reaction. The first stage, however, should not involve diffusional partition of either Mn or C. It can only be postulated that movement of the transformation front at this stage is slowed down by solute drag (of C or Mn) and thus the reaction appears to be diffusion controlled.

6.5 Impingement

It was suggested earlier (sections 5.4.4 and 6.2.5) that the C-shape of the austenitisation finish TTT curve in the two-phase region was due to interaction of several opposing factors. This will now be considered in more detail, and the importance of impingement will be considered.

On isothermal reaustenitisation at increasing temperatures in the two-phase region, the effects of increased driving force and diffusion

rate (and hence growth rate) are offset by the increased volume fraction of austenite which must form. It is difficult to predict the outcome of interaction between these factors in terms of variation of austenitisation finish times with temperature, although it seems likely that the reaction will finish more rapidly at higher temperatures. However, at high volume fractions of transformation, neighbouring growth centres or diffusion fields impinge, and the growth rate slows down. Thus, at temperatures high in the two-phase region, at which large amounts of transformation occur, the growth rate will slow down during the latter part of the reaction. The time taken to reach equilibrium at such high temperatures will be greater than the time taken at lower temperatures, when lower volume fractions of austenite form, and impingement does not occur. The reaction will thus finish most rapidly at a temperature in the middle of the range, and a reaction finish curve in the form of a C-curve will result.

In the foregoing argument, it was assumed that the onset of impingement occurs at a constant volume fraction, regardless of temperature. Since impingement of diffusion fields is in question, and rates of diffusion and boundary conditions for diffusion during transformation vary with temperature, the basis for the assumption is by no means obvious. In order to show that the onset of impingement is not a function of variables such as temperature, impingement theory will now be developed, and a discussion of the experimental results follows.

6.5.1 Development of Impingement Theory

Johnson and Mehl (1939) modelled the transformation kinetics of nucleation and growth processes, and obtained an expression for the volume fraction transformed as a function of time for specific nucleation and growth characteristics, having taken into account impingement of neighbouring growth centres. Avrami suggested a more general growth equation:

$$X = 1 - \exp(-(kt)^n) \qquad (6:1)$$

where X is the transformed fraction, t is time, k and n are constants. The exponent, n, is a function of the growth process and the nucleation and growth characteristics, while other constants and boundary conditions for growth are incorporated in the constant k. Values of n and k have been calculated and experimentally determined for many types of growth process, and are documented eg. by Christian (1975).

The Avrami equation describes sigmoidal growth with time, the reaction beginning slowly, when few growth centres are present, the rate then increasing and reaching a maximum, and finally slowing down towards the end of the reaction because of impingement. The point at which the reaction begins to slow down, ie. at which the growth rate is a maximum, is the point at which the effect of impingement is first felt.

To obtain the time t_o and volume fraction X_o at which the growth rate, dX/dt, becomes a maximum, the Avrami equation is differentiated with respect to time twice. Thus:

$$X = 1 - \exp(-(kt)^n)$$

$$\frac{dX}{dt} = (1-X)nk^n t^{(n-1)} \qquad (6:2)$$

$$\frac{d^2X}{dt^2} = nk^n\left[\exp(-(kt)^n)(n-1)t^{(n-2)} - t^{(n-1)}\exp(-(kt)^n)nk^n t^{(n-1)}\right] \qquad (6:3)$$

At the maximum growth rate, $\frac{d^2X}{dt^2}=0$, giving,

$$t_o^n = \frac{(n-1)}{nk^n} \qquad (6:4)$$

$$\text{and } X_o = 1 - \exp(\tfrac{1}{n}-1) \qquad (6:5)$$

Thus it has been shown that the volume fraction at which impingement sets in is a function only of the exponent n, which is a constant for a particular growth process, and not of any other variable such as time or temperature.

In the reaustenitisation reaction under consideration, growth is volume diffusion controlled, and nucleation is rapid. In these conditions, the exponent, n, has the value $3/2$ (Christian 1975). Thus, from equation 6:5,

$$X_o = 0.2835$$

The temperature at which impingement first occurs in a volume diffusion controlled reaction is thus that at which the fraction transformed reaches about 28%. The nose of the austenitisation finish C-curve will lie a little above this temperature, at the temperature at which the combined effect of impingement and increasing volume fraction overrides the combined effect of increasing diffusion and driving force.

6.5.2 Experimental Results

Because of the fineness of the microstructure obtained on reaustenitisation of martensite in the Fe-1.2%Mn-0.1%C alloy, it was thought that direct measurements of volume fractions would not give reliable results. The temperature at which the volume fraction reaches 28% was therefore calculated (as for Fig. 6.11). After allowance had been made for the known discrepancy between actual and calculated temperatures in this system (taken to be 20°C), the temperature at which the equilibrium austenite volume fraction is 28%, and thus the temperature above which the nose of the C-curve is expected, was found to be about 770°C. This can be compared with the C-curve in the TTT diagram, Fig. 6.2 (band B); agreement is as good as can be expected with such a large scatter of data points.

In conclusion, in the two-phase region the experimentally observed austenitisation kinetics, in the form of a C-shaped reaction finish curve, have been explained in terms of variations with temperature of growth rate, fraction of transformation and impingement effects, the overriding factor at high temperatures being impingement. Such C-curve kinetics have been observed in the reaction-finish behaviour of Mn-diffusion-controlled austenitisation in this alloy (Fe-1.2%Mn-0.1%C), and of C-diffusion-controlled austenitisation and Cr-diffusion-controlled carbide dissolution in an Fe-10%Cr-0.2%C alloy (chapter 5, section 5.4.4). Similar kinetics may be expected in other reactions in two-phase regions, such as austenite decomposition.

6.6 The Reaction above the Ac_3

The continuing reaction until long times at temperatures above the Ac_3 is at first sight somewhat surprising. A typical length v. $t^{1/2}$ plot (1050°C) from isothermal dilatometry is given in Fig. 6.1c. Metallography has shown that complete austenitisation occurs in a few seconds, corresponding to the initial sharp length drop in Fig. 6.1c. The length change in this region is sometimes found to be related to $t^{1/2}$, although partitioning of neither carbon nor manganese should be occurring. This behaviour is attributed to solute drag, as suggested in 6.4.4. The subsequent length change is of a similar order of magnitude as that recorded during ferrite to austenite transformations, although no transformation can be occurring here. The possibility that this

length change is a manifestation of recrystallisation will now be explored.

It is well known that recrystallisation of fine-grained austenite, which is formed by heating martensite, occurs (as discussed in chapter 1, sections 1.2.5 and 1.2.6). The driving force for recovery and recrystallisation is the reduction of energy associated with excess dislocations (introduced by transformation strains) and grain boundaries. Analogies have been drawn between recrystallisation after phase transformation and recrystallisation after heavy cold work (eg Sadovskiy et al 1962). Density changes are known to occur during recrystallisation; for instance, Clarebrough et al (1960) reported a fractional density change of about 2×10^{-4} during recovery and recrystallisation of heavily deformed high purity nickel.

The length change registered at temperatures above the Ac_3 in this work correspond to a fractional density change of up to about 10^{-2}; this is two orders of magnitude larger than that reported by Clarebrough. The density change during recrystallisation after transformation of martensite to austenite may be expected to be large, compared to recrystallisation after cold work, since the removal of many grain boundaries, as well as the removal of excess dislocations, occurs. The observed fractional density change of the order of 10^{-2} seems to be rather large to be attributed to recrystallisation, but no other explanation for the behaviour has been found.

The reaction finish times at several temperatures above the Ae_3 (as at C in the TTT curve, Fig. 6.2), are given in table 6.2. In order to determine the activation energy of the process, these data were used to obtain an Arrhenius plot, which is illustrated in Fig. 6.12. The activation energy was thus found to be $141.9 kJmol^{-1}$, which is remarkably close to the activation energy for carbon diffusion in austenite, $142.3 kJmol^{-1}$ (CRC Handbook of Chemistry and Physics). The kinetics of recrystallisation are known to be largely determined by the effect of impurities on the grain boundary migration rate (see review by Cotterill and Mold 1975, p109). Thus, recrystallisation in austenite may well be controlled by the segregation of carbon atoms to grain boundaries, the rate of boundary migration being controlled by the rate at which carbon atoms can diffuse into and out of the boundary.

Above the Ae_3, therefore, austenite forms rapidly (within a few

Table 6.2: Reaction finish times at temperatures above the Ae_3.

Temperature		Reaction finish time, t(s).
T(°C)	T(K)	
890	1163	15705
917	1190	11329
953	1226	7719
989	1262	5134
1050	1323	3983

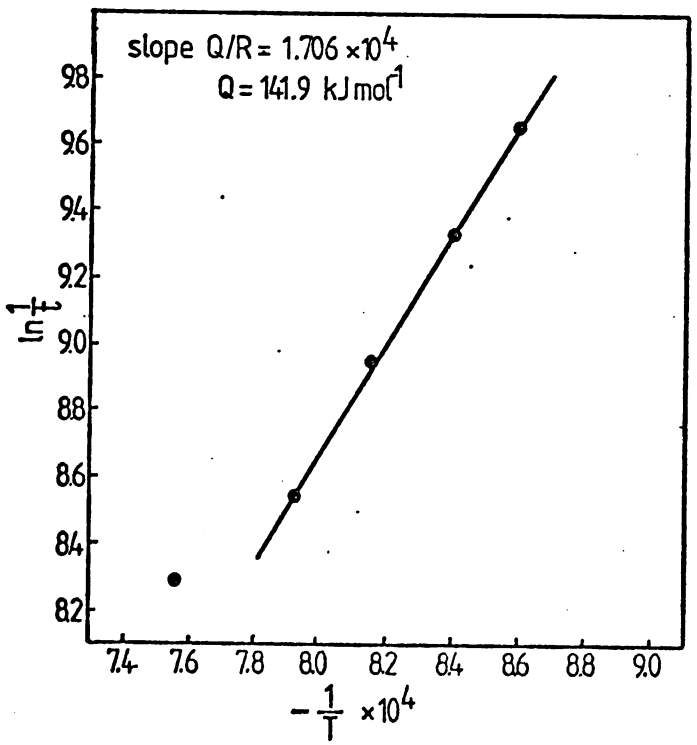

Fig. 6.12: Arrhenius plot for the reaction above the Ae_3.
The activation energy, Q, is found from

$$\frac{1}{t} = A \exp\left(-\frac{Q}{RT}\right)$$

$$\ln \frac{1}{t} = \ln A - \frac{Q}{R}\frac{1}{T}$$

seconds), and another process, thought to be recrystallisation of austenite, continues for long times. The large density change associated with the process is surprisingly large, although some density change during recrystallisation is expected. The activation energy for the process is 141.9kJmol^{-1}, indicating that, if recrystallisation is indeed occurring, it is controlled by carbon diffusion into and out of migrating boundaries.

Below the Ae_3, the austenite regions are generally unconnected and recrystallisation is not expected. However, at the highest temperatures in the two phase region, considerable volume fractions of connected austenite are present (see Fig. 6.4), and some recrystallisation is possible, although it will be restrained by the surrounding ferrite. It is thought that some of the large density change observed in this temperature range may be due to recrystallisation of austenite.

6.7 Conclusions

The processes occurring during reaustenitisation of an Fe-1.2%Mn-0.1%C alloy have been investigated by dilatometry, microscopy and microanalysis; the results and theoretical considerations have led to the following conclusions.

1. At temperatures below the Ae_3' (the no-partition Ae_3) in the two-phase austenite plus ferrite region, the austenitisation reaction proceeds in two stages. The first stage involves partition of carbon but not of manganese, and is carbon diffusion controlled (the no-Mn-partition reaction); it is followed by the second stage which involves the diffusional partition of carbon and manganese and is manganese diffusion controlled (the partition reaction).

2. At temperatures between the Ae_3' and the Ae_3, the first stage of reaustenitisation involves partition of neither carbon nor manganese, and is controlled by solute drag at the austenite-ferrite interface. It is followed by a manganese diffusion controlled partition reaction.

3. Above the Ae_3, neither carbon nor manganese partitions during austenitisation, the rate of which is controlled by solute drag. Austenitisation is followed by a process which involves a large density change and is thermally activated. The process is thought to be the recrystallisation of austenite. The activation energy for the process

is that for carbon diffusion in austenite, indicating that the recrystallisation rate is controlled by the rate at which carbon diffuses away from migrating boundaries.

4. The reaustenitisation TTT curve has been determined (Fig. 6.2). The change from no-partition to partition reaction occurs at shorter times as the temperature increases (A in Fig. 6.2). The austenitisation finish curve in the two-phase region follows a C-curve (B in Fig. 6.2). Above the Ae_3, austenitisation is rapid, but complete recrystallisation takes a long time.

5. In the temperature range between the Ae_1 and Ae_3', the partition reaction starts when it can release free energy more rapidly than the no-partition reaction. The change occurs within a few seconds in this system.

6. During reaustenitisation in the two-phase region, increasing diffusion rate and driving force are opposed by increasing equilibrium austenite volume fraction and impingement as the temperature increases, leading to C-curve reaction finish kinetics. This is also expected to occur in other systems.

CHAPTER SEVEN

CONCLUSIONS AND SUGGESTIONS FOR FURTHER WORK

7.1 Conclusions

A study of reaustenitisation of several microstructures in low alloy steels and in a high alloy steel by metallography, microanalysis and dilatometry, has led to the following conclusions.

1. Reaustenitisation of a carbide-free starting structure (martensite) in a low-alloy steel (Fe-1.2%Mn-0.1%C) at temperatures in the two-phase austenite-ferrite region has been found to occur in two consecutive stages. During the first stage, austenite forms without partitioning of the alloying element, and volume diffusion of carbon is rate controlling. After a few seconds the reaction rate falls sharply, and the slower reaction proceeds for long times (up to several hours). During this second stage, the formation of austenite involves the diffusional partitioning of the alloying element, which is rate-controlling.

At temperatures above the Ae_3' (the no-partition Ae_3) in the two-phase region, the later stages of the reaction are also controlled by volume diffusion of the alloying element, while the early stages appear to be controlled by solute drag at the austenite-ferrite interface. At temperatures above the Ae_3, the austenite reaction again appears to be controlled by solute drag, and austenitisation is followed by recrystallisation.

2. Transformations in two-phase regions have been found to reach completion more rapidly at temperatures in the middle of the temperature range than at higher and lower temperatures. These reaction-finish C-curve kinetics are interpreted as being due to the interaction of driving force, diffusion rate, equilibrium volume fraction and impingement effects. When large volume fractions of transformation products form (eg. at temperatures high in the two-phase austenite-ferrite region during reaustenitisation), the effect of impingement of neighbouring growth centres or diffusion fields is dominant, and the reaction is slow to reach completion.

C-curve reaction-finish kinetics have been observed during Mn-diffusion controlled reaustenitisation of an Fe-1.2%Mn-0.1%C steel, during C-diffusion controlled reaustenitisation of an Fe-10%Cr-0.2%C steel, and during Cr-diffusion controlled dissolution of carbides in the Cr steel.

3. In low alloy steels (containing 1% to 2% Mn or Ni and 0.1% to 0.25%C) nucleation of austenite occurs preferentially at carbides in boundaries; for instance, during reaustenitisation of ferrite containing spheroidised cementite, nucleation occurs at carbides in grain boundaries, while austenite nucleation in a ferrite-pearlite steel occurs predominantly at boundaries between pearlite and adjacent ferrite grains. In certain circumstances however, austenite may nucleate at ferrite-ferrite grain boundaries in the absence of (observable) carbides eg. during reaustenitisation of ferrite containing widely dispersed pearlite regions. In such circumstances, it has been shown that grain boundary nucleated austenite generally obeys a Kurdjumov-Sachs orientation relationship with at least one ferrite grain. The morphology of the austenite is similar to that of proeutectoid ferrite, and most interfaces are partly facetted.

Nucleation of austenite is most prolific when the starting structure is martensite or fine grained ferrite containing many carbides in grain boundaries; thus reaustenitisation is completed more rapidly in these microstructures than in other starting structures.

4. The growth of austenite in low alloy steels containing cementite particles is accompanied by rapid dissolution of cementite, and the austenite growth mode (considering only carbon diffusion controlled growth) is sensitive to the path of carbon diffusion to the advancing interface. The dissolution of cementite in austenite is accompanied by diffusion of carbon through austenite; under these conditions the austenite-ferrite interface follows the carbon diffusion field, Widmanstätten morphologies are never obtained, and dissolution of cementite in ferrite does not occur.

After carbon sources in austenite are depleted, cementite dissolution in ferrite, accompanied by a flux of carbon to the austenite interface, is possible. Under such conditions of ferrite supersaturation, the austenite-ferrite interface may become unstable and break down into a series of regularly spaced Widmanstätten sideplates. The likelyhood of instability of a particular interface depends on the

interface orientation and the crystallographic relationship between austenite and ferrite.

5. Nucleation of austenite in a high alloy steel containing 10%Cr and 0.2%C has been found to occur more slowly than in low alloy steels during conventional heating. However, during induction heating, the formation of austenite occurs very rapidly (ie. virtually as soon as the Ac_1 temperature is reached) in this steel, as in lower alloy steels.

6. The growth of austenite in the same Cr steel has been found to be controlled by the diffusion of carbon, and the partitioning of chromium between austenite and ferrite does not occur. The $M_{23}C_6$ type carbides (rich in Cr) which are present in the starting structure, dissolve slowly during reaustenitisation. Dissolution occurs predominantly in austenite, rather than in ferrite or in the interface, and is controlled by the diffusion of chromium. Undissolved carbides impede the motion of the austenite-ferrite interface, and large closely spaced carbides have a pinning effect.

7.2 Suggestions for Further Work

Much work remains to be carried out on the kinetics of reactions in two-phase regions. The present study has shown that in such temperature regions, the time taken to complete a transformation varies in a complicated way, and that in ternary alloy systems, the factor controlling the rate of the transformation may change throughout the reaction. These problems have been analysed qualitatively for the systems investigated in the current work, but in order to understand more fully the processes which are occurring, and to predict the behaviour of other systems, further work is necessary. Several suggestions for further investigations follow.

1. The kinetics of the transformation from austenite to ferrite, rather than from ferrite to austenite, in an Fe-C-X alloy in the two-phase region can readily be determined by dilatometry, and compared with the kinetics of the reverse reaustenitisation reaction. For instance, investigation of the transformation from austenite to ferrite in an Fe-1.2%Mn-0.1%C alloy would allow direct comparison with the martensite to austenite kinetics reported in chapter 6.

2. Similarly, dilatometric studies of reaustenitisation or austenite

decomposition reactions in two-phase regions could be carried out on a variety of Fe-C, Fe-X and Fe-C-X alloys, yielding further information on the factors which control kinetics.

3. A quantitative analysis of the processes occurring during reaustenitisation of Fe-C-X alloys requires the collection of more experimental data. In particular, careful metallographic measurements of austenite volume fractions and comprehensive surveys of the distribution of X (and if possible, C) during reaustenitisation at temperatures throughout the two-phase region and above are needed. Correlation with dilatometric kinetic data should clarify the exact conditions under which an X-partition reaction takes over from a no-X-partition reaction, allowing a theory of such behaviour to be developed.

4. The kinetic studies can be extended to include reaustenitisation of non-martensitic starting structures, and transformations in two-phase regions in other alloy systems. In particular, the generality of C-curve reaction finish kinetics can be tested.

5. Finally, it would be interesting to study the effect of induction heating on austenite formation in more detail, in order to find a physical explanation for the enhanced austenite nucleation which has been observed to occur under such heating conditions.

APPENDIX A1 ALLOY PREPARATION AND COMPOSITIONS

The alloys used in this work were made up from commercially available high purity elements, which were melted in an Edwards Argon arc furnace and cast as 65g or 2kg ingots. The ingots were reduced in size by both hot and cold work, and specimens were prepared by several techniques, such as swageing, rolling, drawing and machining. All alloys were given homogenisation treatments before use, generally consisting of several days at a temperature between 1100°C and 1300°C in an argon atmosphere. The alloys were chemically analysed, and compositions are given in table A1.

TABLE A1. Alloy Compositions

Alloy	Composition (balance Fe)				Chapter	Microstructure for reaustenitisation.
	C	Ni	Mn	Cr		
A	0.17				2	Ferrite and spheroidised cementite.
B	0.23	1.9			2	Ferrite and spheroidised cementite.
C	0.14		1.41		3	Ferrite-pearlite (coarse).
D	0.10		1.19		3 6	Ferrite-pearlite (fine). Martensite.
E	0.17			9.9	4,5	Ferrite and $M_{23}C_6$ carbides.

APPENDIX A2 EXPERIMENTAL TECHNIQUES

A2.1 Optical Microscopy

Specimens for examination by optical microscopy were hot mounted in perspex and polished to a 1 m finish on diamond paste polishing wheels. Several etches were used to delineate different phases in the different alloys. Details are given in table A2.1.

TABLE 2.1 Etches for Optical Microscopy.

Alloy	Microstructure	Etch	Comments
A,B	Ferrite, spheroidised cementite, martensite.	3%Nital (5-15 seconds)	Grain boundaries and interphase boundaries delineated. Martensite may turn tan, fine carbides appear dark.
C,D	Ferrite, pearlite, martensite.	a) 3%Nital (5-15 seconds) b) Equal proportions of 4% picric acid in ethanol and 1% aqueous sodium metabisulphite. (10-12 seconds)	Pearlite appears dark, martensite may etch tan. Martensite is unstained, ferrite etches tan. Good differentiation of ferrite and martensite.
E	Ferrite, $M_{23}C_6$ carbides, martensite.	Villela's reagent - 2ml picric acid, 10ml HCl, 200ml water. (5-10 seconds)	Carbides etch dark. Ferrite and martensite often indistinguishable.

A2.2 Electron Microscopy

Thin foil electron microscopy specimens were obtained by electropolishing thin discs. The discs, of diameter 3mm and thickness 0.2-0.4mm, were either slit from 3mm diameter rod or punched from thin strip. The discs were ground to a thickness of 0.05mm, and were electropolished in a Fischione twin-jet electropolisher. Details of polishing solutions and conditions are given in Table A2.2. Electron microscopy was carried out in a Philips 300 and a Philips 400 microscope.

TABLE A2.2 Electropolishing Conditions.

Alloy	Microstructure	Polishing solution	Conditions
A,B	Ferrite, spheroidised cementite, martensite.	5%perchloric acid 25%glycerol 70%ethanol	25 C, 55V, 70 - 100mA.
C,D	Ferrite, pearlite, martensite.	10%perchloric acid 20%glycerol 70%ethanol	25 C, 30 - 50V, 75mA.
E	Ferrite, $M_{23}C_6$ carbides, martensite.	5%perchloric acid 25%glycerol 70%ethanol	25 C, 80V, 80 - 100mA.

A2.3 Preparation of Carbon Extraction Replicas

In the Fe-10%Cr-0.2%C alloy (alloy E), $M_{23}C_6$ carbides were extracted from ferrite by a replication technique. The polished specimens were etched in Vilella's reagent (see Table A2.1), and a carbon film was evaporated on to the etched surface in an Edwards 3AM Evaporator. The film was scored into small squares (about 1mm across), and was elecrolytically removed in 20% Nital at a voltage of 5 - 10V. The replicas were washed in distilled water containing a small proportion (about one fifth) ethanol, and were examined on copper grids.

APPENDIX A3 CRYSTALLOGRAPHIC RELATIONSHIPS BETWEEN FERRITE GRAINS

Table A3.1 Crystallographic Relationships between Ferrite Grains which are KS related to a common Austenite (after Bhadeshia, 1978).

1. 0 0 0 0 0 0 0 0 0	2. 60 -52 52 52 41 76 -52 76 41	3. -60 -52 52 52 76 41 -52 41 76
4. 71 48 -48 -48 48 71 48 71 48	5. 11 83 -83 -83 7 90 83 90 7	6. 50 -57 57 57 80 34 -57 80 34
7. -53 -51 60 67 -39 -60 46 -84 85	8. -9 89 -82 89 -19 -71 -82 -71 21	9. 30 -61 -83 60 31 83 88 -80 10
10. 57 -50 58 72 -65 -32 39 51 -88	11. -64 -46 55 65 -44 -57 38 -90 52	12. - 6 -84 -89 84 -21 -70 89 -70 20
13. 61 -33 -75 -61 -60 45 -44 -77 -49	14. 53 -67 -46 60 -60 45 -51 -39 -84	15. 84 -84 - 9 9 84 84 84 - 9 84
16. 57 -72 -39 50 -65 51 -50 -32 -88	17. -90 -85 - 5 14 76 -88 76 -15 85	18. -56 -71 -41 71 41 -56 41 -56 -71
19. 67 69 32 -45 -62 58 54 -36 86	20. -84 76 15 -15 77 -81 -76 -19 77	21. -62 61 43 -75 43 -50 -32 -61 -77
22. 62 38 65 65 -53 48 38 -83 -53	23. 62 55 -48 -65 -59 -42 -40 50 -90	24. -82 83 11 - 8 -89 -82 90 - 7 83

Relationships are expressed as rotation matrices, whose elements are given as angles in degrees, for clarity. To operate the rotation matrix, the cosine of the elements must be taken. The elements of each matrix may NOT be taken in any order. !!!

TABLE A3.2 Experimentally Determined Crystallographic Relationships

Obtained from ferrite-ferrite and ferrite-martensite pairs, in a partially reaustenitised and quenched Fe-1.2%Mn-0.1%C alloy (starting structure, ferrite-pearlite). See Chapter 3, section 3.4;tables 3.1 and 3.2.

Area No.	Pair	Rotation Matrix	Rel.	Pair	Rotation Matrix	Rel.	Pair	Rotation Matrix	Rel.
1.	AB	69 66 32 62 31 78 35 71 61	no	AM	63 32 78 70 66 32 36 71 61	no	BM	B=M	KS 1
2.	AB	69 66 32 62 31 78 35 71 61	no	MA	67 28 75 81 77 16 24 65 88	no	MB	86 14 77 89 77 14 8 87 89	KS 17
3.	AB	69 40 58 58 50 56 41 85 50	KS 23	MA	11 80 89 86 76 14 80 18 76	KS 8	BM	Twin related	KS 4
4.	AB	39 71 57 57 39 71 71 57 39	KS 18	MA	M=A	KS 1	MB	As AB	KS 18
5.	AB	22 76 74 74 16 85 76 81 16	KS 20	AM	14 77 85 77 14 87 87 86 0	KS 17	MB	14 85 76 85 8 87 77 85 14	KS 17
6.	AB	41 61 64 56 35 86 71 73 27	no	AM	75 52 42 14 79 79 88 41 50	no	MB	67 23 87 45 70 52 55 79 38	no
7.	BA	16 81 77 83 11 82 76 84 14	no	AM	A=M	KS 1	BM	As BA	no
8.	AB	69 73 28 60 41 64 31 61 80	no	AM	63 30 79 44 61 60 59 85 33	no	BM	77 60 34 43 61 61 49 44 75	KS 13
	AC	69 73 28 41 49 85 57 46 62	no	BC	54 36 90 79 81 14 39 55 76	no	CM	75 22 74 88 74 16 16 75 88	no

Ferrite is denoted A,B... etc., martensite M. Rotation matrices were derived from the diffraction vectors and angles given in table 3.1, and the matrix elements are expressed as angles, as in table A3.1. The crystallographic relationships were determined by comparison with the matrices in the previous table, and where the crystals are KS related, the number of the corresponding variant is given.

REFERENCES

Aaronson, H.I., (1962): "Decomposition of Austenite by Diffusional Processes." p387. Interscience Publishers, New York.

Aaronson, H.I., Domian, H.A., (1966): Trans. AIME 236 781.

Aaronson, H.I., Domian, H.A., Pound, G.M., (1966a): Trans. AIME 236 753.

Aaronson, H.I., Domian, H.A., Pound, G.M., (1966b): Trans. AIME 236 768.

Albutt, K.J., Garber, S., (1966): JISI 206 1217.

Araki, K., Fukunaka, S., Uchida, K., (1977a): Trans. ISIJ 17 701.

Araki, K., Takada, Y., Nakaoka, K., (1977b): Trans. ISIJ 17 710.

Ashby, M.F., (1966): Phil. Mag. 14 1157.

Austin, J.B., Pierce, R.H.H., (1934): Trans. AIME 22 447.

Austin, J.B., Pierce, R.H.H., (1935): Trans. AIME 116 289.

Avrami, M., (1939): J. Chem. Phys. 7 1103.

Bailey, D.J., (1976): "2nd International Conference on Mechanical Behaviour of Materials", Boston, Mass. p1722.

Bailey, D.J., Stevenson, R., (1979): Met. Trans. 10A 47.

Bayertz, M., (1942): Trans. ASM 30 458.

Bee, J.V., Howell, P.R., Honeycombe, R.W.K., (1979): Met. Trans. 10A 1207.

Bhadeshia, H.K.D.H., (1979): PhD Thesis, University of Cambridge.

Bhadeshia, H.K.D.H., (1980): Personal Communication.

Bhadeshia, H.K.D.H., Edmonds, D.V., (1980): Metal Science

Bleaney, B.I., Bleaney, B., (1976): "Electricity and Magnetism", 3rd Edition, O.U.P. p494.

Bungardt, K., Kunze, E., Horn, E., (1959): Arch. Eisenhütt. 29.3 193.

Butler, J.F., Bucher, J.H., (1979): Iron and Steel International, April 1979 p85.

Cairns, R.L., Charles, J.A., (1967a): JISI 205 1044.

Cairns, R.L., Charles, J.A., (1967b): JISI 205 1051.

Chraska, P., Dubsky, J., (1979): Mat. Sci. and Eng. 41 217.

Christian, J.W., (1975): "Theory of Transformations of Metals and Alloys", 2nd Edition, Part 1. Pergamon Press.

Clarebrough, L.M., Hargreaves, M.E., Loretto, M.H., West, G.W., (1960): Acta Met. 8 797.

Cotterill, P., Mould, P.R., (1976): "Recrystallisation and Grain Growth of Metals", Surrey University Press, p109.

CRC Handbook of Chemistry and Physics, (1977): 57th Edition, ed. Weast.

Davies, R.G., (1978a): Met. Trans. 9A 41

Davies, R.G., (1978b): Met. Trans. 9A 451.

Davies, R.G., (1978c): Met. Trans. 9A 671.

Davies, R.G., (1979a): Met. Trans. 10A 113.

Davies, R.G., (1979b): Met. Trans. 10A 1549.

Digges, T.G., Rosenberg, S.J., (1943): Trans. ASM 31 753.

Dubé, C.A., Aaronson, H.I., Mehl, R.F., (1958): Rév. Met. 55 201.

D'Yachenko, S.S., Fedorov, G.V., (1963): Phys. Met. Metallog. 18 68.

Fong, H.S., Glover, S.G., (1975): Trans. JIM 16 115.

Goldstein, J.I., Costley, J.L., Lorimer, G.W., Reed, S.J.B.,(1977): SEM 1977 1 p315 (Chicago).

Grange, R.A., (1966): Trans. ASM 59 26.

Grange, R.A., (1971): Met. Trans. 2 65.

Green, M., Cosslett, V.E., (1961): Proc. Roy. Soc. 78 1206.

Grozier, J.D., Paxton, H.W., Mullins, W.W., (1965): Trans. AIME 233 130.

Hansen, M., (1958): "Constitution of Binary Alloys", 2nd Edition, McGraw Hill Book Company Inc., New York.

Hayami, S., Furukawa, T., (1977): "Microalloying 75 ", Vol.1, p78. New York, Union Carbide Corp.

Hillert, M., Nilsson, K., Törndahl, L.E., (1971): JISI 209 49.

Homma, R., (1974): Trans. ISIJ 14 434.

Honeycombe, R.W.K., (1976): Met. Trans. 7A 915.

Howell, P.R., Bee, J.V., Honeycombe, R.W.K., (1979): Met. Trans. 10A 1213.

Howell, P.R., Lenel, U.R., Ricks, R.A., (1980): "Developments in Microscopy and Analysis", Inst. Phys. Conf. Ser. No.52, p435.

Jana, S., Wayman, C.M., (1967): Trans. AIME 239 1187.

Johnson, W.A., Mehl, R.F., (1939): Trans. AIME 135 416.

Judd, R.R., Paxton, H.W., (1968): Trans. AIME 242 206.

Karlsson, B., (1973): Mat. Sci. and Eng. 11 185.

Karlsson, B., Sundström, B.O.,(1974): Mat. Sci. and Eng. 16 161.

Kessler, H., Pitsch, W., (1965): Acta Met. 13 871.

King, A.D., Bell, T., (1975): Met. Trans. 6A 1419.

Kinoshita, S., Ueda, T., (1974): Trans. ISIJ 14 411.

Kinsman, K.R., Aaronson, H.I., (1967): "Transformation and Hardenability in Steels", Symposium 1967. Climax Molybdenum Company of Michigan.

Kogan, L.I., Entin, R.I., (1971): Fiz. Met. Metalloved. 31 no.2, 379.

Koo, J.Y., Narasimha Rao, B.V., Thomas, G., (1979): Metal Progress, Sept 1979 p66.

Koo, J.Y., Raghavan, M., Thomas, G., (1980): Met. Trans. 11A 351.

Koo, J.Y., Thomas, G., (1977): Met. Trans. 8A 525.

Koo, J.Y., Thomas, G., (1979): Scripta Met. 13 1141.

Krauss, G.Jr., (1963): Acta Met. 11 499.

Krauss, G.Jr., Cohen, M., (1962): Trans.AIME 224 1212.

Kula, E., Cohen, M., (1954): Trans. ASM 46 728.

Kunio, T., Shimzu, M., Yamada, K, Suzuki, H., (1975): Engineering Fracture Mechanics 7 411.

Kurdjumov, G., Sachs, G., (1930): Z. Physik 64 325.

Lagneborg, R., (1978): "Structure Property Relationships in Dual-Phase Steels", Report of Institutet fur Metallforskning, Sept. 1978.

Law, N.C., (1977): PhD Thesis, University of Cambridge.

Law, N.C., Edmonds, D.V., (1980): Met. Trans. 11A 33.

Lorimer, G.W., Al-Salman, S.A., Cliff, G., (1977): "Developments in Microscopy and Analysis", Inst. Phys. Conf. Ser. No.36, p369.

Mahajan, S.W., Venkataraman, G., Mallik, A.K., (1973): Metallog. 6 337.

Matsuda, S., Okamura, Y., (1974a): Trans. ISIJ 14 364.

Matsuda, S., Okamura, Y., (1974b): Trans. ISIJ 14 444.

Mehl, R.F., Barrett, C.S., Smith, D.W., (1933): Trans. AIME 105 215.

Mileiko, S.T., (1969): J. Mat. Sci. 4 974.

Mirkin, L.I., (1964): "X-ray Analysis of Polycrystalline Materials", Consultants Bureau, New York.

Molinder, G., (1956): Acta Met. 4 565.

Morrow, J., Tither, G., (1978): J. Met. March 1978 p16.

Mullins, W.W., Sekerka, R.F., (1963): J. Applied Physics 34 323.

Nehrenberg, A.E., (1950): J. Met., Trans. AIME 188 162.

Nemoto, M., (1973): J. Microscopy 97 239.

Nemoto, M., (1974): Acta Met. 22 847.

Nemoto, M., (1977): Met. Trans. 8A 431.

Nishiyama, Z., (1934/35): Sci. Rep. Tohoku Univ. 23 637.

Owen, W.S., (1980): Metals Technology (1980), p1.

Pavlick, J.E., Mullins, W.W., Paxton, H.W., (1966): Trans. AIME 236 875.

Pearson, W.B., (1967): "Handbook of Lattice Spacings and Structures of Metals and Alloys", Vol. II, Pergamon Press.

Philibert, J., Tixier, R., (1975): "Electron Microscopy and Microbeam Analysis", Ed. Siegel and Beaman, Wiley, p333.

Plitcha, M.R., Aaronson, H.I., (1974): Met. Trans. 5 2611.

Purdy, G.R., Weichert, D.H., Kirkaldy, J.S., (1964): Trans. AIME 230 1025.

Rashid, M.S., (1976): SAE paper 760206.

Reed, S.J.B., (1975): "Electron Microprobe Analysis" C.U.P.

Roberts, C.S. (1953): J. Metals 5 203.

Roberts, G.A., Mehl, R.F., (1943): Trans. ASM 31 615.

Rose, A., Strassburg, W., (1956): Stahl und Eisen, 15 976.

Ryder, P.L., Pitsch, W., Mehl, R.F., (1967): Acta Met. 15 1431.

Sadovskiy, V.S., Bogacheva, G.N., Solokov, B.K., (1962): Fiz. Met. Metalloved 14 no.3, 414

Sheard, G., Nutting, J., (1979): Met. Sci. 13 131.

Sheard, G., Nutting, J., (1980): Metals Technology 7 192.

Sherman, A.M., Davies, R.G., (1979): Met. Trans. 10A 929.

Shewmon, P.G., (1965): Trans. AIME 323 736.

Smith, C.S., (1953): Trans. ASM., 45 533.

Southwick, P.D., (1980): Research Report, University of Cambridge.

Speich, G.R., Miller, R.L., (1979): "Mechanical Properties of martensite-ferrite Steels", Report from U.S. Steel Corp. Research Laboratory.

Speich, G.R., Swann, P.R., (1965): JISI 203 480.

Speich, G.R., Szirmae, A., (1969): Trans.AIME 245 1063.

Stevenson, R., (1977): GMR 2432, Detroit, Mich.

Stevenson, R., Bailey, D.J., Thomas, G., (1979): Met. Trans. 10A 57.

Tamura, I., Tomota, Y., Akao, A., Yamaoka, Y., Ozawa, M., Kanatani, S., (1973): Trans. ISIJ 13 283.

Tomota, Y., Kuroki, K., Mori, T., Tamura, I., (1976): Mat. Sci. and Eng. 24 85.

Townsend, R.D., Kirkaldy, J.S., (1968): Trans. ASM 61 605.

Wasserman, G., (1935): Mitt. K-Wilh-Inst Eisenforsch. 17 149.

Watanabe, S., Kunitake, T., (1976a): Trans. ISIJ 16 28.

Watanabe, S., Ohmori, Y., Kunitake, T., (1976b): 1st JIM Symposium on "New Aspects of Martensitic Transformation" Kobe 1976 p369.

Webster, D., Allen, G.B., (1962): JISI 200 520.

X-Ray Powder Diffraction File (1968): Index, ASTM Publication PD1S-18i.

Zener, C., (1955): Trans. AIME, J. Met. p619.

Zerwekh, R.P., Wayman, C.M., (1965): Acta Met. 13 99.